The Dependence of Mechanical Properties of Aluminium Matrix Composites on the Size Ratio of their Constituent Powders

by

Adrian Dunne, BE

A thesis submitted as a requirement for the degree of

Master of Engineering

Supervisors: Dr Lisa Looney, Dr Jerry Murphy

Dublin City University
School of Mechanical and Manufacturing Engineering
Sept 2004

DECLARATION

I hereby certify that this material, which I now submit for assessment on the programme of study leading to the award of Master of Engineering is entirely my own work and has not been taken from the work of others save and to the extent that such work has been cited and acknowledged within the text of my work.

Signed: _____ **ID No.: 51172941**

Adrian Dunne

Date: Sept 2004

ACKNOWLEDGEMENTS

Many individuals have come to my assistance during the present work. I offer many thanks to all, and in particular I would like to acknowledge the contributions of:

Dr. Lisa Looney of Dublin City University (DCU) for her guidance, and encouragement and Dr Jerry Murphy of DCU for useful inputs regarding the mathematics of modelling powder packing.

All my fellow students within Dublin City University and elsewhere, for their assistance, support and friendship. Special thanks to Graham Gavin and David Matthews.

Chris Crouch, Liam Domican, and all the technical staff involved in this work, for helpful discussion and for providing me with all I requested and more.

Both the School of Mechanical and Manufacturing Engineering DCU and Enterprise Ireland, without whose funding this project would not have been possible.

My parents and siblings and friends for their encouragement and up-lifting confidence in my ability.

Thanks.

ABSTRACT

In the powder metallurgy method of composite material production it has been noted that the size ratio, between the constituent powders used in Aluminium-Silicon Carbide non-continuously reinforced metal matrix composites (MMCs), has a bearing on the final mechanical strength of the material. The exact mechanism is not understood. This work concentrates on how the difference in size ratios between the powders affects the packing fraction when the powders are poured into a die, before compaction, and how this is related to the final mechanical strength of the material. The packing of binary powders was firstly treated mathematically. An analytical model to predict the packing fraction of the powder was then tested to ensure its accuracy when used with metal powders of this type. The model was found to predict the packing fraction of the powders used to manufacture these materials within a range of 8%. Powder mixtures of various size ratios were then used to prepare material samples and the changes in packing fraction compared to the changes in the mechanical properties of the material. Comparison of the changes of mechanical properties of the materials as size ratio is changed, with the way that packing fraction changes with packing fractions shows that they alter in a similar manner. It is concluded that the change in powder size ratio leads to a change in the packing fraction of the powders before compaction, which leads to a change in the mechanical strength. However it is shown that other factors such as powder size and sintering times and temperatures also have an important part to play. It is also shown that the powders of differing sizes must be present in sufficient quantities to achieve high packing fractions. Therefore it may be easier, and cheaper, to successfully sinter material made from mixtures of powders where significant portions of powders of different sizes are used.

Table of Contents

Chapter 1:Introduction

1.1 Powder Metallurgy and Metal Matrix Composites

The use of Powder Metallurgy (PM) technology is becoming more and more widespread in industry. There are many reasons for this. First is its near net shape characteristics that allow manufacture of complex shapes with the minimum of machining and scrap. Secondly shapes that are difficult to machine or cast can be manufactured cheaply using PM technology. However the area of PM technology that will be focused on in this work is its use in the manufacture of high strength/low weight materials such as Metal Matrix Composites.

Many modern applications (e.g. aerospace components) require materials that can offer low weight combined with high strength, which is not offered by any traditional engineering materials. One such family of materials is that of Metal Matrix Composites. The main body of these materials is made up of a metal phase (e.g. aluminium or steel) and this matrix is reinforced by a hard ceramic phase (e.g. silicon carbide). The reinforcement can come in the form of long continuous fibres. These give great strength in a particular direction, but do not tend to strengthen the material in directions other than that parallel with the fibres. A second means of reinforcement is to use shorter whiskers to reinforce the material. This means of reinforcement has been found to give increases in strength of up to 100% compared to non-reinforced materials. However it was discovered that SiC whiskers are carcinogenic and toxic on inhalation. Research work with them stopped due to the high cost of handling such dangerous materials. The third means of reinforcement is to use particles of the harder phase, otherwise known as discontinuous reinforcement, to reinforce the matrix. This will not give as high an increase in the strength of the material as the fibres will in one direction but the increase in strength offered by the discontinuous reinforcement is isotropic. It is on these Discontinuous Reinforcement Metal Matrix Composites (DRMMCs) that this work focuses.

These materials were originally developed with a view to their use in aerospace applications, where their high specific strength and specific stiffness were seen to be desirable due to the direct relationship between fuel consumption and aircraft mass. However, the low ductility of these types of materials (or DRMMCs) prevented their widespread use in the aerospace industry. Today the application areas of DRMMCs are generally in the automotive and railway fields although they are also widely used in the manufacture of sporting equipment.

1.2 Metal Matrix Composite Manufacture

Several methods for the manufacture of DRMMCs have been implemented. For example it is possible to melt the matrix material and then to stir the reinforcement phase into the molten matrix phase. However it is difficult to get a homogenous distribution of the reinforcement phase throughout the material using this method and the reinforcement particles tend to be gathered in clumps through the MMC. This can actually lead to a reduction in the material's strength. The reinforcement particles can also be co-sprayed with the metallic to form material.

Other processes which have been developed and are in use include preform infiltration or squeeze casting and XD^{TM} (exothermic dispersion) processing [1]. These processes have been developed in recent years in an attempt to increase the volume fraction of reinforcement which can be included in the composites, and also to overcome the problem encountered with the more conventional casting and spray processes.

One relatively simple method of manufacturing these materials is to use powder metallurgy. Mixing of powders together to obtain homogenous mixtures prior to sintering is common practice in the PM field. Thus the matrix and reinforcement phases can be mixed together in the powder mixing phase of the process, then the mixed powder can be compacted into the required shape and sintered. Once the homogeneity of the mixture is assured in the mixing section of the process the reinforcement phase should be homogenously distributed through the matrix phase in the final sintered part.

Work has been carried out in this area investigating the effect on the material of changes in various processing parameters such as sintering temperature and time, compaction rate and pressure, processing atmosphere, etc. One phenomenon that has been noted but not fully explained involves the size ratio (i.e. the ratio of the sizes of the powders used in the mixture to one another) between the powders used to manufacture the material. Work by O'Donnell [1] and German [2] etc. shows the strength of the sintered material decreasing as the size ratio increases to a certain point, and then increasing again as the size ratio is increased further.

Since the powder sintering process is a three stage process it seems logical to assume that there are three distinct explanations for this effect.

1. The size ratio affects the packing density of the powder in the mould, which directly affects the sintered density of the material and thus its strength.
2. Due to the different size ratios the compacted density is different, which affects sintered density and thus sintered strength.
3. The size ratio influences the sintering of the powder. The size ratio of the powders used affects the sintering process, which affects sintered density and thus strength.

A combination of all three effects is likely to affect the final strength of the material. In this work, however, we will concentrate on the first effect and see if we can directly map the effect of size ratio on pre-compaction packing fraction to the mechanical properties of the final sintered material. It is easy to see intuitively that size ratios will affect the packing density of powders before they are compacted. Furthermore it is known that as size ratio is decreased the packing fraction of the powders will decrease and then increase again, in a similar manner to the way the strength of the material is seen to alter with changing size ratio.

If there exists a direct link results between the packing fraction of the powder mixture pre-compaction and the strength of the material post-sintering, then it should be possible to correlate the packing fraction of an un-compacted powder and the strength of the sintered material made from that powder. If no correlation exists then it can be said that the size ratio effect is not a function of the packing fraction of the un-

compacted powder in the pre-compaction stage of the process but rather an effect of another stage/stages or an effect of this stage combined with another stage/stages.

It is this hypothesis that is examined in this work. A review of relevant literature in this area is presented in chapter 2. The problem of the packing of powders of two sizes in a binary mixture where the powders pack in idealised formations is treated mathematically in chapter 4. Results of tests carried out on the powder-packing model of Yu and Standish [3] are presented in Chapter 5 together with results of tensile and hardness tests carried out on Al SiC_p materials manufactured using powder mixtures of various size ratios. Attempts to correlate packing fractions (both as calculated from the model and as measured) with the mechanical properties measured are presented in chapters 5 and 6.

Chapter 2: Literature Review

2.1 Introduction

This review gives an overview of many of the different theories currently available in the literature to model two of the main stages in the manufacture of powder metallurgy (PM) materials viz. pouring of powders during the powder pressing stage of the PM process, and the compaction of these powders to make "green" parts. Some models which describe the overall mechanical behaviour of metal matrix composites are also described.

2.2 Models of Powder Mixtures

Many different models to look at the packing of mixtures of powders of all types exist. Different methods for such modelling have been used by many researchers. An overview of some of the most relevant to the work undertaken here is presented below.

2.2.1 Mathematical Model of Mixtures

The first of these is by Standish and Yu [4]. They use a mathematical model based on a Simplex-Centroid lattice method developed for use in experiments with all types of mixtures by Scheffe [5]. In this design it is assumed that the number of different components in the mixture is equal to q (e.g. for Al-SiC_p powder mixtures q=2). In order to use this method 2^{q-1} measurements of packing fraction are taken, one on each of the following: the q pure components, the $\binom{q}{2}$ binary mixtures with equal proportions, the $\binom{q}{3}$ ternary mixtures with equal proportions and the q-nary mixture with equal proportions. Therefore in the case of a binary mixture (such as the Al powder mixed with SiC_p but with no mixed-in lubrication) only the packing fraction of the two pure powders along with the packing fraction of the mixture with equal proportions of both powders (by volume) needs to be known before it is possible to determine the packing fraction of a mixture of any proportions of these two powders.

For a ternary mixture (such as an Al SiC_p mixture with mixed in lubricant) 7 tests must be carried out before the model can work i.e. the packing fractions of the three pure powders, of the 50-50 mix by volume of the three binary mixtures of the powders (in the Al-SiC_p-Zinc Sterate example the three mixtures would be a 50-50 mix by volume of Al and SiC_p, a 50-50 mix of Al and Zinc Sterate and a 50-50 mix of Zinc Sterate and SiC_p) and the packing fraction of a mixture of equal proportions of all three components.

This model has a number of elements to recommend it. Firstly the calculations are relatively simple. Secondly there is no stipulation that the mixtures be uniform before the model can predict porosity, and thirdly as the equations involved are algebraic the isoporosity lines can be given directly without the need for the results to be interpolated as is the case with physical models such as those presented by Leitzelment et al [6], Ouichiyama and Tanaka [7] or Cross et al [8]. However the model does need a greater number of measurements than the physical models.

In the current study interest is very much focused on the size ratios of the powders that constitute the mixture. This model does not take the relative size ratios of the respective constituent powders of the mixture directly into consideration, although the measured porosities will be inherently dependent on these ratios.

Data is presented by Standish and Yu [4] for the packing of mixtures of three sizes of glass beads and of mixtures of coke, in order to see if the model was successful for irregularly shaped particles as well as spherical particles. The calculated data is compared to experimental data and other data available in literature. The difference between the two is found to be less than 2% and the model is deemed to be more accurate than other geometrical models.

In a further paper Standish and Yu [9] refine the method of calculation, introducing what they call a "D-optimal design". This refinement is needed because of a feature of the original model design. In the original design [4], it is assumed that the minimum porosity for a binary mixture always occurs when the volume of the large spheres is 50%. However for some conditions, depending on the initial porosities and the diameter ratio of the spheres, the minimum porosity in binary mixtures may occur at a

different value. This, in turn, can lead to large errors in predictions. So, in effect, the original Standish and Yu model is limited in the mixtures to which it can be successfully applied by the size ratios between the powders.

To overcome this problem more measurements must be taken. The authors use the so called $\{q,3\}$ design given by Draper and St John [10]. The example of a ternary powder is described in the paper. Here 10 points need to be measured as opposed to 7 in the previous design. These points are again the porosities of the pure powders and a mixture of equal proportions of the three powders along with measurements of 6 other mixtures of varying proportions. The equations to calculate these proportions are also given. The D-optimal design and the simplex-centroid design are compared to measured data and it is clearly shown that below a size ratio of 0.4 the simplex-centroid designed model gives figures which vary greatly from the measured data whereas the D-optimal designed model remains accurate. Thus this latter model provided an improvement so that it can be used in a far wider set of circumstances. It should be noted however that in the D-optimal model, just as in the original Standish and Yu model, size ratio, although taken into account indirectly, is not a prescribed piece of information for the model.

2.2.2 A Model Directly Dependent on Size Ratio

The above models by Standish and Yu were created because the other mathematical models in existence tended to be quite complex and often none too accurate. To overcome this problem Standish and Yu decided to introduce some measured values into a mathematical model. However, while measuring the prescribed information is feasible for mixtures of small numbers of components, the amount of prescribed information that needs to be obtained by measurement quickly increases sharply as the number of components in the mixture increases. This limits the usefulness of these models. Therefore Yu and Standish [3] introduced yet another new approach to the problem, basing the predictions of porosity for multi-component mixtures on binary mixtures alone. Thus the problem of the amount of information that needs to be gathered before the model can be employed was reduced.

If the composition of a binary mixture is changed in the correct manner, the amount of porosity in the mixture decreases as the spaces around the larger particles are filled by the smaller particles. This will be referred to as "void contraction". The paper of Yu and Standish [3] begins with a theoretical treatment of the "relative void contraction" of binary mixtures. To understand this concept we must first understand that, as has been shown by McGeary [11], as the fractional solid volume of large particles increases in a binary mixture the fractional void volume in packing will decrease to a minimum and then begin to increase again. It is also true that the maximum void contraction increases with a decrease in size ratio (small/large) between the component particles. In other words, as the difference in the sizes between the particles in the mixture gets bigger it becomes possible to have lower porosities. This is in agreement with what we will see in Chapter 3. It is also true that the packing fraction of spheres ranges between two well defined limits of about 0.6 and 0.64 as shown by Scott [12] and Rutgers [13]. These limits correspond to loose and dense packing. However these different initial packing fractions will result in a change of the maximum void contraction and the corresponding fractional solid volume. Thus the maximum void contraction and the corresponding fractional solid volume should be a function of size-ratio and initial voidage.

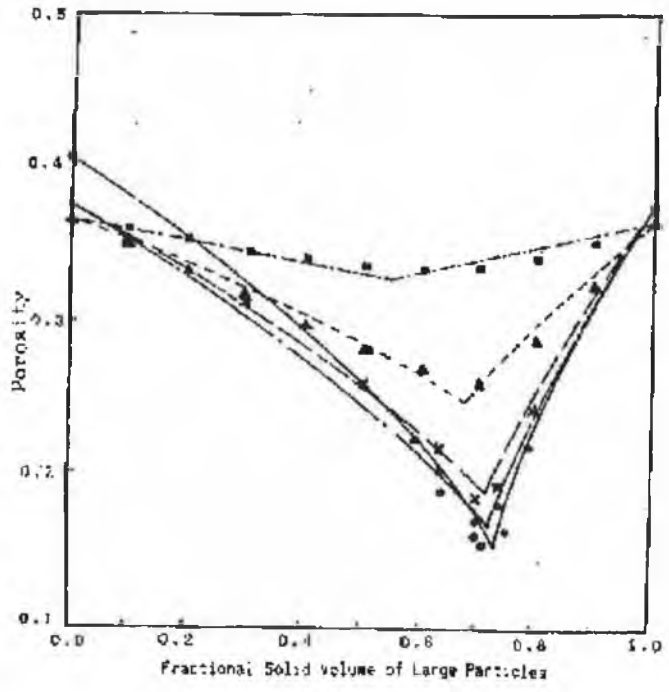

Fig 2.2.1: Porosity vs Fractional Solid Volume of large Particles from the data of McGeary [11]

In the idealised case, size ratio (diameter of the small powder particles/diameter of the large powder particles) equals zero. The maximum contraction and the corresponding fractional solid volume are given, respectively, by Yu and Standish [3] as

$$\Delta\varepsilon(0) = \varepsilon^0\left(1-\varepsilon^0\right) \tag{1}$$

$$X_L^{\max} = \frac{1}{1+\varepsilon^0} \tag{2}$$

Where ε^0 is the initial voidage, $\Delta\varepsilon(0)$ is the maximum contraction and the fractional solid volume of large particles at the maximum void contraction is X_L^{max}.

In order to make the data from existing literature compatible with this method the concept of relative maximum void contraction is introduced. This is defined as the ratio of the maximum void contraction of size ratio r, $\Delta\varepsilon(r)$, to the maximum void contraction in the ideal case when the size ratio equals zero, i.e. $\Delta\varepsilon(0)$. A corresponding relative fractional solid volume of large particles is also introduced. Both relative maximum void contraction and relative fractional solid volume are functions of size ratio only.

A quadratic regression is now introduced which fits measured data [3] for $\Delta\varepsilon(r)/\Delta\varepsilon(0)$ against size ratio r (where r =small particle size/large particle size). The correlation can be expressed by the following quadratic regression:

$$\frac{\Delta\varepsilon}{\Delta\varepsilon(0)} = \begin{cases} 1-2.35r+1.35r^2 & r \le 0.741 \\ 0 & r > 0.741 \end{cases} \tag{3}$$

It is shown in [3] that the following relation also exists between $X_L^{max}(r)/X_L^{max}(0)$

$$X_L^{max}(r)/X_L^{max}(0) = 1-r^2 \tag{4}$$

Therefore combining equations 1-4 we get

$$\Delta\varepsilon(r)=\begin{cases}\varepsilon^0(1-\varepsilon^0)(1-2.35r+1.35r^2) & r\le 0.741\\ 0 & r>0.741\end{cases} \tag{5}$$

$$X_L^{\max}=\frac{1-r^2}{1+\varepsilon^0},\quad X_S^{\max}=1-\frac{1-r^2}{1-\varepsilon^0} \tag{6}$$

Where $X_s^{\max}$ is the fractional solid volume of small particles at the maximum void contraction.

Yu and Standish [3] then discuss the packing of binary mixtures with an infinitely small size ratio, before expanding the theory to include the packing of binary mixtures with larger size ratios. This is done by first considering a packing of purely larger particles with a packing fraction p_L. Small particles are then added to the mix. If the size ratio is small enough then the small particles will fill the voids between the larger particles so that the overall volume of the packing is not increased but the packing fraction is. Letting the solid volumes of the larger and smaller particles be X_L and X_S respectively, the packing fraction p_L^T is then

$$p_L^T=p_L+p_LX_s \Rightarrow p_L^T=\frac{p_L}{1-X_S} \tag{7}$$

The subscript L in this case denotes that we started with a packing composed entirely of the larger particles and the T superscript denotes the total packing fraction of a mixture of small and large particles. Similar equations are derived to express the packing fraction when large particles are added to a packing of smaller ones. These equations can also be written in terms of specific volume V, which is the reciprocal of packing fraction p, as below

$$V_L^T=V_L-V_LX_S \tag{8}$$

$$V_S^T=V_S-(V_S-1)X_L \tag{9}$$

Importantly these two equations show that it is possible to describe the relationship between specific volume and fractional solid volume of binary mixtures with small size ratios by simple linear equations.

Some assumptions must be made to extend the theory to the general packing of binary mixtures. It is assumed that the interactions between two sizes particles only results in changes in maximum void contraction. It is also assumed that the corresponding fractional solid volume and the specific volume will still vary linearly with the fractional solid volume for any size ratio. It is shown that these assumptions do not cause a huge error in the calculation of porosities of multi-component mixtures. Based on these assumptions analytical equations are developed. In terms of packing fraction these are as follows:

$$p_i^T = \frac{p_i}{1-\left(1-\frac{p_i}{p_{ij}}\right)\frac{X_j}{X_{ij}}}, \qquad p_j^T = \frac{p_j}{1-\left(1-\frac{p_j}{p_{ij}}\right)\frac{X_i}{X_{ij}}} \tag{10}$$

where p_i is the packing fraction of one component on its own and p_j is the packing fraction of the other component on its own; X_i and X_j are the fractional solid volume of the components of the mix and p_{ij} and X_{ij} are the maximum packing fraction obtainable for the mixture of the components and the corresponding fractional solid volume. These values can be calculated from equations 5-7 which contain the size ratio.

The model was then extended for multi-component mixtures. Such mixtures are assumed to be composed of equal density spherical particles. Mixtures of irregular shaped components are not considered. Component *i* particles have diameters d_i and initial packing fraction p_i. Diameters are ordered so that $d_1 \geq d_2 \geq d_3 \geq \ldots \geq d_n$ and the fractional solid volume X_i should satisfy the equation

$$X_1+X_2+X_3+\ldots+X_n=1 \tag{11}$$

The binary theory assumptions are again used. Therefore it is assumed that the specific volumes of the multi-component mixtures vary linearly with the fractional solid volumes and there exist no co-interactions among the components. Because of this, it is taken that the calculation of the interaction between component *i* and component *j* in a multi-component mixture is identical to the interaction between these

two components in a binary mixture. Using these assumptions the packing fractions of a multi-component mixture are given by:

$$p_i^T = \frac{p_i}{1-\sum_{j=1}^{n}\left(1-\frac{p_i}{p_{ij}}\right)\frac{X_j}{X_{ij}}} \qquad (i=1,2,\ldots,n),$$

or

$$p_i^T = \frac{p_i}{1-\sum_{j=1}^{i-1}\left(1-\frac{p_i}{p_{ij}}\right)\frac{X_j}{X_{ij}}-\sum_{j=i+1}^{n}\left(1-\frac{p_i}{p_{ij}}\right)\frac{X_j}{X_{ij}}} \qquad (i=1,2,\ldots,n) \qquad (12)$$

where the maximum packing fraction p_{ij} and the corresponding fractional solid volume, X_{ij} can be calculated, as in the binary case, as follows:

$$p_{ij} = \left\{ \begin{array}{ll} p_i + p_i(1-p_i)(1-2.35r_{ij}+1.35r_{ij}^2) & r_{ij} \le 0.741 \\ p_i & r_{ij} > 0.741 \end{array} \right\},$$

$$X_{ij} = \left\{ \begin{array}{ll} \frac{1-r_{ij}^2}{2-p_i} & j<i \\ 1-\frac{1-r_{ij}^2}{2-p_i} & j \ge i \end{array} \right\},$$

$$r_{ij} = \left\{ \begin{array}{ll} \frac{d_i}{d_j} & i \ge j \\ \frac{d_j}{d_i} & i<j \end{array} \right\}. \qquad (13)$$

Predictions of the model were compared in the paper of Yu and Standish [3] with the data published in the literature. It was found that the calculated results are within 8% of the measured data for the packing fraction of mixtures for both binary and ternary mixtures. This is comparable with the models of Cross et al [14] with relative error of 5-13%, Ouichiyama and Tanaka [7] with 3-11% and with Leitzelment et al [6] with 5-15% relative error. Given that this model is much simpler to use and that it directly

takes size ratio into account in its calculations (and size ratio between the constituent powders in the mixture is of prime interest in this work) this model of Yu and Standish was used in the current work.

2.2.3 A Unit Cell Based Model of Particle Mixtures

Many other researchers have looked at this problem. A brief overview of some of their work is included here. Rassouly [15] takes an approach based on a unit cell. A packing of large and small spherical particles is divided up into these unit cells. The cells consist of large and small spheres. The packing density of a local area of the mixture (i.e. some small part of the mixture made up of a number of unit cells) is set to be the same as the overall packing density of the mixture. The packing densities of the unit cells are arranged around the local (and therefore the overall) packing density according to a frequency function. The unit cell's packing fractions are altered by means of changing the amount of smaller particles in them.

To verify these equations, experiments were carried out using mixtures of steel balls and glass beads. Here a linear relation between the packing density of the small spheres (i.e. the glass beads) and the size ratio between small and large spheres was found. However the calculated packing density of the small spheres was found not to fit too closely with the measured data. The author does claim, nonetheless, that this method is more accurate than others in the literature and the data presented supports this claim.

To test the second part of the theory, i.e. the determination of the packing density of a perfect binary mixture, a number of problems had to be overcome. First there is the problem of obtaining a mixture of such high homogeneity and then there is the problem of measuring the quality of mixedness to which the measured packing density can be attributed. To overcome these problems a special rig was devised which allowed two powders to be mixed and then split out into layers and then further into smaller samples. Thus there were 300 samples from each mixture from which 30 were selected randomly to be measured. This method's accuracy and relevance was tested and confirmed. The fact that as the proportion of large particles is increased, the packing density reaches a peak and then drops off again is also noted in this work.

2.2.4 An Analytical Model of Particle Mixtures

Ouchiyama and Tanaka [6] have developed what is described as the sole analytical model to predict the porosity of a mixture of solid particles. This models is based on an expression derived by Westman [19] for the number of contacts in a completely mixed packing, if various sized spheres and the theoretical relationship between the co-ordination number (which is a function of sizes of powders used) and the porosity in a packing of uniform sized spheres. Using these concepts, an expression is derived to describe the overall porosity of the mixture as follows:

$$\bar{\varepsilon} = 1 - \int_0^\infty D^3 f(D)dD \Big/ \left[\int_0^\infty (D \sim \bar{D})^3 f(D)dD + \frac{1}{\bar{n}} \int_0^\infty \left[(D+\bar{D})^3 - (D \sim \bar{D})^3 \right] f(D)dD \right] \tag{14}$$

where $\bar{\varepsilon}$ is the overall average porosity, D the diameter of the larger particles, $\bar{D}$ the average diameter of the smaller particles, f(D) is the number frequency size distribution of particles.

As can be seen the calculations involved in this model are quite complex. However it does contain a number of errors. As such, even though it has been widely used and has been expanded since first published, it does tend to predict an average porosity that is higher than experimental data. Song et al [20] set out to correct these systematic errors.

To this end Song et al [20] present a theoretical correction for the Ouchiyama and Tanaka model. An expression for the average porosity was derived as

$$\bar{\varepsilon} = 1 - \frac{\int_0^\infty D^3 f(D)dD}{\int_0^\infty \left[(D \sim \bar{D})^3 + \frac{(D+\bar{D})^3 - (D \sim \bar{D})^3}{1 + (\bar{n}-1)\frac{g(\Delta V_C)}{g(\Delta V_A)}} \right] f(D)dD},$$

where

$$\Delta V_A = \frac{\pi \bar{D}^3}{96(D+\bar{D})}(20D - 7\bar{D}),$$

$$\Delta V_c = \frac{\pi \bar{D}^3}{96(D+\bar{D})}(8D + 5\bar{D}) \tag{17}$$

and $\bar{n}$ can be found from the equation

$$\int_0^\infty \frac{\left[D^3 - (D \sim \bar{D})^3\right] + \frac{4(7-8\bar{\varepsilon}_0)}{13}\bar{D}(D+\bar{D})^2\left(1 - \frac{3}{8}\frac{\bar{D}}{D+\bar{D}}\right)}{1 + (\bar{n}-1)\frac{g(\Delta V_C)}{g(\Delta V_A)}} f(D)dD$$

$$= \int_0^\infty \left[D^3 - (D \sim \bar{D})^3\right] f(D)dD \tag{18}$$

Thus the average porosity is determined solely by the volume porosity of a packing of equal spheres, $\bar{\varepsilon}$, [20] and f(D) the frequency distribution of the particle sizes.

When comparison is made between the corrected model and experimental data it is found that the changes make the calculated porosities for mixtures match those measured for certain ranges of size ratio (0.0-0.5) and values of porosity $\bar{\varepsilon}$ = 0.4~0.6. In other ranges however, the corrected formulae do not work satisfactorily. The authors claim, however, that these ranges cover most engineering applications. Nonetheless the calculations are still complex in the corrected model.

2.2.5 A Model for Particle Packing Based on Specific Arrangement of the Particles

None of the models discussed thus far have had specific arrangements of particles in them. The model of Stovall et al [21], however, is different. It divides the analysis of

binary and multi-particle systems up into the "crowding" and "non-crowding" states. If the mixture is composed of n components then component *i* grains have effective radii r_i and residual packing density (i.e. the packing density if this component were packed on its own in a large container) α_i. The radii are ordered such that $r_1 \geq r_2 \geq \ldots \geq r_n$. In the mixture the component *i* has partial volume ϕ_i. In the non-crowding state it is possible to add a volume of component *i* grains, ϕ_i^0, to a mixture composed of the first *i*-1 components such that

$$\phi_i^0 = \alpha_i(1-\phi_1-\phi_2-\ldots-\phi_{i-1}) \tag{19}$$

and that the smallest grains will fill of the entire available volume. If crowding exists it is "as if the presence of the large grains deform the available space so as to prevent efficient placement". A non crowding system is an ideal case where the radius of each grain size is infinitely small compared to the next largest size so that it can fully fill the voids left between the larger particles i.e. a system becomes non-crowding as

$$\frac{r_{i+1}}{r_i} \longrightarrow 0 \qquad \text{for i=1,2,3...,n-1} \tag{20}$$

Expressions for the packing density of the system are derived for these two states and a theoretical maximum packing density is also derived. While the non-crowding state is precisely calculated, the crowding state is only approximate. The results are shown to be in good agreement with experimental results from the literature. As expected, for the binary case, packing density reaches a maximum at some percentage of large particles added and then decays. The size ratio is not specifically taken into account in the model although it is vital in determining whether the system is crowding or non-crowding. This makes it unsuitable for use in this work. Also, the exact packing pattern of the particles is again not taken into account.

2.2.6 A Different Approach: A Thermodynamic Analogy

A completely different approach is provided by Marmur [22]. Here, an approach adopted from the thermodynamic treatment of mixtures of fluids is employed. This basically involves defining the partial volume of each particle type in the mixture,

which is analogous to the partial molar volume of fluid mixtures in thermodynamics. This is the same as the increase in the total volume of the packing when one particle of that type is added to the mix. This is different to the volume of the particle itself due to the fact that the particle will normally sit into a void or a gap of some sort in the mixture. The partial volume of each particle type is calculated from the total volume of the mixture, the total number of particles in the mixture and the number fraction of the particular particle type among other factors. In the case of fluid mixture in thermodynamics the partial volume is calculated using the following equation:

$$\underline{V_i} = \frac{V_t}{n} - \sum_{k \neq i} y_k \left[\frac{\partial \left(\frac{V_t}{n} \right)}{\partial y_k} \right]_{y_l} \qquad l \neq i,k \tag{21}$$

where y_k is the fraction of the particles of type k, V_t is the total volume of the particles and n is the total number of particles. This equation is converted by Marmur into a more useful form for particle packings. Firstly y_k is related to the true volume fractions of the particles as follows:

$$y_k = \frac{x_k}{V_k \sum_{i=1}^{N} \frac{x_i}{V_i}} \qquad i = 1, N \tag{22}$$

where, k represents the number of different groups of particles (i.e. particles of a particular size), N is the total number of particles in a group k, x_k is the true volume fraction of the particles of type k and V_k is the volume of a single particle of this type. Using this approach Marmur presents expressions for the volumes of large and small particles in a binary mixture as follows:

$$V_L = \frac{V_t}{n} + (1 - y_L) \frac{d\left(\frac{V_t}{n} \right)}{dy_L},$$

and

$$V_S = V_t - y_L \frac{d\left(\frac{V_t}{n} \right)}{dy_L} \tag{23}$$

where the subscripts L and S denote the large and small particles respectively and where V_t is the total volume of the mixture

The model is applied as the volume fraction of large particles is increased and the volume of the mixture as a whole calculated and compared to experimental results. A good match is shown with the results for binary mixtures. However it was not extended fully to the ternary case due to the fact that sufficient published data from such mixtures was too scarce to calculate the partial volumes. However approximate results were calculated using the specific partial volumes extracted from the data for binary models. This approximation is also found to agree well with experimental data. Again size ratio is not a major concern of this particular work and it is not taken specifically into account.

2.2.7 A Classical Approach

A book on the packing of solid particles by Gray [23] deals in some detail with the packing of regular arrangements of particles. Expressions for the total volume and the density of a bed of particles of multiple sizes are derived. Curves are also reported to express the change in porosity in terms of ratio of the smallest particle size to the biggest in a system, and also to illustrate how porosity changes as the percentage of smaller particles is increased in a binary mixture of set size ratio. These curves are all based on experiment however.

2.3 Compaction Models

A large number of the papers that deal with powder compaction modelling tend to be quite similar and based on a small number of fundamental models. These include the Gurson model that models the material as an incompressible solid containing voids. This model has its roots in the field of soil compaction modelling. The cap model of Druckler and Prager [24] is also in widespread use. This model relies on the old soil compaction modelling techniques developed by Coulomb in the 18^{th} century as its basis.

Cocks [25] gives a good review of many of these models. In that paper it is stated that the majority of these models are based on incremental plasticity theory. What this means is that in the model, force is applied in increments and a "flow rule" exists in the model, which describes how the material will react to each increment of the load. A "yield surface" is also defined. This is basically a diagram that describes where and how the material will yield under loading. The more up-to-date and accurate models also model the compact material like a granular material (e.g. soil) rather than a sintered material to account for the different strengths between compacts and green material especially in tension. The Drucker-Prager cap model is an example of this, as is the Cam-clay model [26].

Certain constants must be determined in order for the cap model described above to work. Chtourou et al [27] present a means of calibrating the cap model for a particular material. Here the powder is modelled using a macro-mechanical approach for computational reasons. Firstly the paper adapts the cap model from its traditional form for dealing with non-ductile powder to a form which can deal with ductile powders. Then experimental determination of the tensile, shear and hardening points of the compact was then carried out in a specially designed rig. This allowed the researchers to find the correct shape of the yield surface i.e. where the compact would fail due to tensile stress, shear stress how it strain hardens etc. Thus in this way they managed to calibrate the cap model for a particular material.

In a second part of the same paper Chtourou et al. [28] addresses some of the computational issues of compaction process modelling. The paper discusses the

numerical implementation of the cap model in the form presented in the first paper [27] in a finite element package.

The cap model is implemented numerically by demonstrating the compaction of a part. The model shows a point of potential failure due to the way the part is originally to be pressed and shows how to modify the pressing to make the green compact stronger and less prone to failure.

Henderson et al [29] present a micro-mechanical approach to the problem of powder compaction modelling. They examine the two oldest and simplest models to get macro properties from the behaviour of constituent elements. These are

1. The same strain in every element. This is then used to calculate the local stress using the elemental stress-strain relations. From this local stress, the macroscopic stress is estimated by averaging. This is known as the Voight method [30]
2. The same stress in each element, which is then used to calculate the local deformation through the elemental stress-strain relations. Some average of these local deformations then gives an approximation to the macroscopic strain. This is known as the Reuss method [30]

Both of these models had been used previous to the paper of Henderson et al [29] with some success for modelling various aspects of powder packing [31, 32]. However in this paper the principle of virtual work (i.e. that for a system of N particles equilibrium can only exist if the virtual work done by all the applied forces is zero) is used in conjunction with the Voight and Reuss approaches to get constitutive laws for the behaviour of powders under compaction. Henderson et al [29] presents the predictions of these two micro-mechanical models alongside an isotropic continuum model.

Looking at the predictions of the 3 models in these situations, the authors concluded the following: for general loading the Reuss method (which is a static method) gives a more physically realistic model for granular compaction than either the Voight approach (which is kinematic) or the simple isotropic continuum model. For the case

of proportional loading however the simple isotropic model gives similar results o the Reuss model. The Voight approach on the other hand, although simple, does not produce models accurate enough in the full range of loading encountered during pressing to be of any real use.

Rednaz [32] considers the models by Gurson [33] and Fleck et al [34] to develop a model for cold compaction of powders. He uses a combination of the older Gurson model and the newer Fleck-Kuhn-McMeeking [34] (FKM) model to describe the compaction. The reason this is done is that the models are appropriate at low and high porosities respectively and the yield condition of a porous material is not only dependent on the yield strength of the particles but also on the porosity. The model presented in the Gurson paper is based on the assumption that the porous material consists of a matrix containing separated, spherical voids. The FKM model on the other hand is more recent and assumes that spherical particles form the porous material. The particles are joined by isolated contacts. The highest possible porosity for the models is 36%. At lower porosities the contacts will start to interact and the particles are less and less spherical and the model starts to break down. Thus the new hybrid model uses the FKM model for the start of the compaction process and the Gurson model for the end of the compaction process, thus results are accurately predicted for the entire compaction process.

A number of simple powder pressing problems are modelled using FEA by Rednaz using the combined model. Results for friction, yield stress and strain hardening of a sample during compaction are all obtained along with porosity gradients for the finished compact. The model is shown to work well although no comparison to experimental data is shown.

A further model of powder compaction is presented by Ransing et al [35]. Here a discrete model is developed which captures the compression of a ductile matrix and a matrix containing ductile and brittle assembly. This model is compared with the Gurson model and is found to match satisfactorily.

The compaction of powders is an area that has been worked on extensively and while many of the models discussed above derive from old models for soil compaction the

basic principle remains the same. The composite model of Rednaz [32] offers a good compromise of the advantages of the older and newer models to describe a powder through all stages of compaction. However the simplicity of the Reuss method [29] makes it worthy of consideration. Both the models of Rednaz and Reuss are more complex mathematically than the model of Yu and Standish [3] however, and neither take size ratio into account in as explicit a fashion as [3]. For these reasons it is felt that the model of Yu and Standish is more suitable for this work where the effect of size ratio on powder packing fraction is central.

2.4 Models of Metal Matrix Composite Mechanical Behaviour

The behaviour of Metal Matrix Composites (MMCs) has been the subject of a multitude of papers and models. However none have dealt in any real detail with the phenomenon that was noted by Gareth O'Donnell [1] and Prasad et al [56] where the relative sizes of the powder of the matrix (e.g. Al) and reinforcement (e.g. SiC) used to make the part through a PM process have a significant impact on the mechanical properties of the material. It is also well known that the volume fractions of the two materials also have a large effect on the final properties. Prasad et al look at the relative particle size in an Aluminium material reinforced with Silicon Carbide particles made through powder metallurgy methods. They found that a decrease in the relative particle sizes (RPS) between the Al and SiC lead to an increase in the strength and ductility. This is attributed to less clustering of the reinforcement in the samples with the lower RPS. An empirical equation to relate RPS to strength was obtained. This given as

$$\sigma_{UTS} = 358\text{-}32.5\ln(X) \tag{26}$$

where X is the ratio of the size of powder used to make the matrix (in this case the Al) to the size of the powder used for the reinforcement (i.e. the SiC) i.e. X:1.

2.4.1 Classical Description of MMC Behavior

There has, however, been much work carried out on modelling of MMCs and their behaviour. This has taken the form of modelling on a micro and a macro scale in an attempt to explain how these materials behave when subjected to stresses. The equations presented by Christensen [57] attempt to use classical methods to explain how the materials behave. This work considers a single embedded reinforcement particle in a matrix that is a composite of the properties of the reinforcement and the matrix. However these classically based theories cannot take into account the size of the particles that reinforce the material, only the percentage volume of the material that they fill.

2.4.2 Mechanism Based Strain Gradient Plasticity Theory

Because of this shortcoming in the classical theories newer ways of modelling the MMC have been developed. One of the more widely used methods is what is known as "Mechanism-Based Strain Gradient Plasticity Theory". This is a theory that can take both volume fraction and size of particles into account. The theory is discussed in a paper by Xue et al [58] among others. In this paper by both rounded and square particles of various sizes are used in a finite element model. The paper looks specifically at how the size of the particle affects the macroscopic work hardening behaviour of the MMC. The results obtained from the model, in the form of stress-strain curves, are compared to experimental data available in the literature and are found to match closely although calculated values are slightly lower than experimental values. In general, this theory describes the size effects of the particles in the MMC accurately.

Another model based on the strain-gradient plasticity theory is presented by Tomita et al [59]. They too make use of the plasticity theory equations. They take into account the fact that both the size and the volume fraction of the reinforcement particles affect the overall material properties. A repeating unit cell is modelled in a matrix of particles that is assumed to be fixed. However two different distribution patterns of the reinforcement particles are modelled to see if the different orientation will alter the results obtained. It is found that the materials with the higher volume fractions of reinforcement are stiffer and that the resistance to deformation increases as the size of the reinforcement particles decreases, all of which is consistent with the evidence of experiment. There is also a marked difference in the properties due to the different distribution patterns of the reinforcement. When laid out in a square pattern, deformation resistance tends to be increased relative to the particles laid out in a triangular pattern. This is attributed to the way that bands of high strain emanating from the particle-matrix boundary relate to particle distribution and how this affects the resistance of the composite. Again the theory gives results broadly in agreement with experimental results and takes into account the size as well as the volume fraction of the reinforcement particles.

2.4.3 Micro-Mechanical Models of MMC Behaviour

Many different micro mechanical models have also been developed for these materials. A paper by Bruzzi et al [60] is one example of such a model for an Al, SiC composite. The model was built assuming elastic and elastic-plastic materials. This paper takes the interesting step of using the same model to analyse a number of different types of particles. A repeating unit cell type model is the basis here. On this basis the paper looks at models of the reinforcement as a circle, a square, a cube, an ellipse and a sphere. The paper also looks at models of the MMC where the position and the shape of the particles was generated by looking at real electron microscope pictures of an MMC. Thus it was hoped that a realistic picture of the deformation characteristics of an MMC and the stress-strain behaviour would be obtained.

The authors also decided to test the validity of the standard approach to problems such as this i.e. using a repeating cell with the boundaries constrained. To do this they set up a model with a core, like a unit cell, which consisted of separate representations of the matrix and the reinforcement. This was surrounded by a homogenous material which represented the combined properties of the matrix and reinforcement and loaded. However, the authors found that the older periodic cell method differed from this "cell embedding" method by only 3%, and they concluded that while the embedded cell method may be slightly more accurate, the difference in the results obtained is not large enough to justify the large amount of extra computation time needed.

This paper also deals with the problem of crystal plasticity i.e. how do you model the flow of material in the actual grains of the specimen that is being strained? A number of different models of the grain structure were implemented with fine and coarse grain structures in 2-D and 3-D. The results obtained show that the re-enforcing particles are a significant barrier to material flow and that the stresses tend to be higher around the particles, as expected.

Other micro-mechanical schemes for describing the behaviour of are presented by Dai and Huang [61], Dai et al [62, 63] and Heness et al [64]. These researchers have used various methods for predicting MMC behaviour using FEA models in each case

attempting to capture as accurately as possible the behaviour of real MMCs under loading. Each of them is successful and each has an area of application where it gives valuable results and insight. For example Dai et al [63] look at the dependence of MMCs on the size of the particles that make up the reinforcement whereas Heness et al [64] have implemented a model based on the microstructures of real materials.

2.4.4 Crack Growth in MMCs

Crack growth through a material as a load is applied or as the material is fatigued is, of course, an important mechanism. Authors such as Boselli et al [65], Ding [66] and Steglich et al [67] have looked at the behaviour of MMCs in these terms.

Boselli et al [65] present a model for crack growth in MMCs. The authors built a model in the ANSYS FEA package for crack growth through a composite where the particles are homogenously distributed and through composites where the reinforcement particles are clustered. This model, in agreement with other published models, showed that as the crack approaches a particle, a shielding effect is seen where the stress intensity value at the crack tip drops. As the crack grows past the particle anti-shielding is observed where the stress intensity value grows. The model showed that cracks were primarily deflected when interacting directly with an individual particle.

However, the most important part of the model concerns the crack growth rates. The model shows that the composites with the clustered particles tended to have the cracks that grow much faster through them than the composites with the homogenously distributed particles.

Ding [66] et al. focus exclusively on a crack tip area of the MMC. The model is based on the low-cycle fatigue life of composites. It suggests a number of interesting points about the behaviour of MMCs in service. Firstly, the low cycle fatigue life on an MMC is shorter than that of the unreinforced matrix. Secondly, MMCs with a higher volume fraction of reinforcement particles exhibit shorter fatigue lives than composites with smaller fractions of reinforcement at comparable sizes.

One of the major issues in the mechanical behaviour of MMCs involves the cracking of the reinforcement particles. Steglich et al [67] attempt to look at this problem via a micromechanical model. The model is based on a model developed by Gurson, Tvergaard and Needlemann [68] for a description of nucleation, growth and coalescence of voids in a ductile matrix. The model can accurately give stress-strain curves for a unit cell with a cracking particle. It can also provide accurate curves of force applied to the unit cell vs. the crack mouth opening displacement. Fracture resistance curves too agree well with experiment. However the authors note that the calculation time for the model is too long to be of any great use in a practical engineering situation. Therefore they develop a "phenomenological" model based only on the original void fraction of the matrix and the critical void volume fraction, which is the fraction at which the voids begin to interact. The authors found that this simpler approach, gave surprisingly accurate results at a fraction of the computation time.

2.4.5 Using Images of Real Material to Establish a Model

Another novel approach to the problem of characterizing particle reinforced MMCs is given by Baxter et al. [69]. The method presented in their paper is a combination of two different methods, namely the moving window (MW) technique [70] and the generalized method of cells (GMC) micromechanics model [71]. Basically this procedure takes a digitized image of a real microstructure and performs local micromechanical analysis on small parts of it to build up a picture of the whole. Thus material property fields can be built up directly from digitized images provided that the different phases of the material are different enough in colour from each other that the computer can distinguish one from the other on the grayscale.

A simulated specimen was generated and the model was used to generate bulk modulus fields for it (although any property could be calculated). A 3-D and a 2-D analysis was done on one slice of the microstructure and shows that the 3-D analysis does differ significantly from the 2-D and that therefore the "out of plane" parts of the matrix are important to the analysis. It was also shown that as the window size is increased the field becomes smoother, although naturally some resolution is lost on the actual properties of the field.

2.4.6 The Problems of Inclusions, Using Elastic and Plastic Models in Tandem

The problem of how native inclusions affect the stress in MMCs is examined in a paper by Wilkins and Shen [72]. The problem is specifically looked at in the context of an Al SiC composite. It was found that it was necessary to develop two models for this problem, a simplistic one that dealt with the elastic problem and a more complex model to deal with the modeling of the composite in the plastic regime. However while the authors claim that the results obtained in the model match experimental data there appears to be a direct contradiction with the data presented by Ding et al [66]. In the paper of Wilkins and Shen [72] it is claimed that as SiC concentration goes up fatigue strengths of the composites increase. This is exactly the opposite of that which is claimed by Ding et al [66] for the low cycle fatigue case.

2.5 Final Overview

It can be seen that many models exist for the overall properties and behaviour of MMCs. Some are contradictory and so great care must be taken with the route followed. The advantage of the plasticity theories is that they can take particle sizes into account as well as volume fractions. However it must be noted that they do tend to produce stress-strain results lower than those seen experimentally. This has led to this route being dismissed by some researchers. Crack growth and nucleation will always be an important feature of the properties of any material and several models have looked at this. The building of the model for these shapes has also been approached in a variety of ways with repeating unit cells, with and without periodicity, and by using a moving window technique to produce extremely complex models of the full composite. Once again most of the models presented above have some degree of agreement with experimental data and seem to be accurate in the areas where they were designed to be effective. The choice of model, therefore, is all-important.

In this work two models will be concentrated on. It is wished to examine the connection between the size ratios of the powders used to make material using PM methods and the mechanical properties of those materials. It is intended to focus on

how size ratio effects the packing of the metal powder mixture and how this change in packing, before the material is compacted or sintered relates to changes in mechanical properties after sintering. Therefore a model to describe powder packing which deals explicitly with size ratio is desired. One such model is that of Yu and Standish [3] as presented above. In this model the size ratio of the powders used in the mixture is a prescribed piece of information and so it can be manipulated in order to see how it affects packing fraction. Thus comparisons with changes in mechanical properties for the same change sin packing fraction can be examined.

Firstly, however, a model based on simple geometrical ideas and simple mathematics is developed in chapter 4. It will be seen if such a simple model can predict the increases and decreases in packing fraction as powder sizes and the amount of different powder in a mixture are changed. It will also be seen in chapter 5 how the accuracy of such a model compares to the real world situation or to a model based on a more complicated premise such as that of Yu and Standish [3].

Chapter 3: Experimental Work

The present experimental research focuses on powder metallurgical (PM) powder pressing and sintering production of particle reinforced aluminium matrix composite (PRAMC) material. Aluminium alloys AA6061 was selected as the matrix material and silicon carbide (SiC) particulate was selected as reinforcement. The basis of selection for both the matrix and reinforcement materials chosen for this work is discussed in section 3.2. The aluminium alloy was supplied in prealloyed powder form and these powders were produced by argon atomisation. The SiC particulate used was industrial abrasive grade SiC which was supplied in an unconditioned form (mechanically pulverised only).

Figure 3.1 outlines the main steps involved in the processing route which was used in the present experimental research. These steps include the mixing of the matrix and reinforcement powders, the uniaxial pressing of the resulting composite powder into either cylindrical or tensile test sample shaped green compacts and the liquid phase sintering of these green compacts.

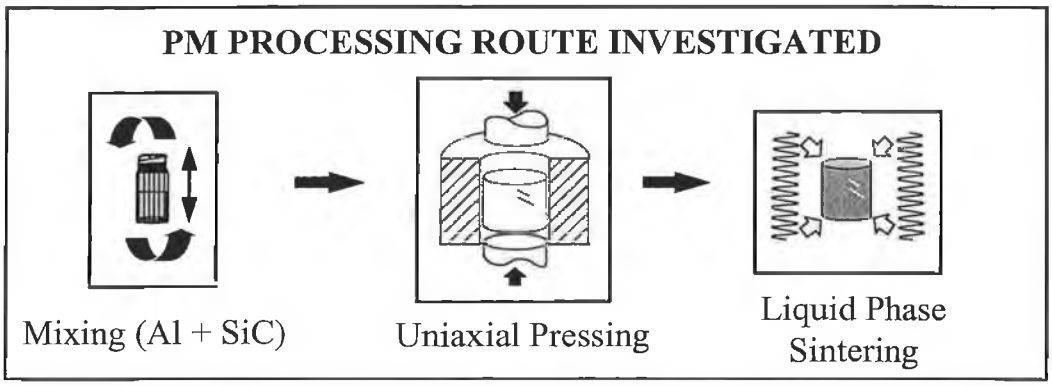

Figure 3.1. The fundamental steps involved in the processing route investigated in the present experimental research [1]

Additional steps involved the heat treatment of the material post-sintering and the addition of lubricant. Unlike the majority of processing methods used for the

production of materials of these types, the process used did not involve composite powder canning, degassing or isostatic pressing stages. This was in order to keep the cost down and to show that such costly methods do not need to be used to produce viable MMCs.

The testing work carried out was done in three main batches. The first involved the processing of cylindrical samples (17mm diameter) which were used to test the hardness of the material. The second and third involved the manufacture of tensile test samples. The processing of the material is described in detail in section 3.3.

3.1 Experimental Work Overview

The main focus of this work was on the relationship between the relative sizes of the powders used to manufacture the Al-SiC_p material and the strength of the material when produced, as well as the packing fraction of the powder mixtures before compaction and how that changed with the changing relative sizes of the powders. This was based on previous work [1]. Thus the methods used for the production of the initial samples were exactly those laid out in [1]. Lessons learned in the manufacture of these materials were applied to the subsequent samples where longer sintering times and higher sintering temperatures were used. An overview of the work carried out is shown below:

Table 3.1.1: Packing fraction measurement experiments carried out in this work

Packing Fraction Measurements		
% by volume SiC_p	10%	20%
Al powder size used	38μm, 41μm	10μm, 25μm, 33μm, 38μm
SiC_p powder size used	23μm	23μm
Al: SiC_p size ratios	1.65, 1.78	0.43, 1.086, 1.43, 1.65
No. of measurements taken	10 each	10 each

Table 3.1.2: Hardness tests carried out in this work

Hardness Tests				
17mm diameter samples (produced using initial sintering parameters). 20% by volume SiC_p				
Al Powder Sizes used	10μm	22μm	33μm	38μm
SiC_p powder size used	23μm	23μm	23μm	23μm
Number of Samples	10	10	10	10
Number of readings per sample	6	6	6	6

Table 3.1.3: Tensile strength tests carried out in this work

Tensile Tests					
20% by volume SiC_p dog-bone samples sintered at 617°C for 70 minutes					
Al Powder Sizes used	10μm	25μm	39μm		
SiC_p powder size used	23μm	23μm	23μm		
Al: SiC_p size ratios	0.43	1.086	1.65		
Number of Samples	5	5	5		
20% by volume SiC_p dog-bone samples sintered at 640°C for 80 minutes					
Al Powder Sizes used	10μm	10μm	25μm	19μm	25μm
SiC_p powder size used	23μm	13μm	23μm	13μm	13μm
Al: SiC_p size ratios	0.43	0.76	1.086	1.4	1.92
Number of Samples	5	5	5	5	5

The analysis techniques employed in the present experimental work include laser diffraction powder size analysis, hardness compression and tensile testing and the optical microstructural investigation of the sintered composite. These analysis techniques and the analysis procedures followed are described in section 3.4.

3.2 Material Selection

3.2.1 Matrix Material

The aluminium alloy AA6061, which was selected as the matrix material for the present work, is regularly used in engineering applications. AA6061 is a common medium strength heat treatable alloy. This alloy was selected on the basis of availability, cost, heat-treatable characteristics, SiC compatibility and suitability to PM processing as shown by the available comparative data [1].

The nominal chemical composition by weight of AA6061 can be seen in table 3.1. Also, table 3.2 lists various material properties of this alloy. A variety of powder sizes, including 10μm, 18μm, 25μm and 38μm have been used. All powders were produced and supplied by the Aluminium Powder Company, England.

Table 3.2.1. Nominal chemical composition by weight of AA6061

	Aluminium	Magnesium	Silicon	Copper	Chromium	Iron	Manganese
AA6061	97.6%	1.01%	0.75%	0.30%	0.18%	0.16%	0.00%

Table 3.2.2 Physical properties of monolithic AA6061, AA2124 & SiC_P [1].

	Density (g/cm^3)	Solidus/Liquidus (°C)	U.T.S. (MPa)	Elastic Modulus (GPa)
AA6061	2.7	552-652	310-380 (PM)	70 (PM)
SiC_P	3.2	-	>3000	450

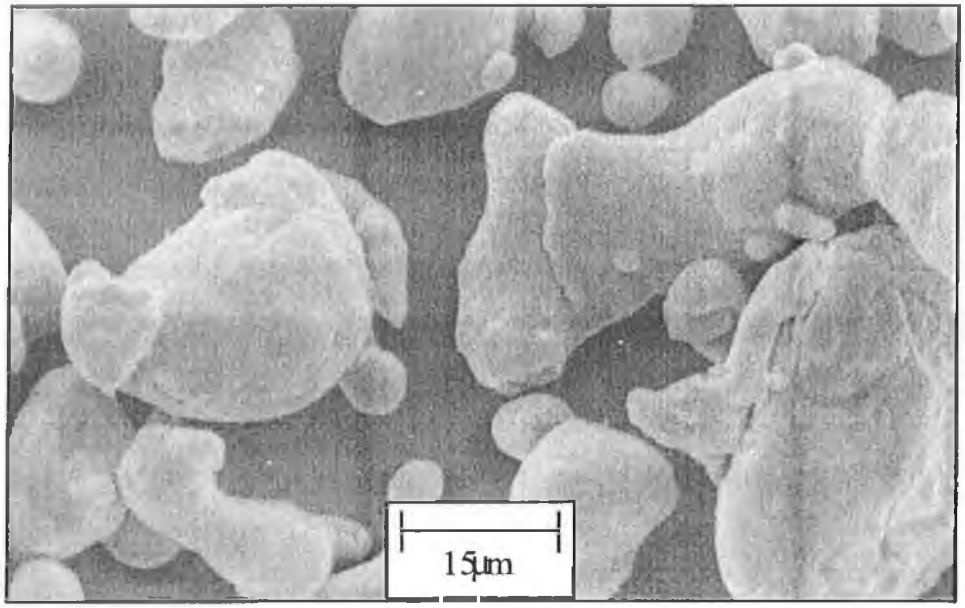

Figure 3.6. SEM micrograph of the argon atomised 16µm ($d_{50,3}$) AA6061 used in the present experimental research, Mag. x 1120[1].

3.2.2 Reinforcement

SiC particulate was selected as the reinforcement material for the present investigations. These ceramic particles are commonly used as abrasive grit in polishing, grinding and cutting applications and are therefore widely available in a variety of sizes and are also relatively inexpensive.

The SiC used in this work was angular α-SiC particulate with a density of 3.2 g/cm^3 compared to 2.7 or 2.77 g/cm^3 for the matrix materials. The main sizes used in this research were 13µm and 23µm. Table 3.2 lists various nominal material properties of SiC particles. Figure 3.7 shows the angular nature of the SiC particulate.

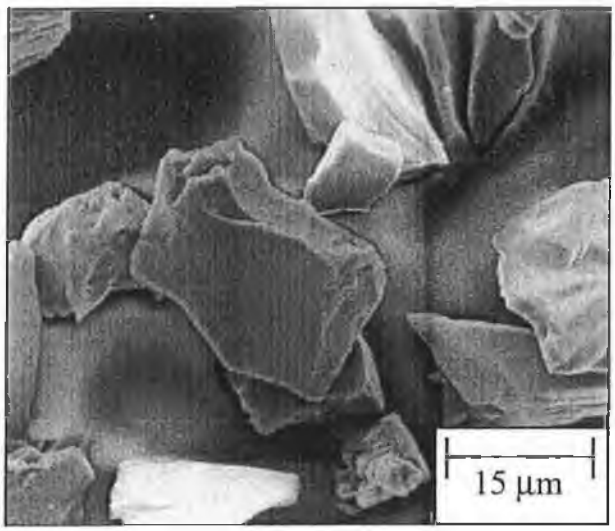

Figure 3.7. SEM micrograph of the as-supplied 25µm SiC particulate used in the present experimental research, Mag. x 1120 [1].

3.2.3 Lubricant

Zinc stearate powder lubricant was used to reduce die wall friction during sample ejection in the majority of the present research. These powder lubricants were either mixed with each blend of composite powder in various quantities including 0.5, 0.75, 1, 2 and 3% by weight or used as die wall lubricants. The solid lubricant was subsequently burnt off from the green components at either 450°C or 415°C. This burn off procedure was incorporated into the presintering stage of the sintering heat treatment process.

Table 3.2.3. Properties of the zinc stearate solid lubricant [1].

Common Name	Softening Temperature (°C)	Melting Temperature (°C)	Density (g/cm^3)	Auto-Ignition (°C)
Zinc stearate	77-110	190	1.09	302

The physical properties of zinc stearate are listed in table 3.3. The particle size of this powder was found by laser diffraction to be approximately 11µm. The selection of lubricant types was based on their lubricating properties, burn off characteristics and availability.

3.3 Sample Preparation

Samples were prepared for tensile testing in accordance with Metal Powder Industries Federation (MPIF) standard 10 [73]. The dimensions of the test specimens and for the die set are slightly modified from the MPIF flat bar dimensions and can be seen in Appendix E.

3.3.1 Powder Mixing and Preparation

The Al and SiC_p powders were first weighed to attain a mixture with 10% by volume SiC_p and were then placed together in a plastic container. The lid was fastened onto the container and it was then rapidly reciprocated by hand for approximately three minutes. The method followed here is that of O'Donnell [1]. In that work samples of powders mixed in this fashion were taken and compared to samples of powder mixtures mixed in a v-mixer turned in a lathe for 30 minutes at 90rpm. O'Donnell found that this method gave a mixture which was as homogeneous as that obtained using the more traditional mixing methods. Since it is the intention of this work to follow on from the work by O'Donnell [1, 74], noting a link between powder size ratio and mechanical properties, the same production methods are followed here.

The powders were now annealed in order to drive off any moisture as well as making the powder easier to compress. The powder was placed into a four-chamber kiln, with a quarter of the mixture in each chamber of the kiln and the lids of the chambers put in place. An industrial N_2 gas supply was connected to the furnace and allowed to flow at approximately 14 l/min for three minutes in order to purge any air out of the kiln. The gas flow was then set at 3 l/min and the furnace was heated to 480°C$\pm$ 5°C at 130 °C/hour, soaked for $1^1/_2$ hours, followed by cooling at a rate of 45°C/hour to 100°C in the furnace. After cooling the powders were placed back into the plastic container and reciprocated for a further three minutes in order to break up any caking which may have occurred during the annealing process.

3.3.2 Weighing and Compaction of Samples

Next the powders were weighed out. The weight of powder was calculated so that a charge of powder, which would give a sample thickness of 6.5mm if the powders achieved 100% sintering density, could be placed into the die and pressed. The bottom punch was placed into the die. Where no mixed in lubricant was used the walls of the die and the top of the bottom punch were brushed with zinc sterate in order to act as a die wall lubricant. In samples where mixed in lubricant was used, no zinc state was applied to the walls of the die. Next the powder was poured into the die and the die was tapped to level the powder. At this stage any excess powder left on the surface of the die was scraped away. The die was again tapped until the powder was levelled. The lower punch was then lowered and allowed to rest in place for the compaction step. The surface of the top punch was now brushed with zinc sterate and placed into the die cavity ready for the compaction stage.

Great care was taken during the compaction stage of the process. The die set was mounted on a single action hydraulic press, which sat on top of a calibrated load cell connected to a display unit giving a read-out of the force applied. A manual control switch controlled by an operator controlled the direction of movement of the hydraulic ram and a flow control valve controlled the speed of movement.

With the powder and punches in place and aligned correctly, the top section of the die set was brought rapidly down to meet the bottom section. As the top section was about to make contact with the top punch the speed was reduced to its minimum, which was approx 15mm/min. The ram was then steadily advanced at this speed until the force indicated on the readout was just below that desired. In this case it was wished to compact the samples at a force of 235 $\pm$ 5 kN. When the control switch was released, the force was found still to increase slowly. Thus the advance switch was released just below 235kN and then the operator waited for the force to "creep" up to 235kN at which point the ram was retracted.

In order to release the sample before ejection the ram was not fully retracted. Rather approximately 10kN of force was left on the part while the four screws holding the two halves of the split die together were released by a half a turn. This allowed the part to be ejected without breaking. The ram was then fully retracted.

To eject the part, the top punch was removed and spacing blocks were placed on top of the die on either side of the cavity. The top of the die set was then brought rapidly down until nearly in contact with these blocks and the speed of advance was then reduced to approx 20mm/min for safety reasons. The ram was advanced at this speed until the sample had been fully pushed, by the bottom punch, out of the die cavity. At this stage the top of the die set could be retracted, again at approx 20mm/min.

3.3.3 Powder Sintering and Post Processing

With the part now pressed it could be sintered. The green part was placed into the kiln in the furnace and the lid put in place. An industrial N_2 gas supply was connected to the kiln and allowed to flow at 14 l/min for three minutes. The flow was then reduced to 3 l/hour. In the cases where zinc sterate had been used as a mixed in lubricant the furnace was first heated to 450°C $\pm$ 5°C and this temperature maintained for 30 minutes in order to burn off the lubricant. The furnace was then heated to 617°C $\pm$ 5°C at a rate of 130°C/hour and soaked at that temperature for 70 minutes. The samples were then cooled on the furnace to 100°C before being removed. Where zinc sterate was brushed onto the die walls and not mixed into the powder the 450°C step was left out of the process.

The samples were then repressed in the original die at 235kN to ensure dimensional consistency and removed manually before precipitation heat treatment was carried out on them to improve their mechanical properties. In order to carry out the required heat treatment, the samples were placed back into the furnace, heated to 515°C in a nitrogen atmosphere and soaked at this temperature for between one and two hours. While at this temperature they were placed into iced water. Solution heat treatment followed, either by natural ageing at room temperature for four days or more (T4) or

the samples were re-heated in air in the furnace to between 168°C and 175°C for times between 4 hours and 5½ hours, depending on the composition of the material (T6).

A later batch of material was processed in exactly the same manner with the exception that it was sintered at 640°C± 5°C and soaked for 80 minutes. In all other respects their processing was identical to the above.

Again, the methods used here are those described by O'Donnell [1,74] and are followed for the reasons noted in section 3.1.1 above.

3.4 Mechanical Testing of Samples

3.4.1 Packing Fraction Measurement

All measurements of packing fraction were carried out in accordance with MPIF standard 04 [73]. A funnel is held in a clamp over a beaker of known volume. The powder which is to have its packing fraction measured is then poured through the funnel into the beaker until it overflows. The excess is then scraped off the top of the beaker and the beaker given a tap so that the powder settles.

The mass of the powder can then be measured and the actual volume of the powder determined by using the size of the powder particles and the density of the material. Once this is determined the packing fraction can be found by dividing the volume of the powder by the volume of the beaker.

3.4.2 Tensile Testing

Tensile testing of the samples produced was carried out on an Instron 4204 universal testing machine at a tensile deformation rate of 1mm/min. The strain measurements were obtained with the use of an Instron extensiometer over a gauge length of 25mm. An Instron X-Y recorder was used to recorded the force and extension during testing. The recorded data was converted manually from this form to the true stress and true strain form. The tensile testing procedure carried out followed the MPIF test standard 10 [73]. The test sample was also based on this standard, however, the sample used in this work was slightly larger than that suggested in the standard. The geometry and

dimensions of the die cavity within which these samples were pressed are shown in appendix E

3.4.3 Hardness Testing

Following sintering, Rockwell B macrohardness tests were carried out using an AFFRI 206RT hardness testing machine. Each sample was machined and polished before testing to minimise errors due to either the roughness or the surface oxide layer created during processing. To improve the reliability of this test procedure two readings from each end were taken for all samples. The Rockwell B testing (1/16" ball, 100 kg) was used. The hardness test procedures carried out were in accordance with the MPIF test standard 43 [73].

3.4.4 Optical Microscopy

The optical microscope used in this work was a Reichert MeF3 optical microscope. This microscope was fitted with a Sony colour video printer and linked to PC image capturing software.

The sintered materials in the present work were prepared for optical microscopy by grinding and careful polishing. Grinding and polishing was carried out by hand on a Stuers DAP-V polishing machine following the Buehler recommended polishing procedure for aluminium SiC composites [214]. Polishing of the samples proved difficult due to the SiC particle pull out experienced. This had the effect of contaminating the polishing surfaces at the fine polishing stages, which in turn caused damage to the surface of the samples. A number of green samples were also prepared for the microscope, however the results were unsuccessful and the images hard to decipher. The images obtained are presented in chapter 5.

Chapter 4: The Problem of Particle Packing

4.1 Introduction

In chapter 2 a number of complex models for powder packing were presented. They use a number of mathematical methods to predict powder packing, all of which are designed to take the complexity of the system into account and thus provide a high level of accuracy. In this chapter we will investigate the possibility of developing a model which is based on simple geometric assumptions and simple maths in order to ascertain whether such a model will correctly predict the rise and fall of packing fraction as the amount of both powders in the mixture changes, and whether it can accurately predict the levels of packing fraction when compared to measured data or to one of the more complex models such as that of Yu and Standish [3].

It is known that in the manufacture of Al SiC_p composite materials by standard powder metallurgical methods the sizes of the two powders relative to each other has a marked effect on the material properties. However the exact mechanism at work is not understood. Some effects related to the ratio (i.e. the size of one powder relative to that of the other in a two-powder mixture) are known. German [2] notes that if a certain volume of a powder consisting of large particles is added to a sample of a powder consisting of smaller particles, the "specific volume" filled by the powder decreases to a minimum. Specific Volume is the volume filled by the particles divided by the actual volume filled by the mixture (i.e. the volume of the powder particles and the spaces around them). Adding more of the larger powders beyond this point increases the specific volume again. This is an empirical observation and is attributed by German to the smaller powder filling in the gaps around the bigger powder as closely as possible in the case of the minimum specific volume. Adding less of the bigger powder means that there is small powder without any gap to fill, adding more of the bigger powder means that there are large powder particles without any small powder to fill in the spaces around them.

In order to appreciate fully what mechanism is at work here, we need to firstly look at how powders of different sizes pack together. It is proposed to look at the idealised case of circular discs as representative of the different powders and to discover what

effect altering the particle sizes has on the specific area filled. It will be instructive to see how the equations presented here compare to the real data for packing fraction and the predictions of packing fractions from the published Yu and Standish [3] model. This comparison is made in chapter 5. The accuracy, or otherwise of the simple model presented below, will show how real metal powder packing vary of otherwise from idealised packing modes due to their irregular shapes and the distribution in sizes that will always occur in real metal and SiC_p powder batches.

4.2 Square packed 2-D Analysis

Begin with a number of discs, all of radius R, that are packed in a square formation as shown below:

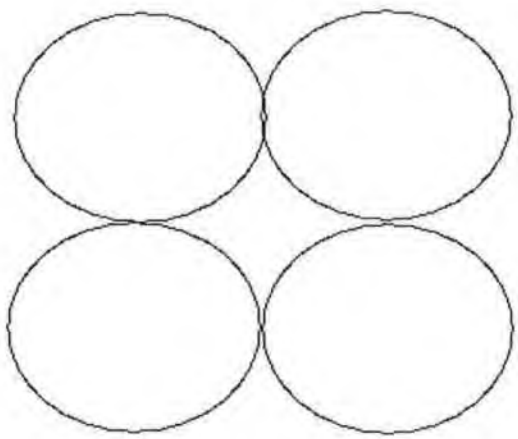

Fig 4.2.1: Discs in square packed formation

It can be shown that the area of each particle is πR^2 and that the effective area that each disc fills is $4R^2$. If there are m discs in total, then the Specific Area (SA) can be expressed as follows:

$$SA = \frac{m\pi R^2}{m4R^2} = \frac{\pi}{4} \tag{1}$$

Now n discs of a smaller size are mixed in. It is desired that the small discs fit in the spaces between the larger discs so therefore the radius of the smaller discs, r, must be as follows:

$$r < (\sqrt{2} - 1)R \tag{2}$$

In this idealised model these smaller discs fill up the gaps between the larger discs. Note that there are less small discs than would be needed to fill up all the spaces between the larger discs. The number of small discs which will totally fill the spaces between the large discs, without distorting the packing of the large discs, is referred to as n^*. SA is now calculated again it is as follows:

For $n \leq n^*$ $$SA = \frac{m\pi R^2 + n\pi r^2}{m4R^2} \tag{3}$$

Treating n as a continuous variable it can be seen that

$$\frac{\partial SA}{\partial n} = \frac{r^2\pi}{4mR^2} > 0 \tag{4}$$

Which implies that for $n \leq n^*$, SA increases as n increases, i.e. as more and more smaller discs are added and they fill the gaps between the larger particles so the specific area increases as expected.

As the number of smaller particles is increased beyond n^* we see that

$$SA = \frac{m\pi R^2 + n\pi r^2}{4mR^2 + (n - n^*)4r^2} \tag{5}$$

Again treating n as a continuous variable:

$$\frac{\partial SA}{\partial n} = \frac{(4mR^2 + 4nr^2 - 4n^*r^2)\pi r^2 - (m\pi R^2 + n\pi r^2)4r^2}{(4mR^2 + 4nr^2 - 4n^*r^2)^2} \tag{6}$$

$$= \frac{-4n^*\pi r^4}{(4mR^2 + 4nr^2 - 4n^*r^2)^2} \tag{7}$$

$$\therefore \frac{\partial SA}{\partial n} < 0 \qquad \text{where } n > n^* \tag{8}$$

In other words as the number of small particles is increased beyond the point where the smaller discs fit in the spaces between the larger discs, the specific area decreases. As well as n^* which is the number of small discs which need to be added before there are too many small discs to fit in the spaces between the large discs, we will also define a value r^*. If we were to increase the radius of the small discs to the size where they no longer fit in the spaces between the large discs, that radius will be referred to as r^*.

If the change in specific area versus the number of smaller particles is plotted for various values of r between r^* and $r^*/2$ then we see the pattern shown in fig4.2.2. The case of percentage by volume of smaller discs in the mix is shown below. The case shown is for $r=r^*$.

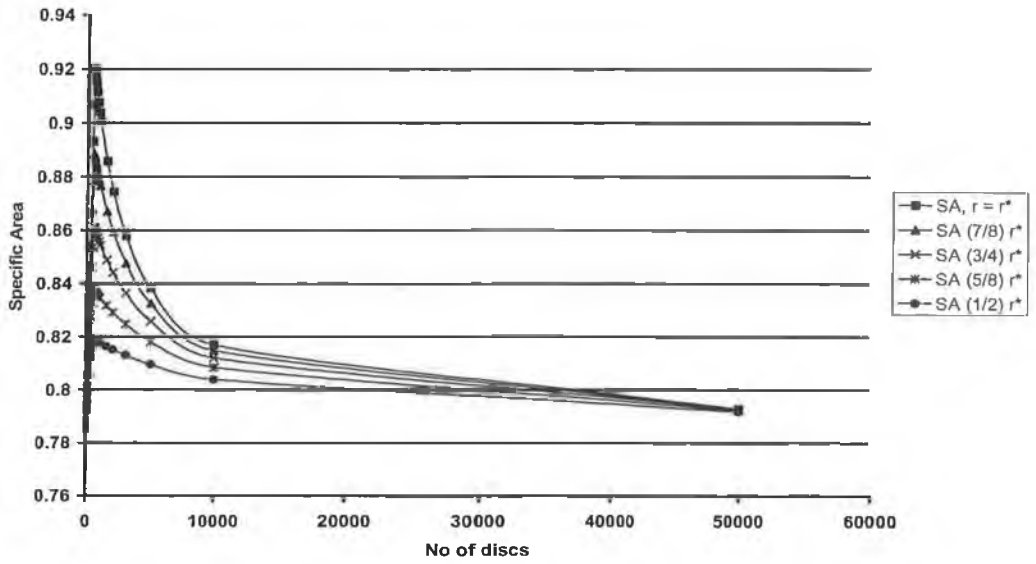

Fig 4.2.2: Specific Area of 2-D Square Packed Formation as Number of smaller particles of various sizes are added.

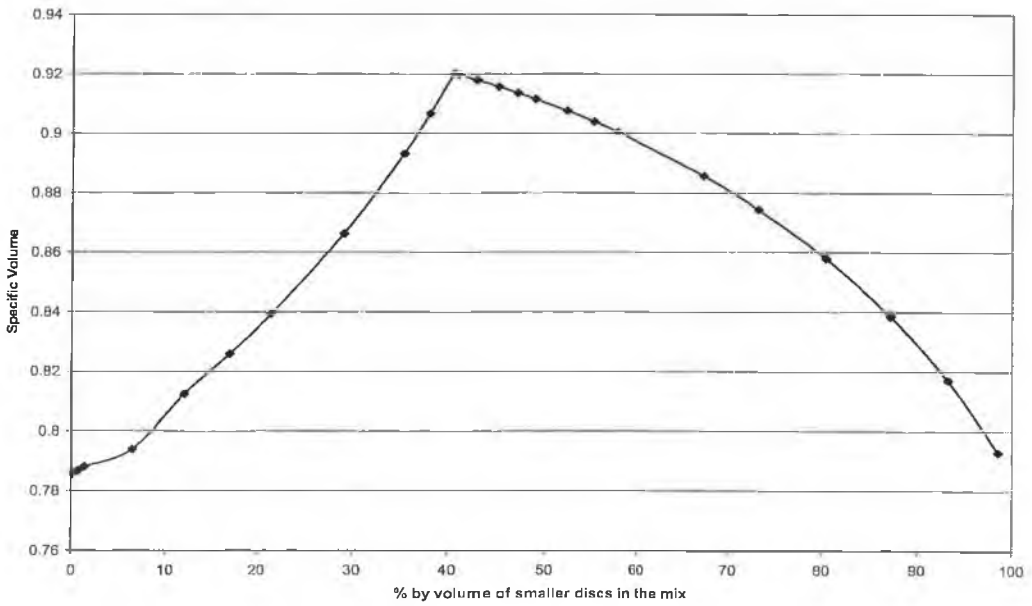

Fig 4.2.3: Change in SA of a mixture as the % volume of smaller particles is changed where the radius of the smaller discs is r^*

It should be noted that all graphs in this chapter are presented so that the data can is clearly displayed. However the absolute level of specific area or specific volume and the changes in them as the smaller particles are added differ between them. In some cases the differences are quite large, in others they are very small.

Fig 4.2.2 above shows a very sudden increase in the Specific Area of the mixture (i.e. a decrease in porosity) as the number of the smaller particles is increased and then a gradual return to the original value of SA as the number of smaller discs approaches infinity. However it should be noted that for a real mixture the amounts and sizes of the two powders used are often such that we operate in the area between 10% and 20% or, alternatively, between 80% and 90% volume small particles where a slight change in the composition can have a huge effect on the SA of the mix.

Fig 4.2.3 also illustrates the fact that the highest value of SA obtainable when the discs are packed in this formation is 0.92.

Now let n→∞ (i.e. we add a large number of small discs into the mixture). Then

$$SA_{\infty} = \lim_{n\to\infty} \frac{\frac{m}{n}\pi R^2 + \pi r^2}{\frac{4m}{n}R^2 - \frac{n^*}{n}4r^2 + 4r^2} \tag{9}$$

$$= \frac{\pi}{4} \tag{10}$$

So it can be seen that as the number of smaller particles added is increased, the specific area of the sample increases to a maximum and then back down to its starting point at π/4. This is in line with the effect noted by German.

This shows what to expect as we add more particles of one size to the mix. But what happens if we maintain the numbers of particles as a constant and change the size of one of the particles?

To start let us assume that the small particles fit easily into the gaps between the big particles i.e. $r < (\sqrt{2}-1)R$. Also assume that n<n*. Then

$$\therefore SA = \frac{m\pi R^2 + n\pi r^2}{4mR^2} \tag{11}$$

Now treat r as a continuous variable.

$$\frac{\partial SA}{\partial r} = \frac{2n\pi r}{4mR^2} \tag{12}$$

$$= \frac{n\pi r}{4mR^2} > 0 \tag{13}$$

Therefore as the radius of the smaller discs is increased up to r* (i.e. $r = (\sqrt{2}-1)R$) so the specific area of the sample increases too. Once r>r* the smaller discs no longer fit into the gaps between the larger discs. However the smaller discs replicate the packing of the larger discs in this packing model so SA does not change as shown below:

$$SA = \frac{m\pi R^2 + n\pi r^2}{4mR^2 + n4r^2} \tag{14}$$

$$= \frac{\pi(mR^2 + nr^2)}{4(mR^2 + nr^2)} = \frac{\pi}{4} \tag{15}$$

As the size of the radius is increased, eventually we reach a size where $R = (\sqrt{2}-1)r$. In other words, a stage is reached where the discs with radius R fit in the gaps between the discs with radius r. Call this radius r**. At this point

$$SA = \frac{m\pi R^2 + n\pi r^2}{4nr^2} \tag{16}$$

but
$$R^2 = (\sqrt{2}-1)^2 r^2 \tag{17}$$

$$\therefore \quad SA = \frac{m\pi(\sqrt{2}-1)^2 r^2 + n\pi r^2}{4nr^2} \quad = \text{a constant.} \tag{18}$$

So as r increases beyond r^{**} specific area decreases again as the smaller discs are no longer big enough to fill the gaps between the big discs.

4.3 3-D Square Packed Analysis

Now the case of packing of powders in three dimensions is considered i.e. the packing of spheres instead of discs. Specific Volume (SV) will now be discussed rather than Specific Area as in the section 4.2. SV is the volume actually filled by the spheres divided by the volume occupied by the spheres (i.e. volume of a container necessary to take all of the spheres). The volume of a sphere is

$$V = \frac{4}{3}\pi R^3 \tag{1}$$

So for the first case where spheres are in a square packed formation with no small spheres in the spaces between the larger spheres, Specific Volume (SV) is expressed as follows

$$SV = \frac{m(\frac{4}{3}\pi R^3)}{m8R^3} = \frac{\pi R^3}{6R^3} = \frac{\pi}{6} \tag{2}$$

If smaller spheres are introduced into the spaces such that the radius of the smaller spheres $r<r^*$ and such that $n<n^*$, where, as before, r^* and n^* are the critical radius and number of the smaller spheres respectively where the smaller spheres will no longer fit into the spaces between the larger spheres and start to distort the packing formation of the larger spheres, then

$$SV = \frac{m(\frac{4}{3}\pi R^3) + n(\frac{4}{3}\pi r^3)}{m8R^3} \tag{3}$$

Again for $n<n^*$,

$$\frac{\partial SV}{\partial n} = \frac{\frac{4}{3}\pi r^3}{m8R^3} = \frac{\pi r^3}{6mR^3} > 0 \tag{4}$$

Thus, as more of the smaller spheres are added up to n^*, porosity decreases. If small particles of size $r<r^*$ are now added into the spaces such that $n>n^*$ then

$$SV = \frac{m(\frac{4}{3}\pi R^3) + n(\frac{4}{3}\pi r^3)}{8mR^2 + (n - n^*)8r^3} \tag{5}$$

How SV changes as n is increased is now investigated for the case where $n>n^*$. For this case

$$\frac{\partial SV}{\partial n} = \frac{-32n^*\pi r^6}{3(m8R^3 + (n-n^*)8r^3)^2} \tag{6}$$

$$\Rightarrow \frac{dSV}{dn} < 0 \tag{7}$$

So we see that if we have a mixture of large and small spheres in a square packed formation that once the number of small spheres goes above the critical number n^* that an increase in the number of small spheres leads to a decrease in specific volume (i.e. an increase in the porosity of the packing).

Suppose the case of 3-D square packing is taken with one small sphere (of radius r where $r^*/2<r<r^*$) in each of the spaces between the larger spheres. How does the value of SV change as the radius of the smaller sphere is increased (i.e. increase r) while holding the radius of the larger spheres (R) and the numbers of small and large spheres (n and m respectively) constant? Since $r<r^*$,

$$SV = \frac{\frac{4}{3}m\pi R^3 + \frac{4}{3}n\pi r^3}{m8R^3} \tag{8}$$

$$\frac{\partial SV}{\partial r} = \frac{n\pi r^2}{m2R^3} > 0 \tag{9}$$

So as the radius r is increased up to r^* so the SV increases. The case of $r>r^*$ is now considered. Here

$$SV = \frac{\frac{4}{3}m\pi R^3 + \frac{4}{3}n\pi r^3}{m8R^3 + n8r^3} = \frac{\frac{4}{3}\pi(mR^3 + nr^3)}{8(mR^3 + nr^3)} = \frac{\pi}{6} \tag{10}$$

$$\Rightarrow \frac{\partial SV}{\partial r} = 0 \tag{11}$$

As r is increased still further, a point is reached where the spheres of radius R fit into the spaces between the spheres of radius r. We call this radius r^{**}. Once the radius is increased beyond this point, SV will decrease back to its original value as was shown for the 2-D case earlier. A graph of the increase and decrease of SV as more small spheres are added to the mix is shown below

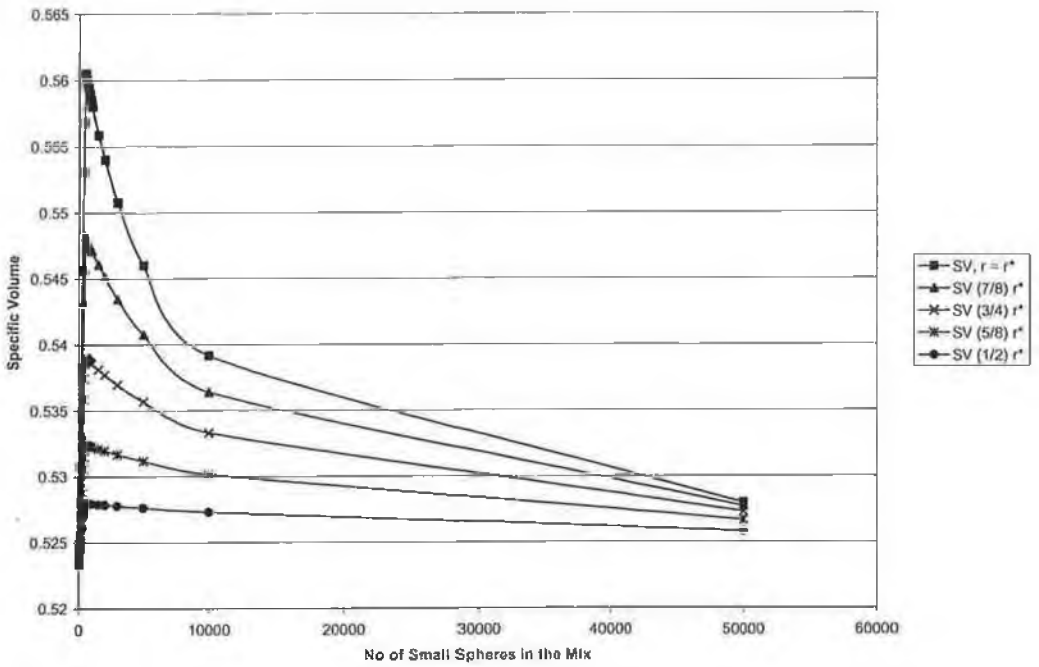

Fig 4.3.1: Specific Volume of 3-D Square Packed Formation as Number of smaller particles of various sizes are added.

Graphs of the change in SV vs the percentage volume of smaller spheres are shown below for the cases of r=r* and r=(1/2)r* in figures 4.3.2 and 4.3.3 respectively:

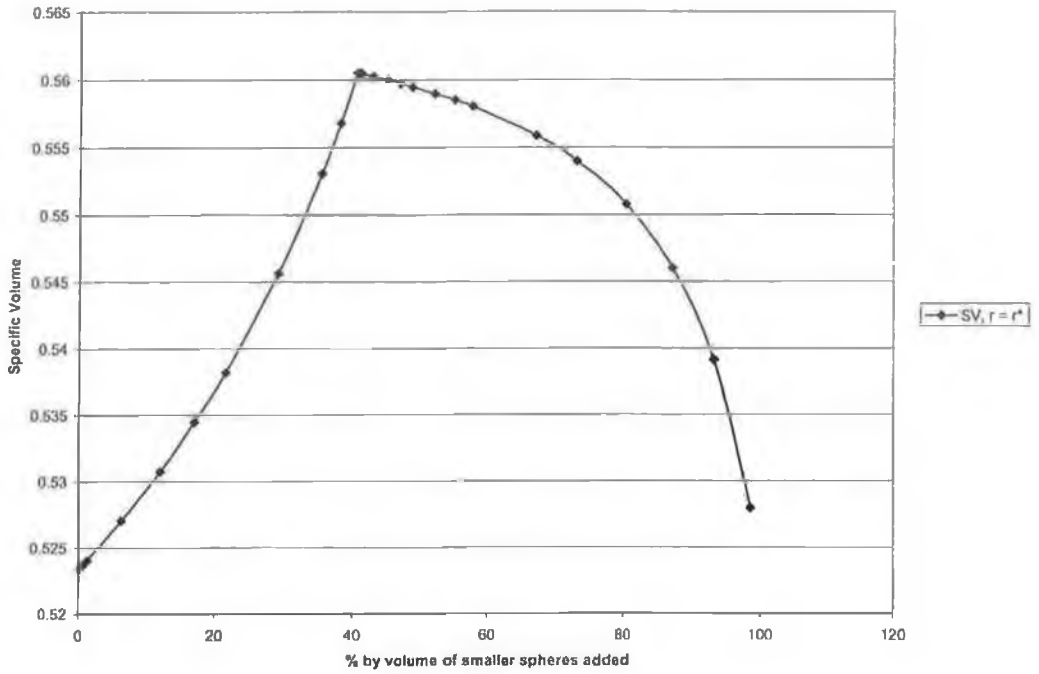

Fig 4.3.2: Change in SV of a mixture as the % volume of smaller particles is changed where the radius of the smaller discs is r*

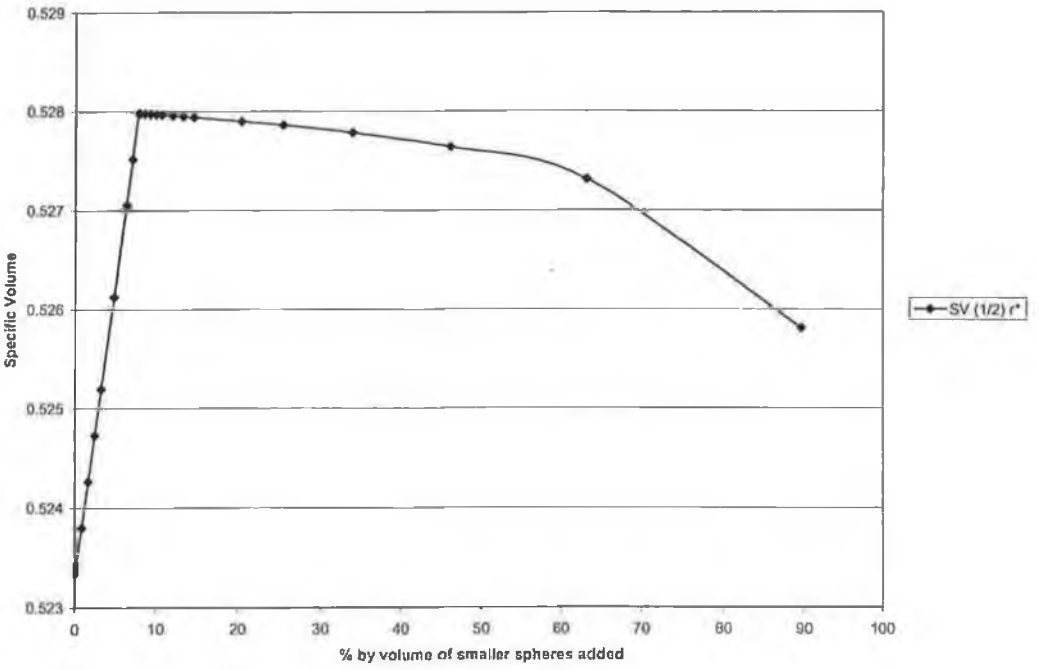

Fig 4.3.3: Change in SV of a mixture as the % volume of smaller particles is changed where the radius of the smaller discs is (1/2)r*

4.4 2-D Close packed Analysis

Let us now consider that the discs are not packed square but in a more compact triangular fashion as seen below.

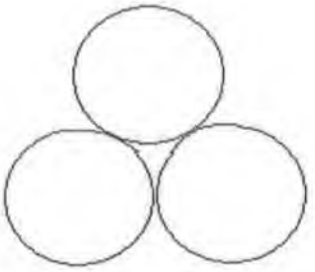

Fig 4.4.1: Compact particle packing

In the case of triangular packed discs in 2-D we take a unit cell in the form of a triangle between the centres of three adjacent discs as shown below. The area of this triangle is equal to $(1/2)R^2Sin60$ or $\sqrt{3}/4\,R^2$. Each disc which is added to the mixture will contribute four new unit cells so the total volume of unit cells is the volume of one unit cell multiplied by four times the number of discs.

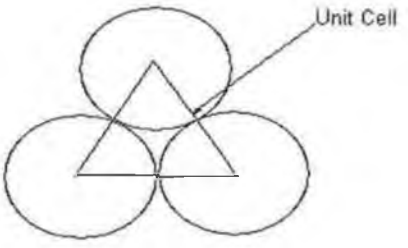

Fig 4.4.2: The unit cell as used in the 2-D triangular packed analysis

The sector of each disc within the unit cell is one sixth of the area of the disc therefore the actual area filled by the discs in each unit cell is $1/2\pi R^2$. Thus the specific area is

$$SA = \frac{2m\pi R^2}{\sqrt{3}mR^2} = \frac{2\pi}{\sqrt{3}} \tag{1}$$

One small disc is now added into the spaces between the large discs. The radius of the smaller discs is such that $r<r^*$ and $n<n^*$ (where n^* and r^* are the critical number and radius as defined before). Thus

$$SA = \frac{2m\pi R^2 + n\pi r^2}{m\sqrt{3}R^2} \tag{2}$$

The effect on SA as the number of small discs is increased up to n^* is now examined. So for $n<n^*$

$$\frac{\partial SA}{\partial n} = \frac{\pi r^2}{\sqrt{3}mR^2} > 0 \tag{3}$$

Thus the value of specific volume is seen to increase as the number of small discs is increased to n^*. Now what happens as the number of smaller discs is increased beyond n^* is considered. For $n>n^*$

$$SA = \frac{2m\pi R^2 + n^*\pi r^2 + 2(n-n^*)\pi r^2}{\sqrt{3}mR^2 + \sqrt{3}(n-n^*)r^2} \tag{4}$$

As the number of smaller discs is increased to a very large number (infinity):

$$SA_\infty = \lim_{n\to\infty} \frac{2\,{}^{m}\!/_{n}\,\pi R^2 + {}^{n^*}\!/_{n}\,\pi r^2 + 2\pi r^2 - 2\,{}^{n^*}\!/_{n}\,\pi r^2}{\sqrt{3}\,{}^{m}\!/_{n}R^2 + \sqrt{3}r^2 - \sqrt{3}\,{}^{n^*}\!/_{n}\,r^2}$$

$$= \frac{2\pi}{\sqrt{3}} \tag{5}$$

In other words the specific area of the mixture returns to its starting value as a large number of small discs are added. Differentiating the expression it is seen that

$$\frac{\partial SA}{\partial n} = \frac{(\sqrt{3}mR^2 + \sqrt{3}(n-n^*)r^2)2\pi r^2 - (2m\pi R^2 + n^*\pi r^2 + 2(n-n^*)\pi r^2)\sqrt{3}r^2}{(\sqrt{3}mR^2 + \sqrt{3}(n-n^*)r^2)^2}$$

$$= \frac{-\sqrt{3}n^*\pi r^4}{(\sqrt{3}mR^2 + \sqrt{3}(n-n^*)r^2)^2} < 0 \qquad (6)$$

i.e. the value of SA decreases with an increase in the number of small particles beyond n^* as expected.

Fig 4.4.3 is the graph of the change in SA with a change in the number of smaller discs. Below the change is plotted against % by volume for the case of r=r*.

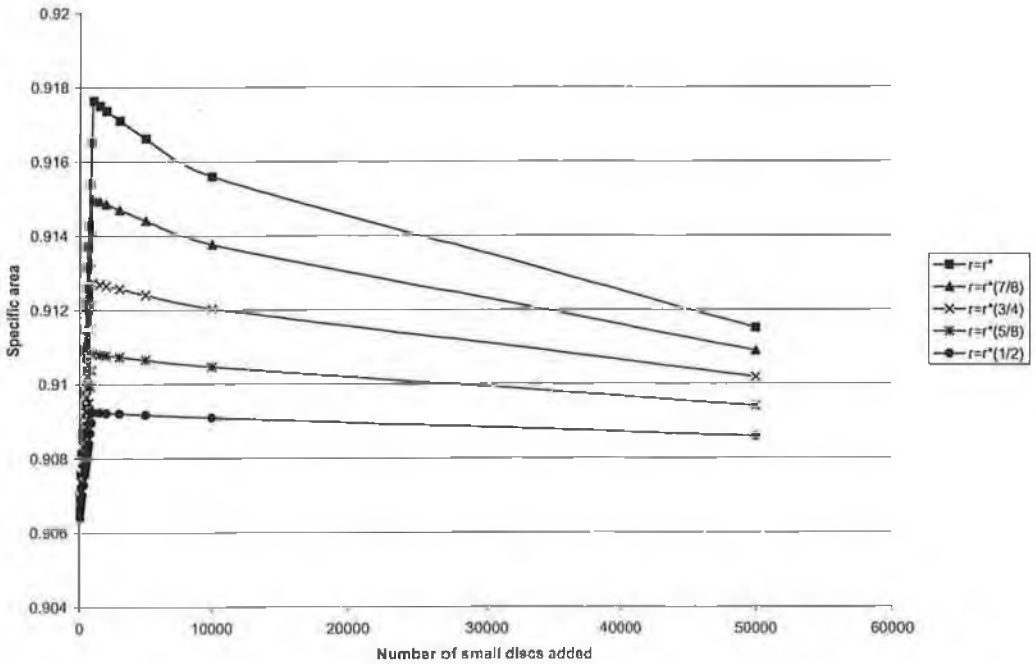

Fig 4.4.3: Specific Area of 2-D Close Packed Formation as Number of smaller particles of various sizes are added.

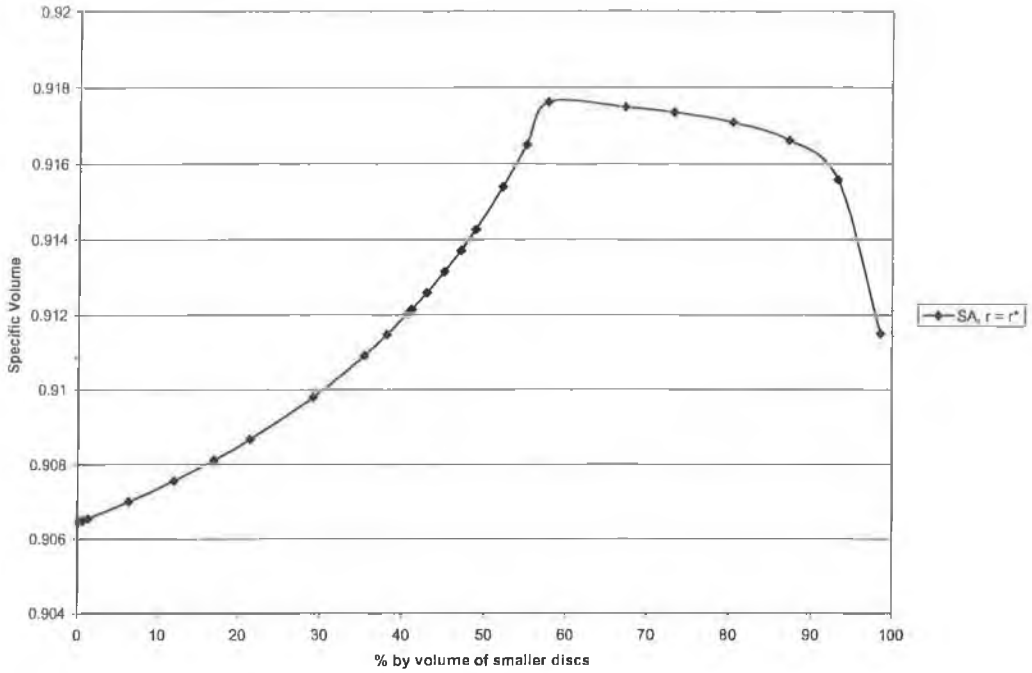

Fig 4.4.4: Change in SA of a mixture as the % volume of smaller particles is changed where the radius of the smaller discs is r^*

The above has shown how changes in the percentage of the mixture occupied by either the small or large discs effects the specific area of the mixture. The effect of keeping the numbers of each type of disc constant and varying the size of one relative to the other is now considered.

Start with a mixture of large discs with one small disc in each space between the large discs. The radius of the smaller discs is such that $r < r^*$ and $n < n^*$. Now SA is given by

$$SA = \frac{2m\pi R^2 + n\pi r^2}{\sqrt{3}mR^2} \tag{7}$$

$$\therefore \frac{\partial SA}{\partial r} = \frac{2n\pi r}{\sqrt{3}mR^2} > 0 \tag{8}$$

Therefore the value of specific volume increases as the radius of the small discs is increased up to the point where they are too big for the gaps between the large discs. At this stage $r > r^*$. This means that

$$SA = \frac{2m\pi R^2 + n\pi r^2}{\sqrt{3}mR^2 + \sqrt{3}nr^2} \tag{9}$$

$$\frac{\partial SA}{\partial r} = \frac{-2\sqrt{3}mn\pi R^2 r}{(\sqrt{3}mR^2 + \sqrt{3}nr^2)^2} < 0 \tag{10}$$

Thus it is seen that as long as $r>r^{*}$ specific area decreases as radius, r, increases. As it is increased further, at a certain point r will be such that the discs of radius r are large enough for the discs with radius R fit into the gaps between them. Call the radius where this occurs r^{**}. Increasing r beyond this point is the same as decreasing r when $r<r^{*}$. In other words as r in increased and $r>r^{**}$ specific volume will decrease. This is shown by eqn. (10) above.

4.5 3-D Close Packed Analysis

Now let us look at the most closely packed case in 3-D. This can be either Cubic Close Packing (CCP) or Hexagonal Close Packing (HCP). We will look at the case of cubic close packing in this case as the calculations are simpler. However the overall principle remains the same in either case. The packing can be illustrated as shown below. Each unit cell consists of eight octants of spheres and six hemispheres. The total volume of the spheres in the unit cell is therefore

$$V = (8.1/8 + 6.1/2)\frac{4\pi}{3}R^3 \quad (1)$$

$$= \frac{16}{3}\pi R^3 \quad (2)$$

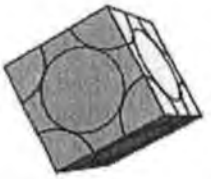

Fig 4.5.1: A section of spheres in CCP packing

Looking at the face of the unit cell it can be seen that the diagonal is equal to 4R. This implies that the length of a side is $2\sqrt{2}R$. Thus the volume of a unit cell is $(2\sqrt{3}R)^3$ or $16\sqrt{2}R^3$. Thus the specific volume of CCP can be seen to be

$$SV_{CCP} = \frac{(m/4)16/3\,\pi R^3}{(m/4)16\sqrt{2}R^3} = \frac{\pi}{3\sqrt{2}} \quad (3)$$

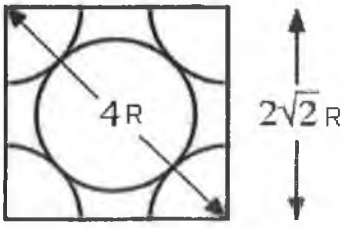

Fig 4.5.2: A cross section of spheres in CCP packing

Smaller spheres are now added into the gaps between the spheres in the CCP mix. The small spheres are small enough to fit into the spaces and there are less small spheres than spaces between the large spheres i.e. $n<n^*$ and $r<r^*$.

$$SV = \frac{\left(\frac{m}{4}\right)\left(\frac{16}{3}\right)\pi R^3 + n\,4/3\,\pi r^3}{\left(\frac{m}{4}\right)16\sqrt{2}R^3}$$

$$= \frac{m\pi R^3 + n\pi r^3}{3\sqrt{2}mR^3} \tag{4}$$

How does this alter as the number of small spheres is increased?

$$\frac{\partial SV}{\partial n} = \frac{\pi r^3}{3\sqrt{2}mR^3} > 0 \tag{5}$$

We will now look at the case where $n>n^*$. It can be shown for this case that the specific volume is given by

$$SV = \frac{m\pi R^3 + n^*\pi r^3 + (n-n^*)\pi r^3}{3\sqrt{2}mR^2 + 3\sqrt{2}(n-n^*)r^3} = \frac{m\pi R^3 + n\pi r^3}{3\sqrt{2}mR^3 + 3\sqrt{2}(n-n^*)r^3} \tag{6}$$

Therefore,

$$SV_\infty = \lim_{n\to\infty} \frac{\left(m/n\right)\pi R^3 + \pi r^3}{3\sqrt{2}\left(m/n\right) + 3\sqrt{2}r^3 - 3\sqrt{2}\left(n^*/n\right)r^3} \tag{7}$$

$$= \frac{\pi r^3}{3\sqrt{2}r^3} = \frac{\pi}{3\sqrt{2}} \tag{8}$$

Therefore as the number of small particles added becomes very large so the specific volume returns to its original value. We can see how it changes by differentiating. As follows

$$\frac{\partial SV}{\partial n} = \frac{(3\sqrt{2}mR^3 + 3\sqrt{2}(n-n^*)r^3)\pi r^3 - (m\pi R^3 + n\pi r^3)}{(3\sqrt{2}mR^3 + 3\sqrt{2}(n-n^*)r^3)^2} \tag{9}$$

$$= \frac{-3\sqrt{2}n^*\pi r^6}{(3\sqrt{2}mR^3 + 3\sqrt{2}(n-n^*)r^3)^2} < 0 \tag{10}$$

Fig 4.5.3 is a graph of how specific volume changes as the number of smaller spheres is changed. We more usually look at % by volume. This is graphed below for the two cases where r=r* and r=r*(7/8) in figures 4.5.4 and 4.5.5 respectively.

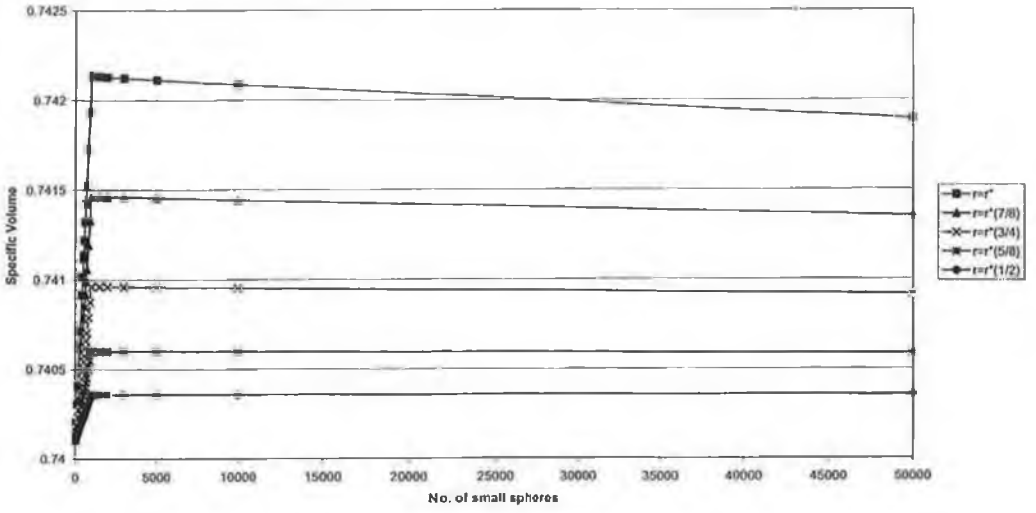

Fig 4.5.3: Specific Volume of 3-D Close Packed Formation as Number of smaller particles of various sizes are added.

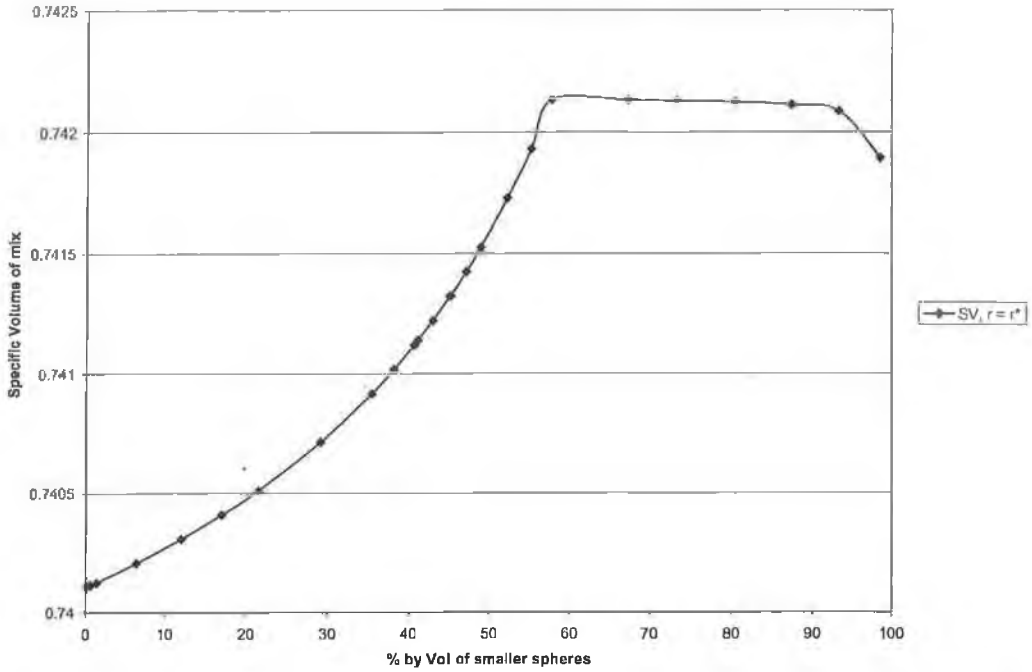

Fig 4.5.4: Change in SV of a mixture in 3-D Close packing as the % volume of smaller particles is changed where the radius of the smaller discs is r^*

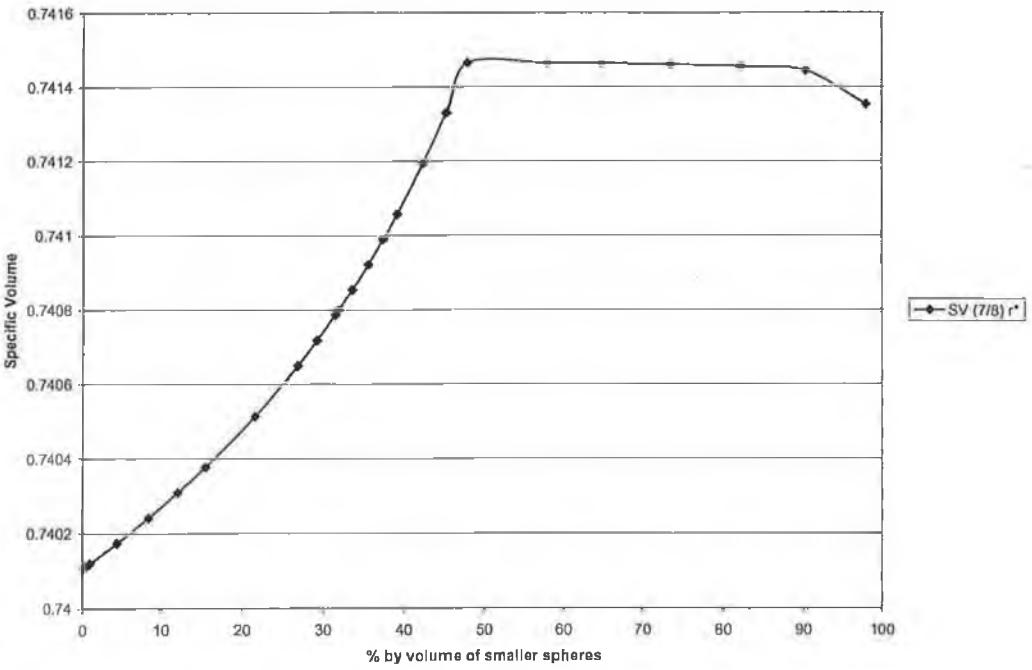

Fig 4.4.5: Change in SV of a mixture in 3-D Close packing as the % volume of smaller particles is changed where the radius of the smaller discs is $(7/8)r^*$

The case where we hold the numbers of each sphere type constant and vary the radius of one of them must now be considered in order to see what effect changing the relative sizes of the spheres has on specific volume. Consider first the case when $n<n^*$ and $r < r^*$. Then

$$SV = \frac{m\pi R^3 + n\pi r^3}{m3\sqrt{2}R^3} \tag{11}$$

$$\therefore \frac{\partial SV}{\partial r} = \frac{n\pi r^2}{m\sqrt{2}R^3} > 0 \tag{12}$$

For the case where r is increased beyond r^* such that $r^* < r < r^{**}$ (where, as before r^{**} is the radius that the "smaller" spheres must be increased to so that the "larger" spheres can fit in the spaces between them without distorting their packing) we can see that

$$SV = \frac{m\pi R^3 + n\pi r^3}{3\sqrt{2}nR^3 + 3\sqrt{2}nr^3} = \frac{\pi}{3\sqrt{2}} = \text{A Constant} \tag{13}$$

The examples shown above are simplifications of the real situation. However they do indicate a fact that has been observed by many authors i.e. that the size ratio has an effect on the maximum packing fraction obtainable for a mixture and that a certain proportion of large and small particles will lead to the maximum packing fraction. Changing proportions of each component in the mixture can lead to dramatic changes in the packing fraction obtainable and in certain cases a small change in the proportion of a single component of a mixture can lead to a large increase or decrease in packing fraction.

The models also seem to indicate the percentage volume of smaller spheres is a key element in determining the packing fraction obtained. As the percentage volume of the smaller component of the mixture is increased so the packing fraction increases up to a certain point. At that point a certain plateau is reached where further increases in the percentage volume lead to only very small changes in the overall packing fraction of the mixture. This is important because if real mixtures of metal powders behave in the

same way then there will be a wide range of mixture compositions which will tend to give high packing fractions. This in turn should lead to denser green compacts and denser, stronger sintered parts.

It is interesting to note that the 3-D models both give lower specific areas and volumes than their 2-D equivalents as can be seen in figs 4.5.3, 4.4.3 4.3.1 and 4.2.2. This is unsurprising as the extra space created around the sphere is greater than the difference in volume between a sphere and a circle. The values of specific volume which are given by the 3-D examples are closer to the values encountered in experiment than the higher values which are given by the 2-D models. Again this to be expected as the 3-D models are more realistic.

It should be noted that in the models described above a large proportion, by volume, of the mixture will be made up of the smaller particles before any significant change in specific volume or area is seen. This also seem to agree with the phenomenon described by O'Donnell [1] and by German [2] who both note that the strengths of PM composite materials which are manufactured using large powders to form the matrix material tend to be weaker than expected and certainly weaker than comparable materials where small powders were used to for the matrix of the composite. This is discussed in greater detail in chapter 6. Here the weakness of composite materials manufactured where large Al powder sizes are used is shown.

Chapter 5: Results

Results are presented as mixture packing fractions and mechanical properties of sintered samples (tensile and hardness). Discussion of these is reserved until chapter 6 however the data itself is commented upon.

5.1 Comparison between Measured Packing Fraction and the Yu and Standish model

Yu and Standish [3] present a model that predicts the packing fraction of a mixture of particles. One of the prescribed pieces of information for this model is the size ratio between the large and small particles. The individual packing fraction of the unmixed powders must also be found before the model can be used. They claim that their model predicts the packing fraction to within 8% of the measured value. To test that claim, packing fractions of various mixtures were measured and compared to the packing fraction as predicted by the Yu and Standish model [3] calculated using equations 10, 11, 12 and 13 as presented in chapter 2. The model was tested for both binary and ternary mixtures. It is important to note that in this form the Yu and Standish model deals with powders of a uniform size. Obviously the powders in this case are not of a single size. The size distribution the aluminium metal powders can be seen in appendices B-D. Nonetheless, in this section, for the sake of simplicity of calculation, the powders are treated as if they were of a single size. The implications of this assumption will be looked at later in chapter 6. All binary mixtures contained aluminium and silicon carbide powders of various sizes. All Ternary mixtures contained Aluminium, Silicon Carbide and Zinc Sterate powders of various sizes. The measurement of the powder's individual and mixed packing fractions were carried out in accordance with MPIF Standard 04 [73] as discussed in chapter 3. The individual packing fractions obtained are shown below in table 5.1. The calculation of the results from the Yu and Standish model was done via a spreadsheet.

Table 5.1: Individual powder's measured packing fractions.

Al Results					
Powder Size	10μm	25μm	33μm	38μm	41μm
Unmixed Powder Packing Fraction	0.407	0.439	0.432	0.407	0.48
SiCp Results					
Powder Size	13μm		23μm		
Unmixed Powder Packing Fraction	0.27		0.357		

The results can be seen below:

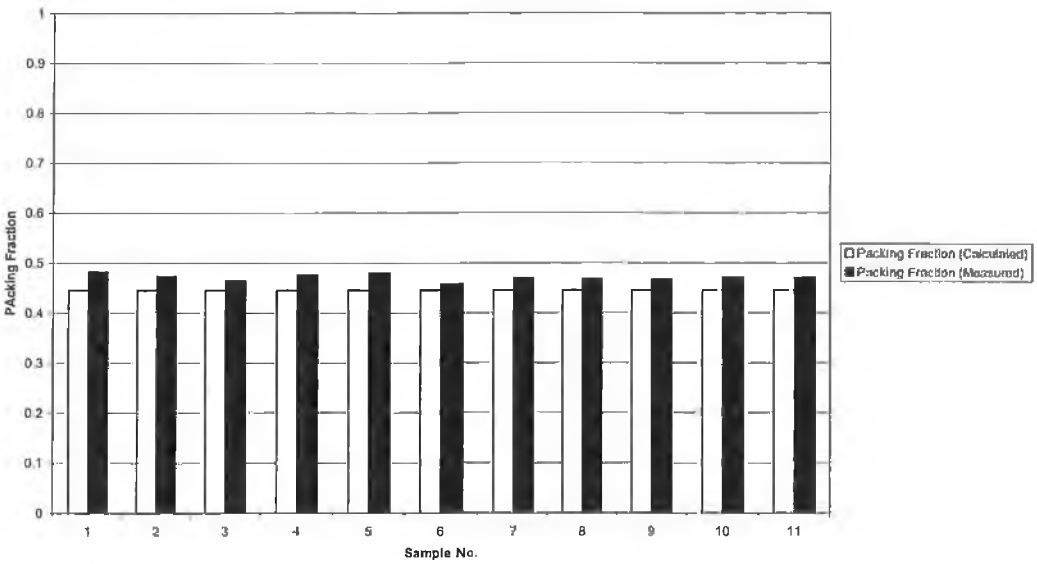

Fig 5.1.1: The Packing Fractions Measured, and those Calculated Using the Yu and Standish Model for a Binary Powder Mixture of 10μm Al and 20% by vol. 23 μm SiC_p, r=0.43

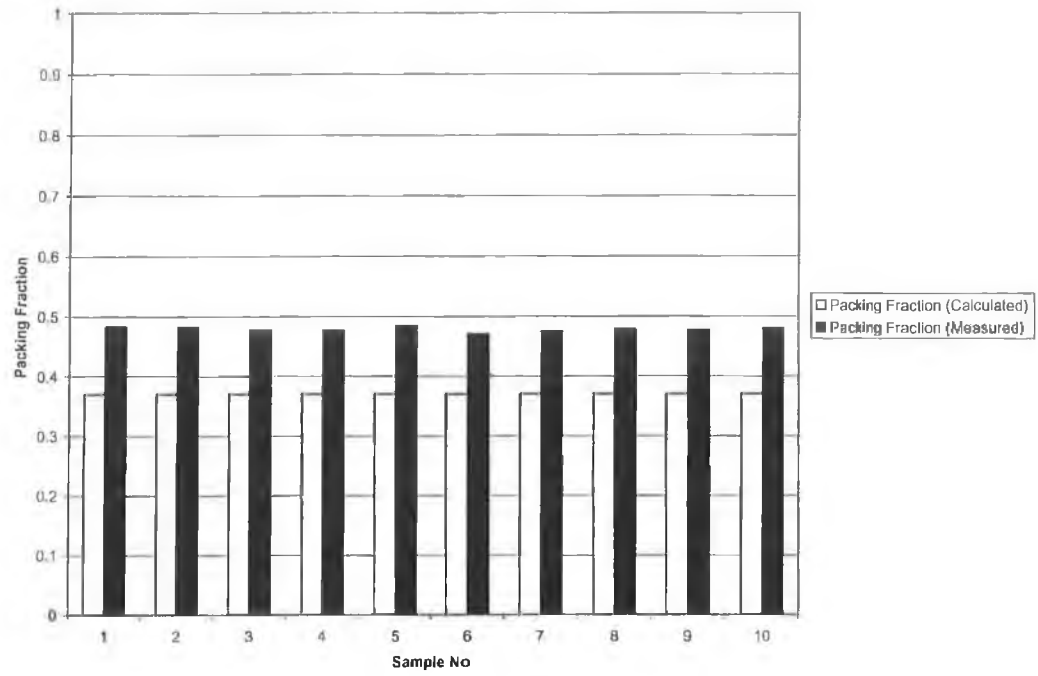

Fig 5.1.2: The Packing Fractions as Measured, and those Calculated Using the Yu and Standish Model for a Binary Powder Mixture of 33μm Al and 20% by vol. 23 μm SiC_p r=1.65

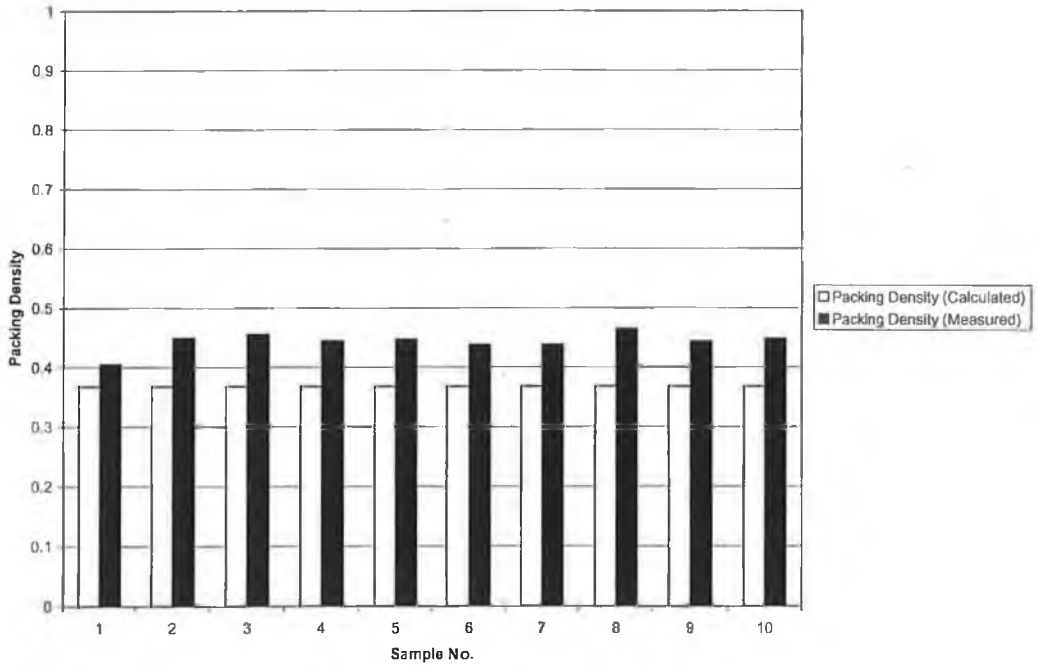

Fig 5.1.3: The Packing Fractions Measured, and those Calculated Using the Yu and Standish Model for a Binary Powder Mixture of 25μm Al and 20% by vol. 23 μm SiC_p, r=1.086

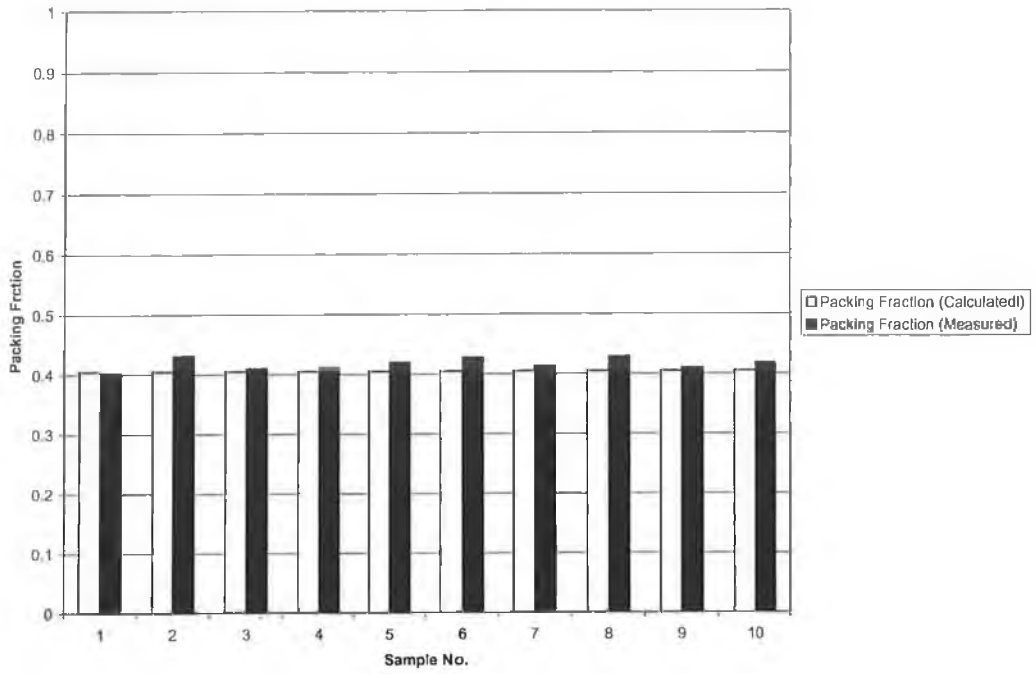

Fig 5.1.4: The Packing Fractions as Measured and those Calculated Using the Yu and Standish Model for a Ternary Powder Mixture of 38μm Al and 10% by vol. 23 μm SiC_p and 1% by vol Zinc Sterate

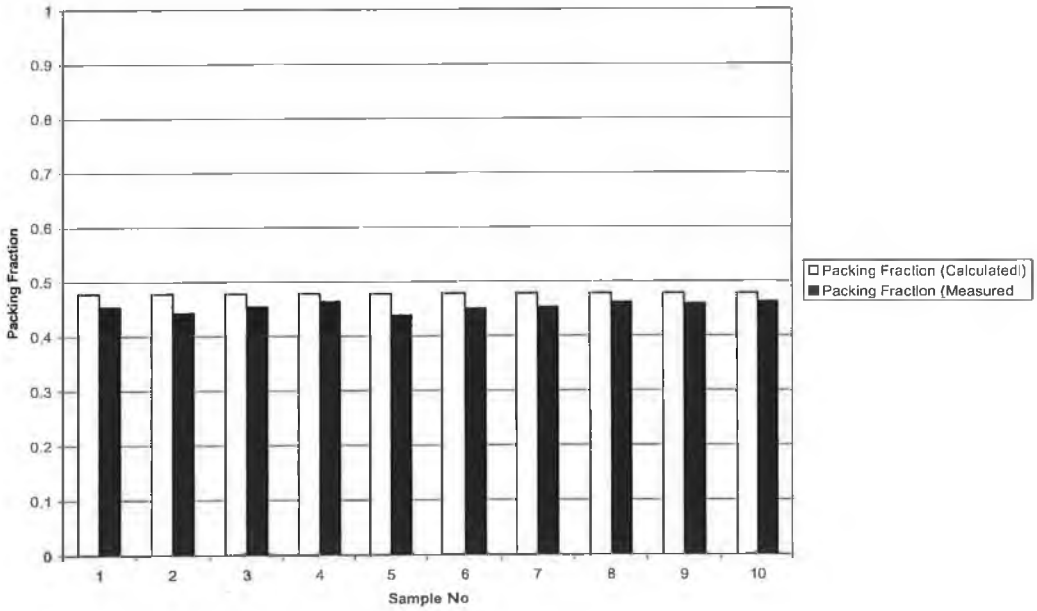

Fig 5.1.5: The Packing Fractions as Measured, and those Calculated Using the Yu and Standish Model for a Ternary Powder Mixture of 41μm Al and 10% by vol. 23 μm SiC_p and 1% by vol Zinc Sterate

The above data confirms the accuracy for the model reported by Yu and Standish [3]. Indeed, while they present data that shows a relative error of less than 8% on the measurement of packing fraction for spherical single sized glass beads, here the data suggests that the model is equally successful in dealing with powders that are not spherical. In Figs 5.1.1, 5.1.3, 5.1.4 and 5.1.5 the average relative error is less than 8% while in Fig 5.1.2 the relative error averages less than 10%. This in spite of the fact that we know that the powders have a size distribution in reality, that the sizes we have entered into the model represent only an average size for the powders and that they are of an irregular shape. This comparison is discussed in greater detail in Chapter 6.

It should be noted that there is a degree of scatter in the results shown above and that some of the powder mixtures packing fractions were seen to have more scattered measurements than others. This is largely as a result of the manner in which the various powders flowed through the funnel and into the beaker in the measurement of the packing fraction. The mixtures containing larger powders tended to flow less freely than those containing smaller sizes. Also the mixtures containing lubricant flowed more freely than those without. All of this lead to differing levels of scatter. This is discussed in more detail in chapter 6.

Below is a graph showing packing fraction as measured compared to as calculated by Yu and Standish and by the model as shown in chapter 4 of this work. The version of model in chapter 4 which predicts the powder packing in the mode of 3-D close packed was chosen for this comparison as it is felt that this will be the most applicable to a real packing situation. To this end equation 4 in section 4.4 was used. It can be seen that the results of the model in chapter 4 are much too high compared to the measured packing fractions of the powders. This model cannot take into account the random shape, size distribution and random way in which these real particles pack. By contrast the model of Yu and Standish is seen to be quite accurate in spite of these problems.

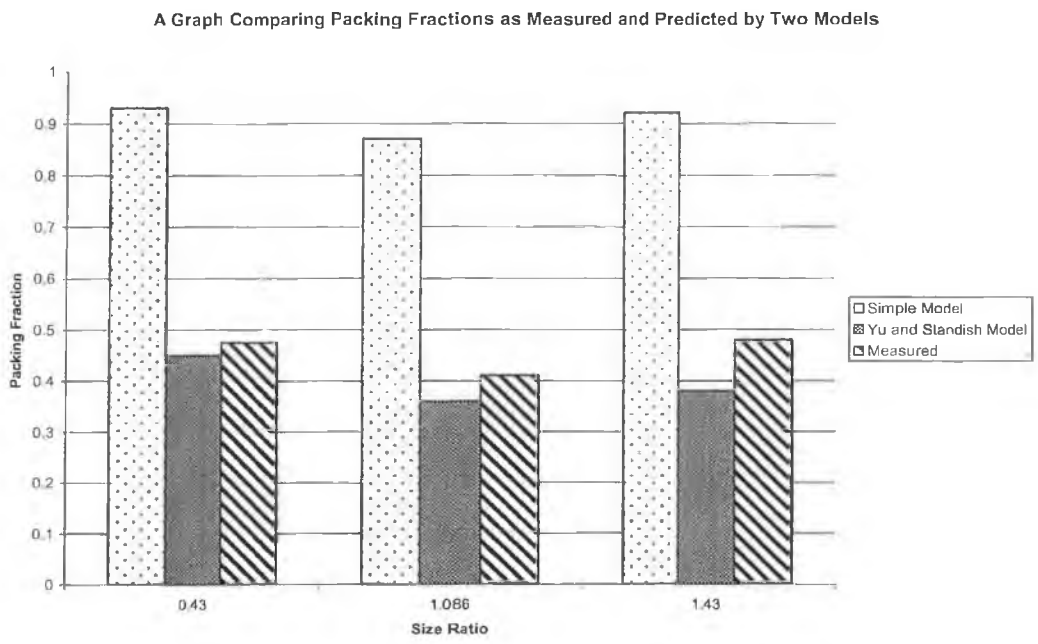

Fig 5.1.6: A graph comparing the packing fractions as predicted by the Yu and Standish model and the simplified model presented in chapter 4 to measured packing fractions of real Al SiCp powder mixtures.

Three graphs are presented below representing the packing fractions as predicted by Yu and Standish [3] for the size ratios of powder mixture from which the tensile samples in section 5.2 and hardness samples in section 5.3 were manufactured. It is seen below that the packing fractions as predicted by Yu and Standish move around as the packing fraction of the powder mixtures change. Packing fraction decreases rapidly as size ratio approached one (where size ratio r = Al powder size / SiC_p powder size) and the increases as the packing fraction increases further. The only change in this trend below is for the largest packing fraction of all. Here the packing fraction decreases. This is mainly down to the fact that this powder mixture was made using a large (41μm) Al powder which was seen to flow in clumps into the beaker during the packing fraction measurement as described in chapter 3. This caused the powder to trap air in it and thus to decrease its packing fraction. The effect of this is discussed further in chapter 6.

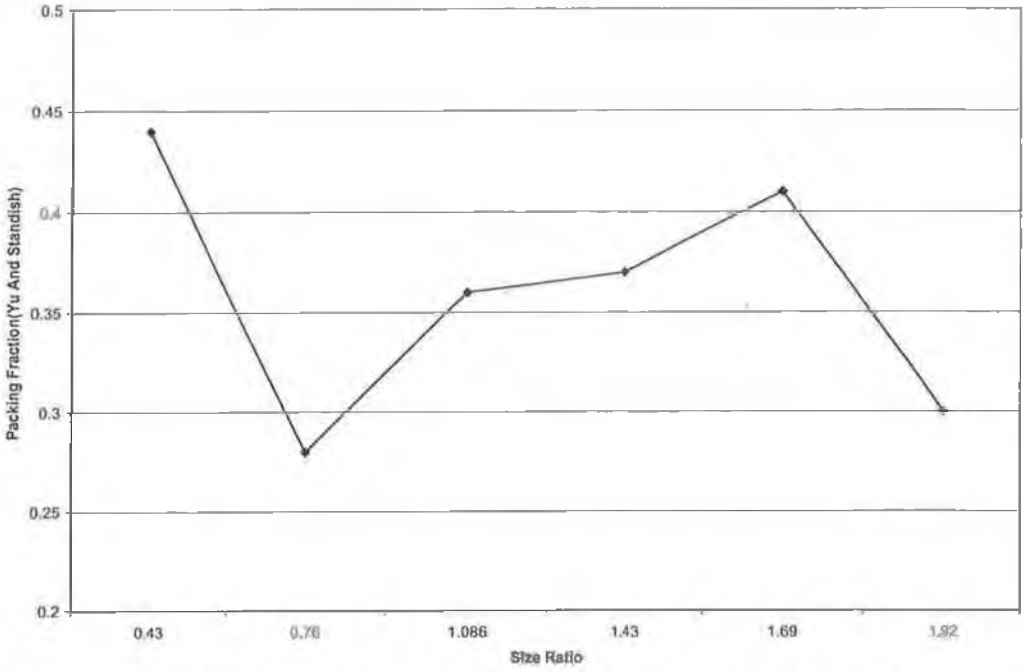

Fig 5.1.6: Packing Fraction as predicted by Yu and Standish Model for various size ratios.

5.2 Tensile Response

In order to examine whether or not a correlation exists between the packing fraction of the powders pre-compaction, and the mechanical properties of the material post sintering, a number of samples were prepared as specified in chapter 3. 40 samples were made from a variety of sizes of Al powder mixed with SiC_p powder in order to give a variety of size ratios. The materials were then tested for both UTS and Rockwell B hardness. The tensile response of the material is discussed in this section.

Note that all size ratios (r) quoted in this section are in the form of (size of Al Powder/size of SiC_p powder) for the sake of clarity. This differs somewhat from the Yu and Standish [3] model where size ratios are always given in terms of (small powder size/large powder size). Also note that not all samples produced are shown below due to problems with sintering. The results presented below are representative of the whole sample however.

5.2.1 Tensile Results

Once they had been manufactured, the samples were then ready for testing in accordance with MPIF standard 10. The samples were tested in an Instron 4204 universal testing machine. The results were obtained in terms of load and displacement and converted into stress and engineering strain by hand.

The graph below shows the tests for samples which were manufactured from powder mixtures comprised of 10μm Al, 25μm Al and 39μm Al respectively mixed with 20% by vol. 23μm SiC_p. Thus the mixtures have size ratios, r, (Al/SiC_p) of 0.43, 1.086 and 1.69 respectively. Samples which are presented on the same graph were processed together in the furnace and as such received exactly the same heat and gas supply. Thus differences in strengths etc cannot be put down to differences in processing regime.

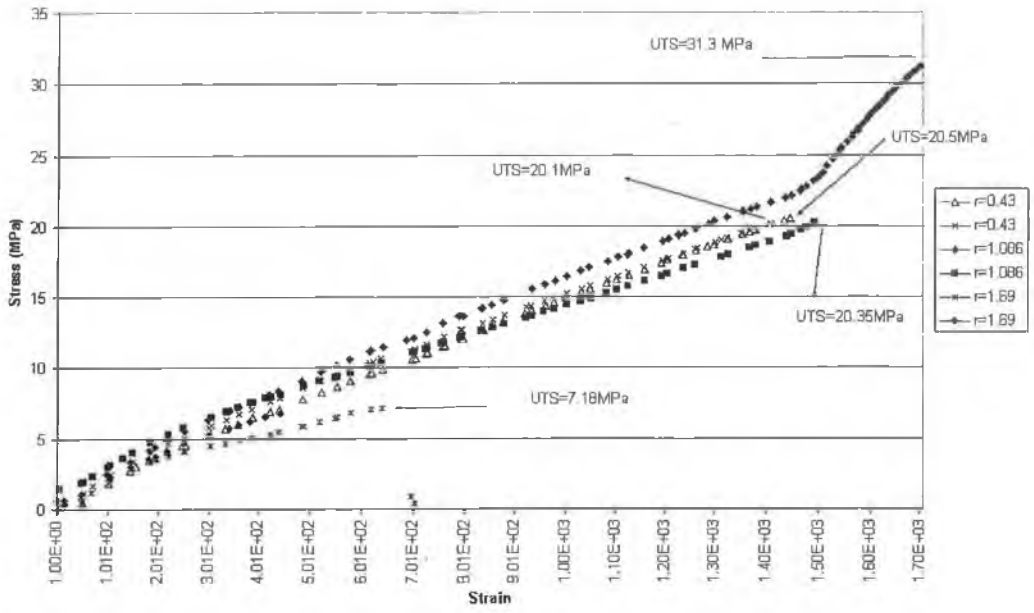

Fig 5.2.1: Stress vs. Strain graphs for samples of different size ratio, r.

As expected there is quite a difference in the strengths of the materials shown in Fig 5.2.1 depending on the sizes of the powders used. How do the changes in UTS as size ratio is changes tally with the changes in the packing fraction as size ratio is changed? Does an increase in packing fraction correspond with an increase in UTS? Or does the compacting and sintering the powder totally cancel out the differences in density seen pre-compaction as a result of differences in size ratio?

The graph presented below show the average UTS of the samples by size ratio. A comparison between fig 5.2.2 and 5.1.6, which presents the values of packing fraction as predicted by the model of Yu and Standish [3] and be made. Thus it is possible to compare how packing fraction changes with a certain change in size ratio and how UTS changes with the same change in size ratio.

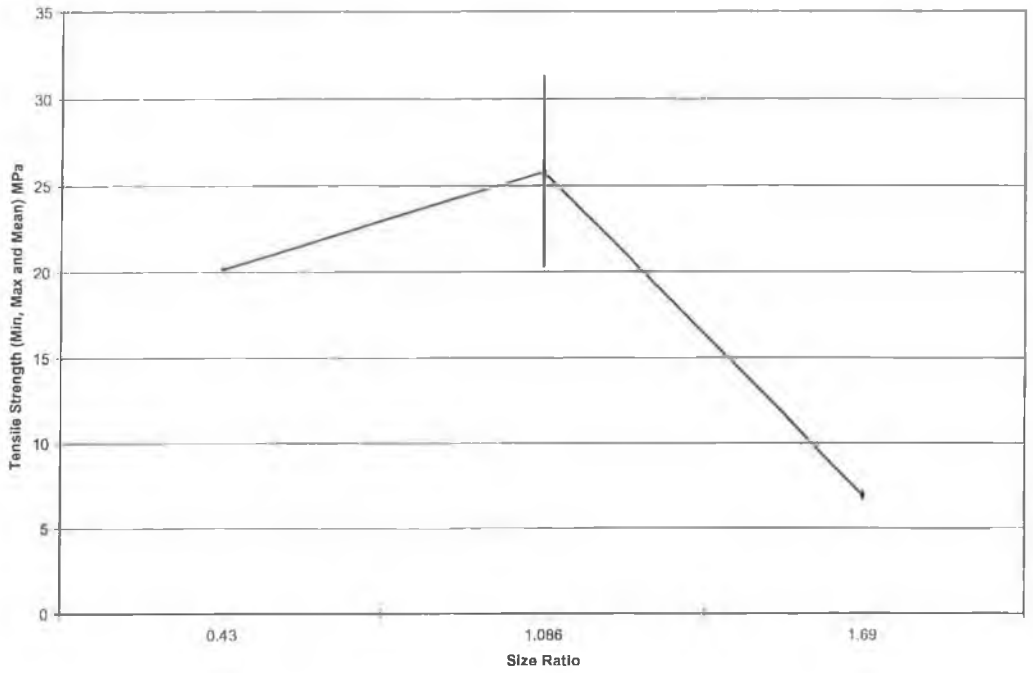

Fig 5.2.2: Average UTS of Samples of manufactured from powder mixtures of various size ratios arranged by size ratio. Minimum, maximum and mean values of tensile strength indicated.

No correlation can be drawn between the packing fraction and the UTS from the above data. For example the average value of UTS for the samples made from the powder with a size ratio of 1.086 is higher than those made from a powder with a size ratio of 0.43. This is exactly the opposite of what is predicted if the UTS changes in a similar way to the packing fraction of the powder mixtures pre-compaction shown in fig 5.1.6. However problems with the processing of the material (discussed in chapter 6) may have a part to play in this.

The above powders were sintered at 617°C for 70 minutes in accordance with the procedure provided by O'Donnell [1]. However the samples below were sintered at 640°C for 80 minutes to see what effect this had on the comparative UTSs.

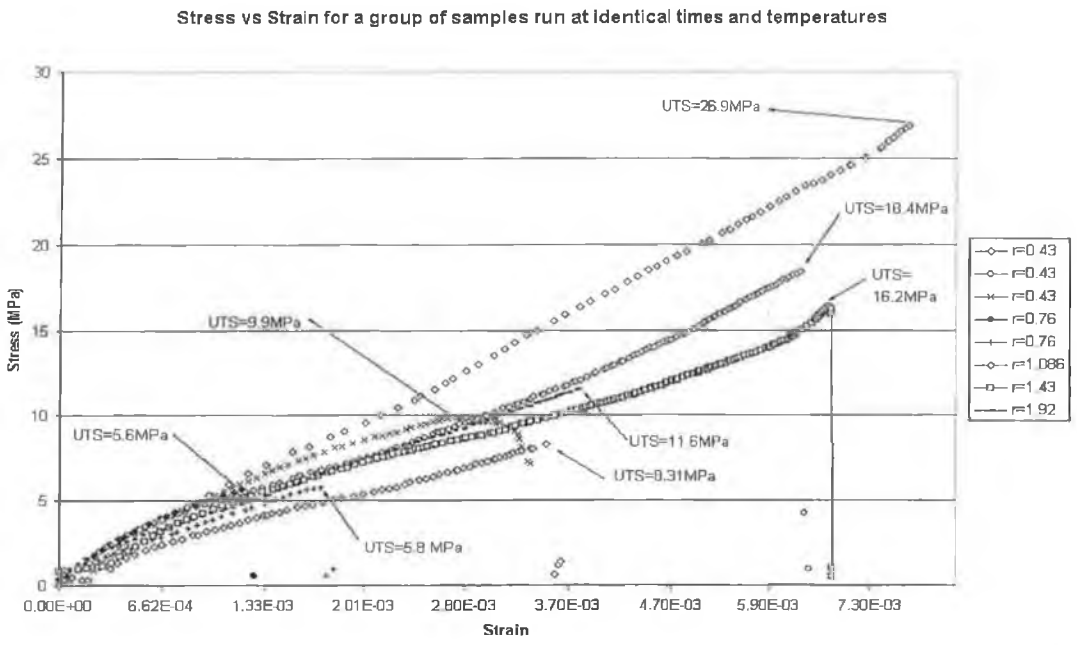

Fig 5.2.3: Stress vs. Strain graphs for MMCs of different size ratios, r.

The average UTS of the above samples per size ratio is presented below. This may be compared to the packing fractions for the same size ratios as presented in fig 5.1.6.

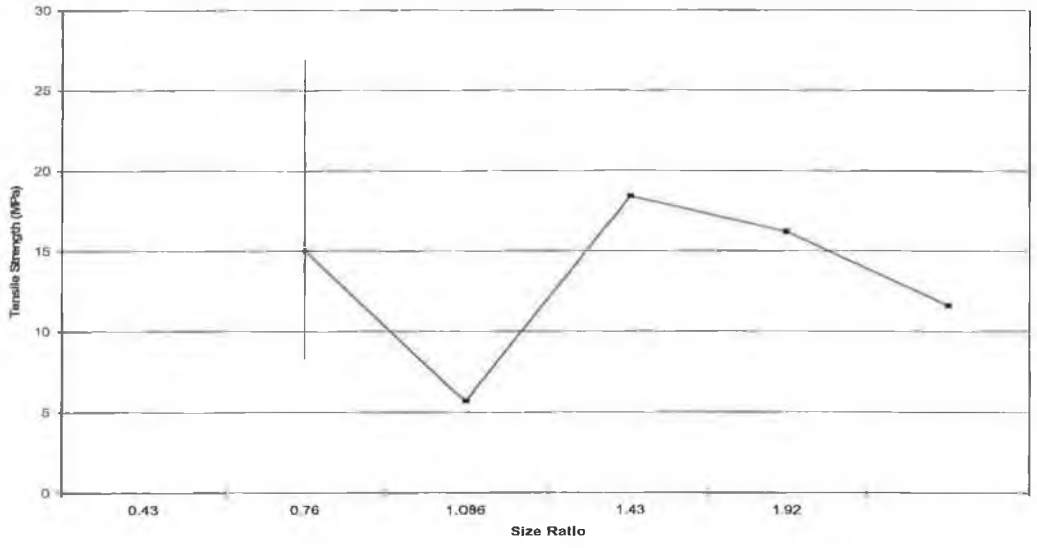

Fig 5.2.4: Average UTS of Samples of manufactured from powder mixtures of various size ratios arranged by size ratio. Minimum, maximum and mean values indicated.

If the values for UTS obtained for each of the size ratios is averaged then a certain similarity between the above plot and the changes in packing fraction as shown in fig 5.1.7 can be observed. This would seem to suggest that there is some link between the packing fraction pre-compaction and the strength of the material post-sintering. It can be seen that an increase or decrease in packing fraction in fig 5.1.7 from one powder mixture to another tends to be matched by an increase or decrease in the tensile strength of the material manufactured from that mixture, although the percentage of change is not the same. The sample size is small here however, and problems with processing of material has effected the results somewhat, however. These problems, as well as results and how they compare to the packing fraction data shown in fig 5.1.6 are discussed in Chapter 6.

Some of the tensile samples were prepared for viewing under an optical microscope so that their structure could be viewed in detail. These images are presented below. Note that some of the materials pictured below are not of the same composition as the material presented in the data above but they were manufactured using the same mixing and sintering process. They are included as they illustrate the structure of the material.

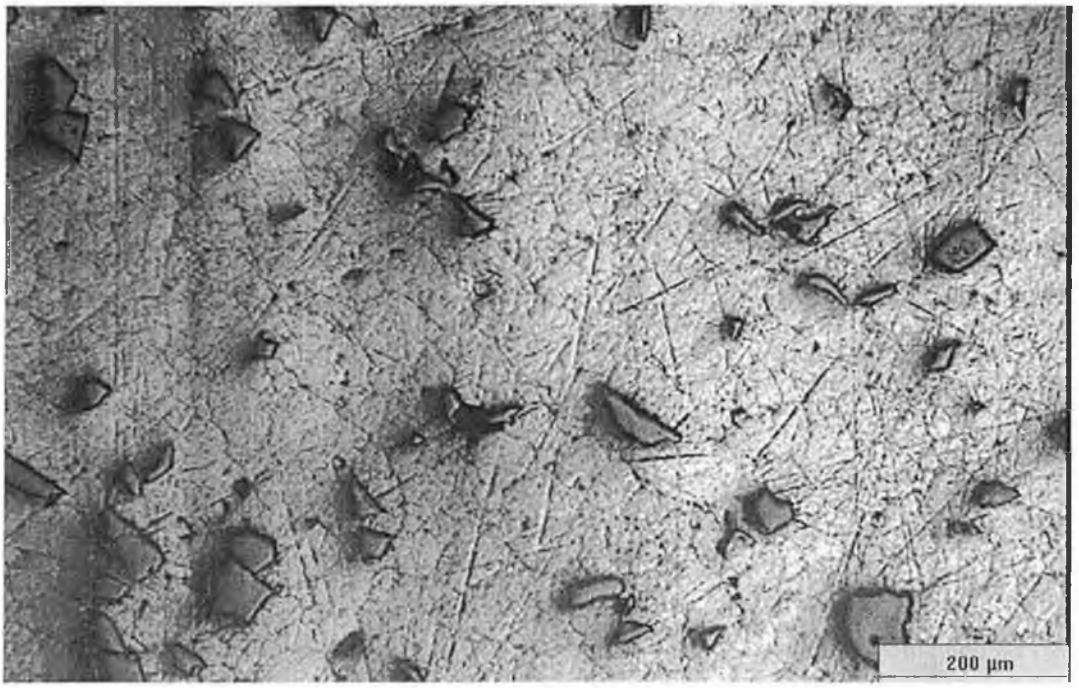

Fig 5.2.5: A sample of 10µm Al + 10% by 23µm vol. SiC_p

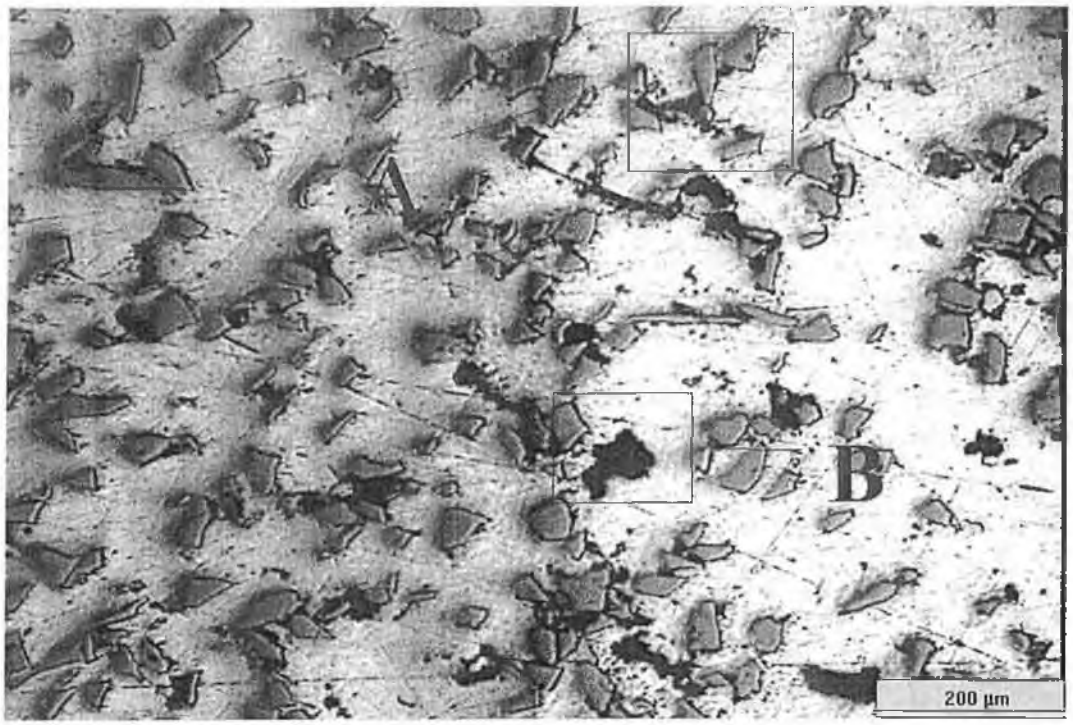

Fig 5.2.6: A sample of 10µm Al + 20% by vol. 23µm SiC_p. Note (A) the areas of porosity as well as (B) areas where SiC_p particles have been torn out during the tensile testing process.

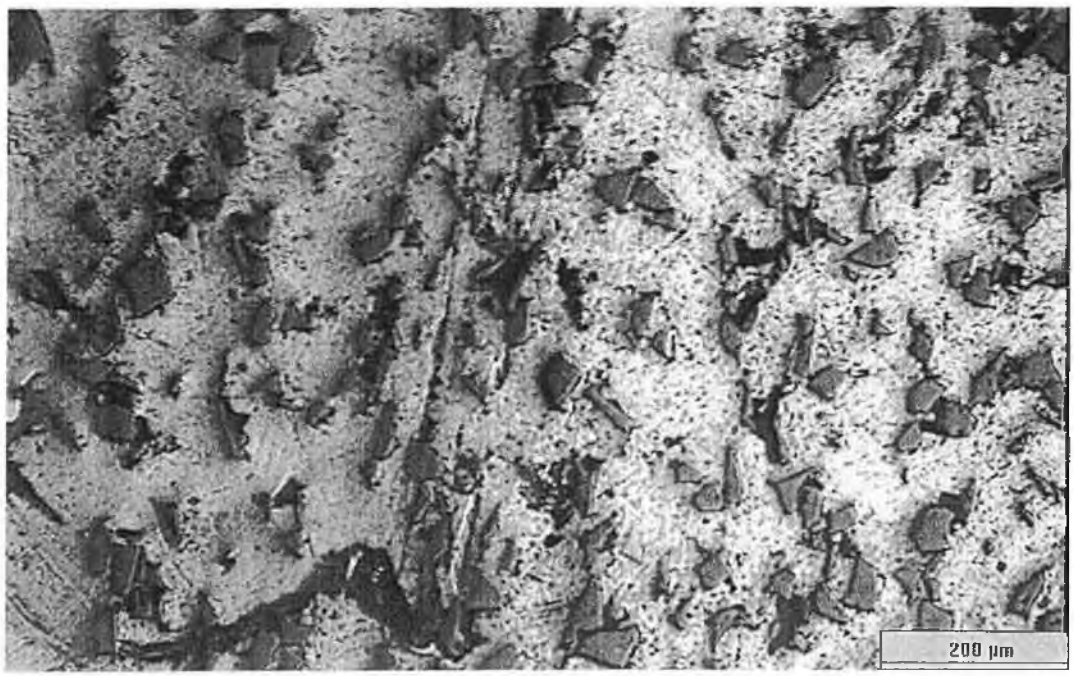

Fig 5.2.7: A sample of 18µm Al + 20% by vol. 23µm SiC_p. Note the increase in porosity from Fig 5.2.6.

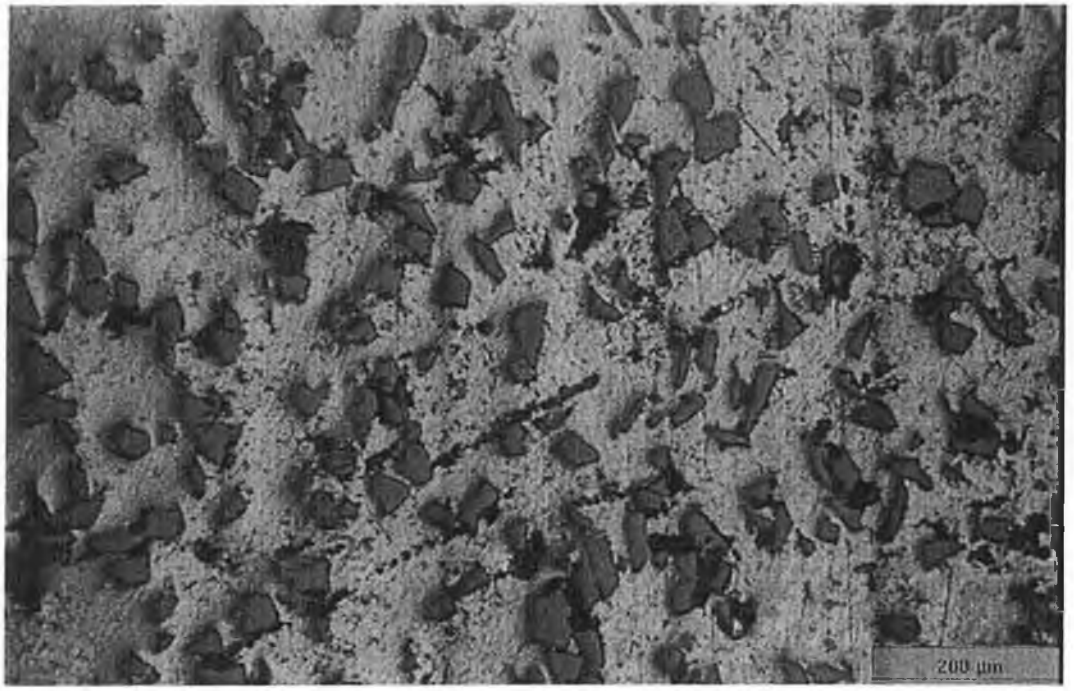

Fig 5.2.8: A sample of 25µm Al + 20% by vol 23µm SiC_p. Again note that there is a high level of porosity throughout the material.

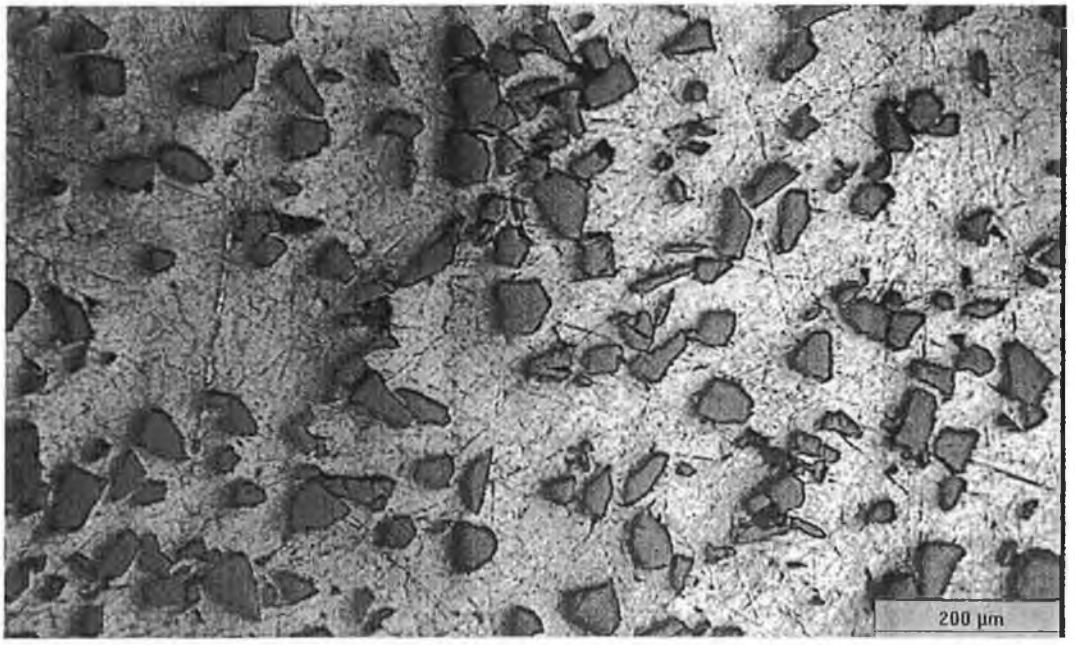

Fig 5.2.9: A Sample of 39µm Al + 20% by vol. 23µm SiC_p. Note the areas where the silicon carbide particles are crowded together. This will tend to make the material weaker as no active sintering of the aluminium can take place in these areas.

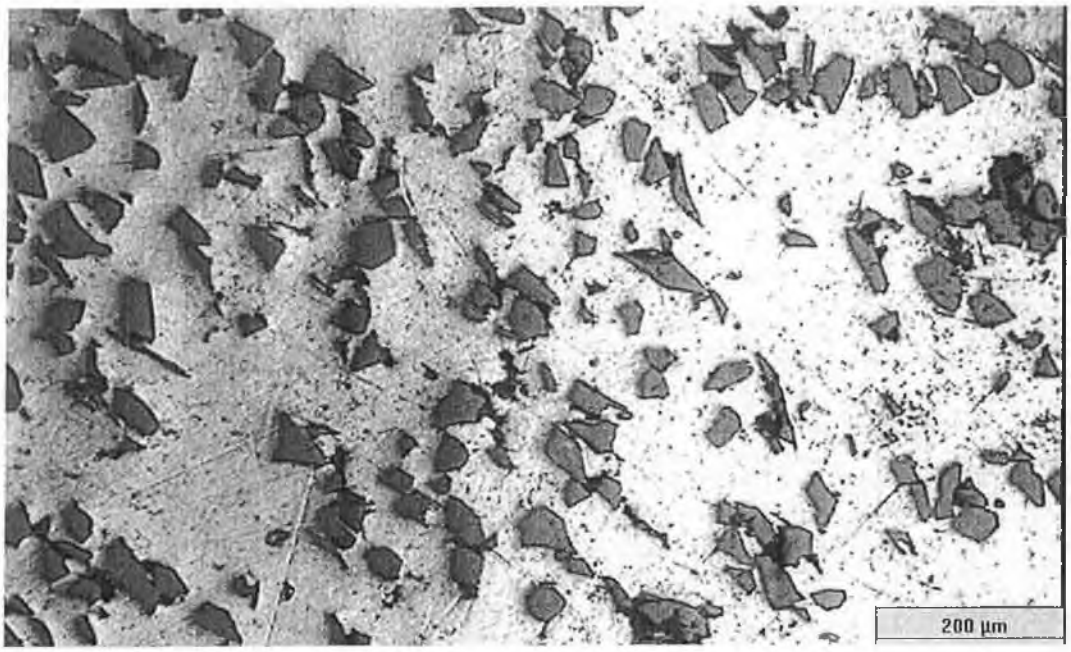

Fig 5.2.10: A sample of 25µm Al + 20% by vol 23µm SiC_p. This sample was sintered at higher temperature and for a longer time than the comparable sample in fig 5.2.8 above.

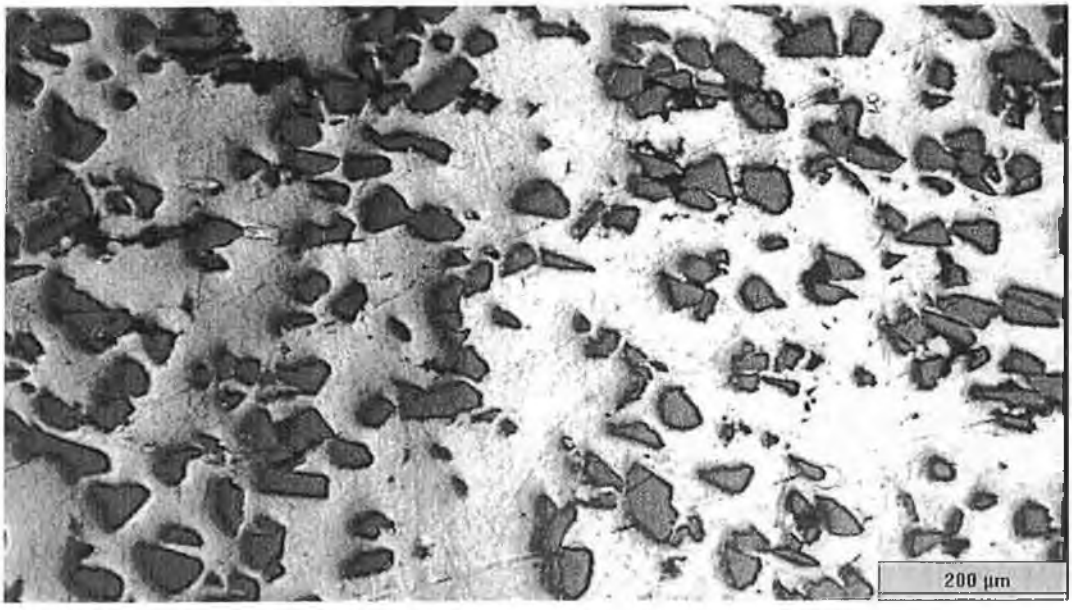

Fig 5.2.11: A sample of 39µm Al + 20% by vol. SiC_p. This sample was also sintered at higher temperatures and for longer time than the comparable sample in fig 5.2.9. Note however that the decrease in porosity is not as noticeable as it was for the case where the powder particle sizes were close together.

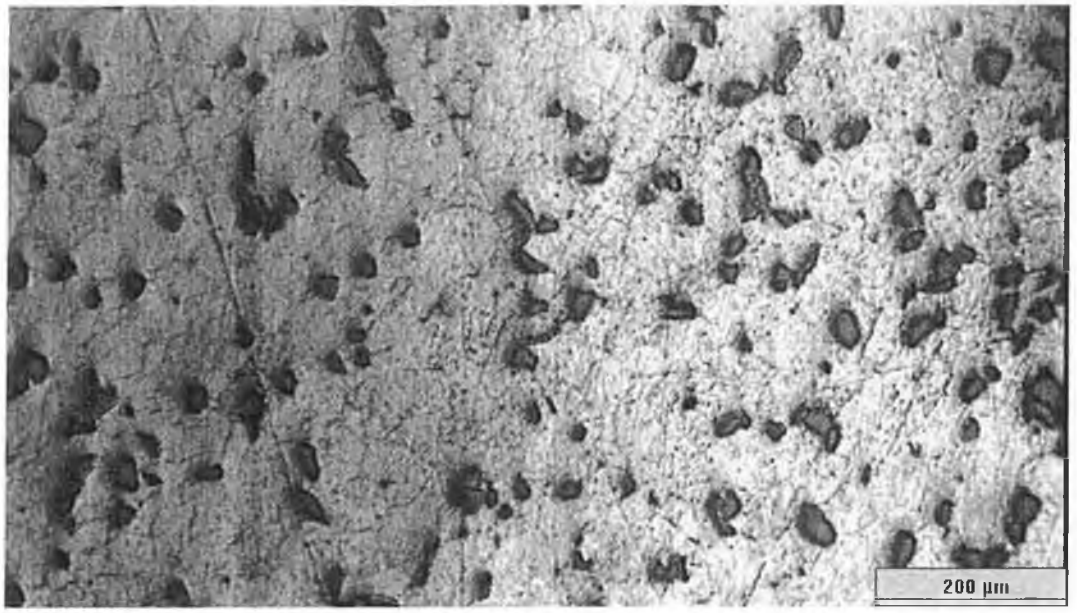

Fig 5.2.12: A sample of 10µm Al + 10% by vol. 13µm SiC_p. Note that incomplete sintering has occurred and that the shape of the Al powder particles is still visible.

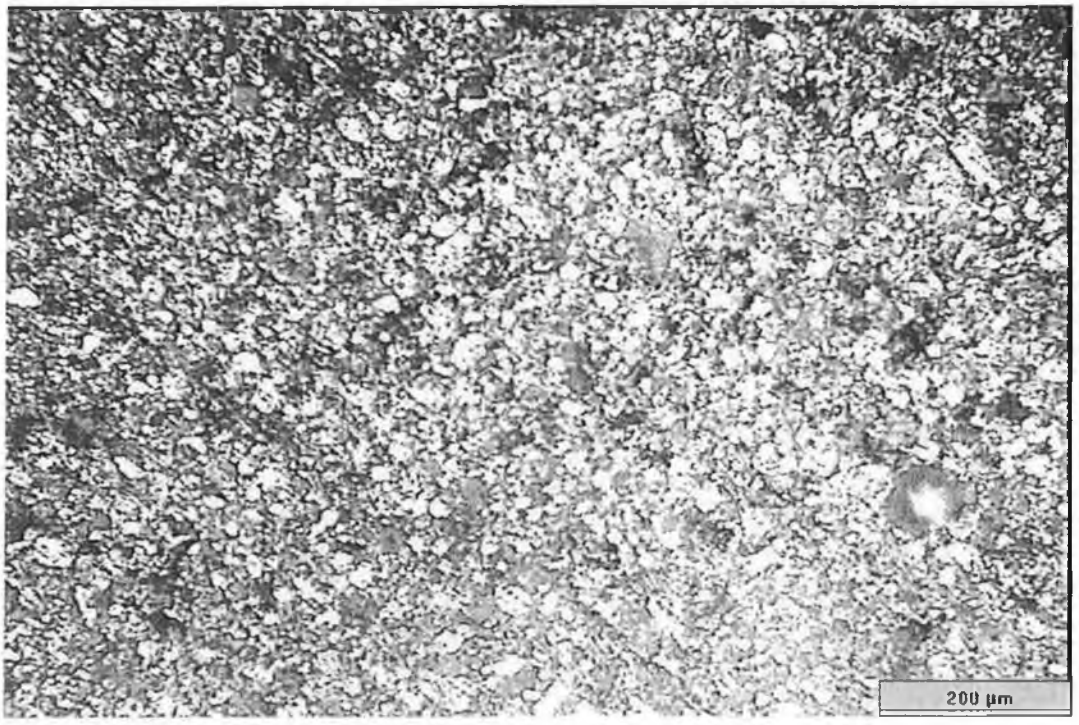

Fig 5.2.13: A green sample consisting of 39µm Al + 10% by vol. 13µm SiC_p.

5.3 Comparison between packing fraction from Yu and Standish and published data

O'Donnell [1, 74] was successful in making a large number of samples by the methods described above. In order to attempt to test the relationship between packing fractions as predicted by the Yu and Standish [3] and the mechanical strength of finished material it was decided to make a comparison between the Yu and Standish model and the data as presented by O'Donnell. Thus below are presented graphs which shows variation in UTS with powder mixture size ratio from O'Donnell [1] and variation in packing fraction with size ratio as generated using the Yu and Standish model. How the two values vary as size ratio is varied can thus be compared.

The material produced by O'Donnell was produced using the same methods as described in chapter 3. The samples were prepared from mixtures of 16μm, 11μm 7μm aluminium powders and 6μm, 25μm and 28.5μm silicon carbide powder. All mixtures used to generate the data used below contained either 10% or 20% by volume silicon carbide and so the results are presented as such, figure 5.3.1 showing the material with 10% by volume and fig 5.3.3 showing the material with 20% by volume.

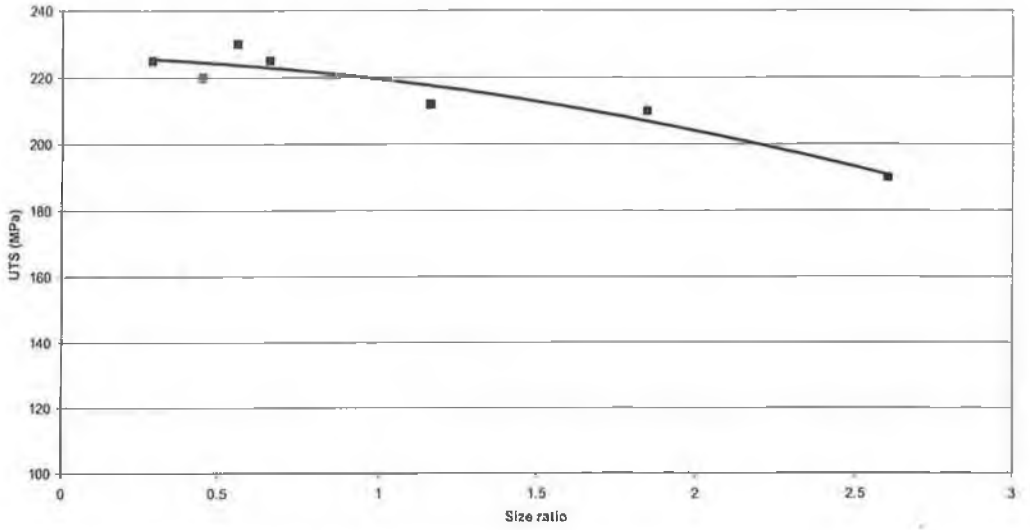

Fig 5.3.1: Variation in Tensile strengths of Al SiC_p MMCs with 10% by volume SiC_p with changing size ratio [1]

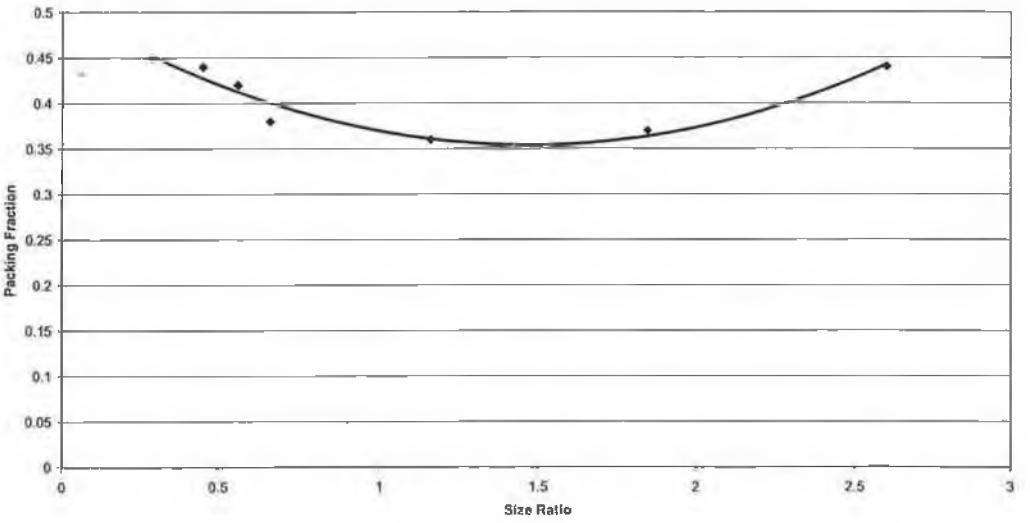

Fig 5.3.2: Variation in packing fraction as calculated by the Yu and Standish Model of Al SiC_p powders with 10% by volume SiC_p with changing size ratio

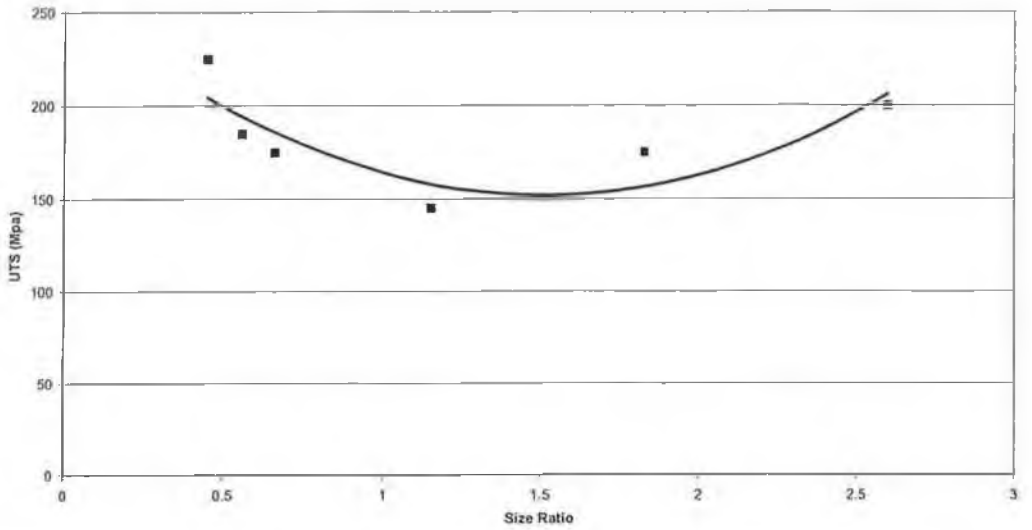

Fig 5.3.3: Variation in Tensile strengths of Al SiC_p MMCs with 20% by volume SiC_p with changing size ratio

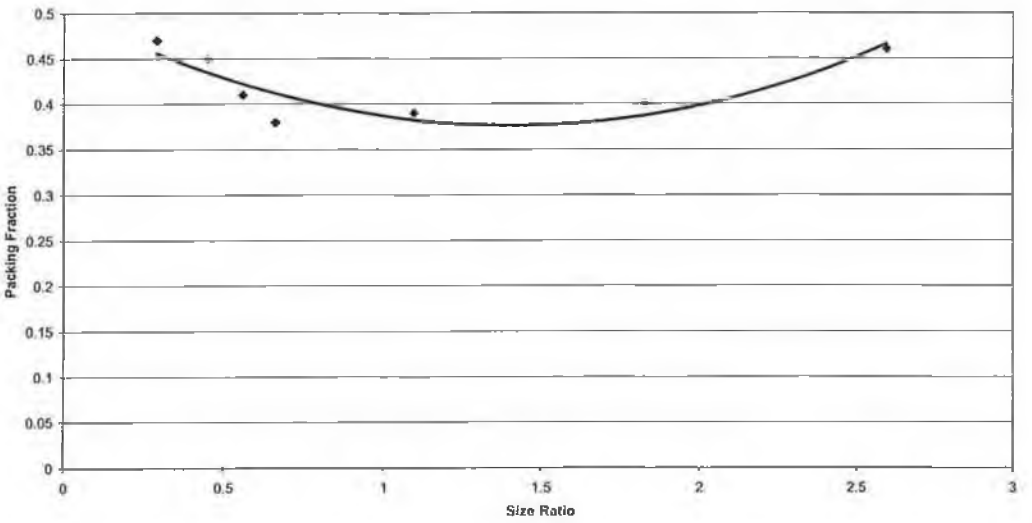

Fig 5.3.4: Variation in Packing Fraction of Al SiC_p powders with 20% by volume SiC_p with size ratio

The above results can be interpreted as showing that while a relationship exists between packing fraction and size ratio that is dependent on other factors. In the case of the powders with 10% SiC_p, the variation in the tensile strength is less clear than in the case where 20% SiC_p is used. Indeed there is very little variation in tensile strength at all, until the size ratio is increased to 1.1. The trend line on the graph seems to show

a linear decrease. The last point has a large influence on this. This data point represents a material made using a large Al powder as the matrix material. Thus the low strength of this material may be explained by the mechanisms involving the use of large powders described in Chapter 6.

In the case of the powder with 20% by volume SiC_p the variation in UTS is much larger. The packing fraction of the powders and tensile strength of the samples made from them are both seen to vary in the same way, so that as packing fraction decreases, so tensile strength decreases and visa versa. It must be noted, however, that there is a greater change in packing fraction too for the powder containing 20% SiC_p than that with 10% SiC_p.

From the above a relationship between packing fraction and UTS may be inferred. However it is known that packing fraction is effected by size ratio. It has been shown that as size ratio changes so the UTS of the material and the packing fraction tend to change in a similar way in certain circumstances. Therefore this may explain the relationship between size ratio and mechanical strength as noted by O'Donnell [1] and German [2] etc.

The strength of the relation between the tensile strength and packing fraction and the reasons why there should be a difference between a powder with 10% by vol. SiC_p and one with 20% by vol. are discussed in detail in Chapter 6.

5.4 Hardness

The hardness of samples made from powders of various size ratios was measured. Ten samples from each of the size ratio groups shown below were measured, except for the samples with a size ratio of 1.65 where only five samples were measured due to availability of powder. The hardness of the samples was measured six times in different locations around the sample to get a good average hardness. All of the results obtained are presented below in the form of a chart showing minimum, maximum and average Rockwell B hardnesses obtained.

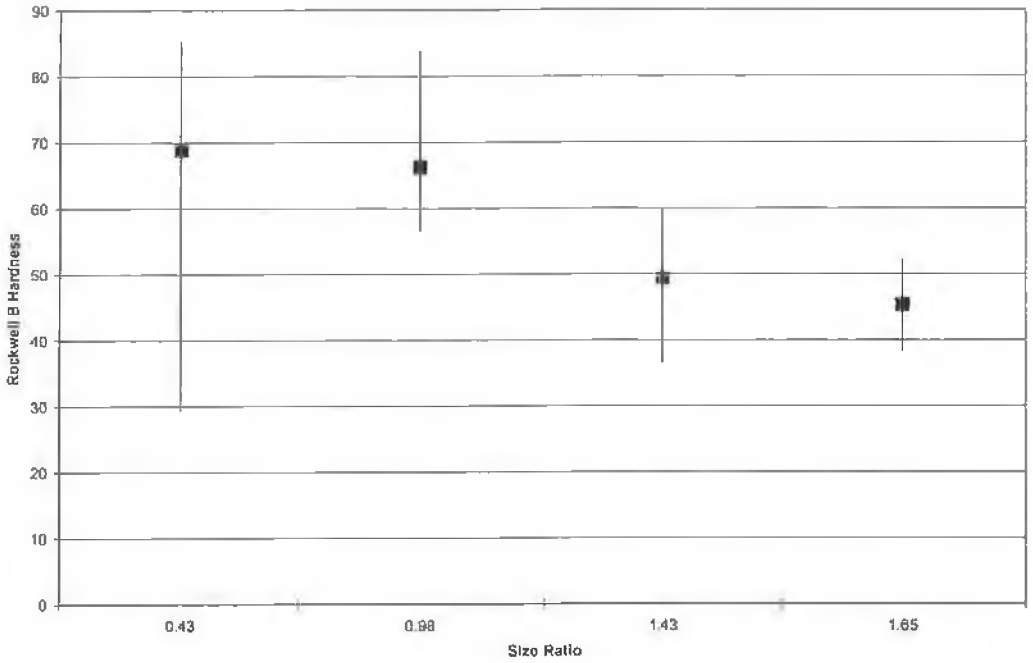

Fig 5.4.1: Rockwell B Hardnesses by Size Ratio
Maximum, minimum and mean values shown

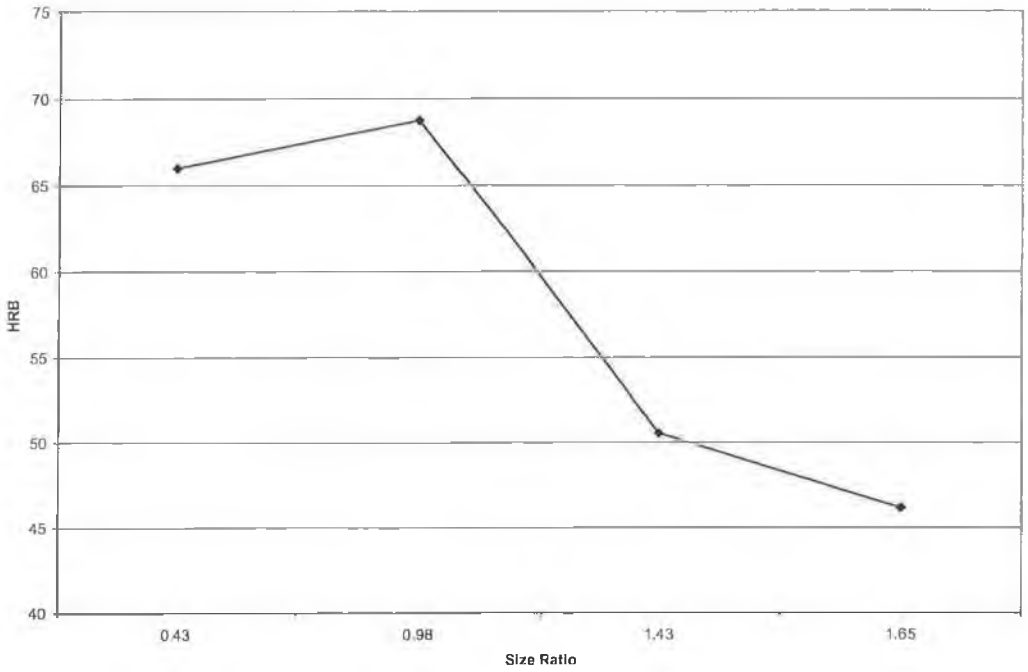

Fig 5.4.2: Average Rockwell B Hardness by size ratio of the constituent powders.

It is apparent that the spread of results for the samples prepared with a powder of size ratio of 0.43 is wider than that of the other powder mixtures. On close inspection of the data, however, it is clear that this wide spread is due to one particularly low sample, a result probably due to poor processing rather than due to an underlying feature of material made from powder with this size ratio. If this sample is disregarded, the difference between the maximum and minimum hardnesses obtained for the first three size ratios shown above are comparable, though rather high, at approx 25 HRB. The lower variation in the results from the samples manufactured using the powder with a size ratio of 1.65 HRB is due to the presence of only two readings here.

Average hardnesses obtained from the samples are presented above by size ratio. These results may be compared to the packing fraction of the powders used to make them which are also presented by size ratio in fig 5.1.6. Comparing fig 5.4.2 and fig 5.1.6 some similarity can be observed suggesting that the packing fraction of the powders before compaction does have an effect on the hardness of the finished

material. This may, in turn explain the effect of size ratio on hardness as noted by German [2] and O'Donnell [1]. These results are discussed in detail in Chapter 6.

Chapter 6: Discussion

6.1 Powder packing results

The data collected for the comparison of the Yu and Standish [3] packing model and the packing fraction of real powder mixtures confirms the accuracy for the model, notwithstanding the problems caused by the distribution of the powder sizes and their irregular shapes. In Figs 5.1.1, 5.1.3, 5.1.4 and 5.1.5 the average relative error is less than 8%, while in Fig 5.1.2 the relative error averages less than 10%.

There is variation in the measured data. However, this may be in large part due to the method of measuring packing fraction as described in MPIF Standard 04 [73]. This test involves flowing powder through a funnel into a beaker. The powders will tend to flow in a different manner each time the test is carried out leading to a different packing fraction as air is trapped in the mixture to a larger or lesser extent. Different sizes of powders also have different flow characteristics, with larger powder sizes tending form clumps and flow less freely, so in each case, it is important to point out that the measured packing fraction is a function of the way powders of this size flow through the funnel into the beaker as well as the size of the particles in the mixture. However, powders would be expected to flow in a similar manner into a die and so the packing fractions achieved by this method may be seen as representative.

Looking at the data for the binary mixtures alone, the data suggests that the amount of scatter increases as the sizes of the powders approach each other i.e. as the size ratio, r tends to 1. Certainly the case where r is closest to 1 (i.e. the case for 25μm Al with 20% by vol 23μm SiC_p where r=0.92) has by far the highest standard deviation of the data sets presented above. This seems be due to the fact that when the particle sizes are close to each other, the mode of packing will tend to have its lowest packing fraction. However due to the irregularity of the shape of the particles in the mixture the amount of porosity will tend to be very dependent on the orientation of the particles in relation to each other. Thus in this mode of packing, the level of porosity could be changed greatly by small changes of orientation of particles in relation to

each other. When the size difference is greater, the smaller particles, whichever material they might be, will tend to fill in the spaces around the larger particles regardless of the orientation of the particles in relation to each other. Thus these mixtures are less susceptible to scatter caused by this mechanism.

For the ternary mixtures, the same seems to apply except in the case of the 45μm Al and the 23μm SiC_p powder. Upon inspection, this data set has a high variance due to one unexpectedly high value of packing fraction that was obtained. This value lies outside two standard deviations of the mean value of the set, possibly as a result of experimental error, and it appears that this data point is not representative of the real level of packing fraction that would normally be measured for a powder mixture like this. If this data point is disregarded, the value level of scatter falls into the pattern described above.

It is interesting to note that in four of the five cases the model predicts packing fractions lower than those measured. Indeed in figures 5.1.1, 5.1.2, 5.1.3, and 5.1.4 there is only one single data point where the measured packing fraction was lower than the calculated value of packing fraction. However in the case of Fig 5.1.5 the model has consistently overestimated the value of packing fraction. It should be noted that this is the largest Al powder used in these tests at 41μm diameter. This will have a two-fold effect.

First, the way the powder aluminium flows into the beaker to measure the packing fraction will be changed by this larger size of aluminium powder. Larger powders tend to form clumps and flow less smoothly in to the beaker. Great care was taken in gathering the data presented here that this was kept to a minimum by strict adherence to the MPIF standards. However, some change in the flow of the mixtures containing larger size powders could not be avoided. Secondly the size ratio (r=0.56 where r=small diameter/large diameter) is quite small. This size ratio is similar to the size ratio for the 10μm aluminium powder mixed with the 23μm SiC_p powder (where r=0.43), but in this case the larger powder comprises much more of the volume of the volume of the mixture i.e. 90% as opposed to 20%. The model does take this difference in volume into account as well as the value of r. However there is a

difference in the shape of the aluminium powder and the SiC_p powder and the way the different powders flow into the beaker and trap air. This makes it inevitable that the packing fraction as poured for a powder mixture where SiC_p is the larger powder and fills 10% of the volume of the mixture will be of a different type to the packing for a mixture where the aluminium powder is the larger constituent and makes up 90% of the volume of the mixture. The way that these powders flow during the test is seen to be different and thus the way they form into clumps and trap air, creating voids is different. This will be the case even though the value of r might be the same. This difference in the mode of packing is not explicitly taken into account in the model and this may explain why the packing fraction measured for this mixture alone out of those sampled here is consistently greater than that predicted by the model.

Indeed this phenomenon will affect every different mixture of differing size ratio that has been measured. As it is not specifically dealt with in the Yu and Standish model [3] this will be a contributory factor to the error between the model and the measured values of packing fraction. However the predictions are always close to the measured values.

We need to consider whether there is any relationship between the difference between the model and measured values of packing fraction and the value of size ratio, r. Certainly in the case of the binary mixtures the data seems to suggest that the larger the Al powder used, the larger the percentage divergence observed, as can be seen by comparing figures 5.1.1, 5.1.2 and 5.1.3. However, as stated above, the model of Yu and Standish [3] calculates the values of r as (r =small diameter/large diameter) so that as the size of the Al powder used increases from 10μm to 38μm the value of r first increases and then decreases again. The change in error can be attributed to the above effect whereby, as the size of the Al particle increases, the large, irregularly shaped Al particles give a mixture of higher porosity than the model predicts. A second contribution to the change in error comes from the fact that two powders can have the same size ratio but contain completely different size powders, which will have different flow characteristics and thus different errors introduced in the measurement of the packing fraction as required for the model.

The difference for the ternary mixtures seems to remain constant across the whole range of Al powder sizes used in the data presented above. However the effect of the way different powder mixtures flow on their measured packing fraction is seen very strongly for the binary powders. The amount of zinc sterate used in the ternary mixtures is very low (1% by volume). Despite this small amount of lubricant, the powders with the mixed-in lubrication were seen to flow more smoothly from the funnel into the beaker when packing fraction was being measured. This, in turn, tends to cancel out some of the variability in the flow between the different mixtures caused by the different sizes of powders used. This may explain the why the divergence between the model and measurements tends to remain reasonably constant, at around 2.5%-3%, for the ternary mixtures. This also points to the cause of the increasing error for the binary mixtures being related to the difference in the way the powders of larger size particles flow when measuring the packing fraction. This seems to rule out any relationship between size ratio and the model's accuracy as such.

The particle sizes which were entered into the model of Yu and Standish in this work were mean sizes. However the actual powders measured to compare with the model consist of many different sizes of particle distributed around the mean. The size distributions of three of the Al powders can be seen in Appendices B-D. It can be seen quite clearly in these graphs that the size distribution is reasonably bell shaped, although there is quite a large variation in the sizes of the particles between the smallest and the largest. The different size distributions of the powders will also be a contributory factor in the differences between the measurements and the model. Each of the powders has its own distinct size distribution and this will affect the measurement of packing fraction.

Further work needs to be done however to fully integrate the distributed nature of the powders used, into the calculations of packing fraction. Yu and Standish [3] allow for this in their model. However, a reliable method of measuring packing fraction while taking into account the distribution of particle sizes in the powder needs to be found before this can be done successfully.

It should be noted that none of the tensile or hardness samples prepared in this work used a mixed in lubricant. Thus they can all be considered to be manufactured from

ternary mixtures. However such samples may also be manufactured using mixed-in lubrication and so the ternary data is included above in figures 5.1.4 and 5.1.5 for completeness.

So, it is seen in chapter 5.1 that the percentage difference between the packing fraction of the un-compacted mixture and the packing fraction as predicted by the Yu and Standish [3] model for that mixture is well within the 8% as reported in the literature, with the ternary mixtures in figures 5.1.4 and 5.1.5 averaging around 3%. Thus the model appears to give more accurate results than claimed by the authors in their work for these powders.

6.2 Tensile Results Discussion

The tensile strength data is somewhat inconclusive. For of the first group of samples generated and shown in fig 5.2.1 there is very little observable correlation between ultimate tensile strength (UTS) and packing fraction as predicted by the Yu and Standish model. This can be seen by comparing fig 5.2.2 and fig 5.1.6. These samples did not sinter well so it is probable that any size ratio effect that might exist will be unobservable due to the poor sintering. However for the second group of samples, shown in fig 5.2.3, there does exist some comparison between the variations in UTS and the calculated packing fraction in fig 5.1.7. A different processing regime was used to produce this second group of samples (i.e. they were processed at 640°C and for 80 minutes as described in Chapter 3) and it is probable that the longer processing times and higher temperatures used for the second batch of samples led to a better material. While the material is not shown to be stronger in any significant sense with more energy and time available for sintering the micrographs in chapter 5 seem to show that the materials sintered more fully. Thus any size ratio effect that exists would be more likely to be seen in these samples than in the first group where the materials did not sinter well at all.

A more accurate method of showing that the samples were sintered more fully would be to carry out density tests on the samples. This could show any differing level of sintering and quantify it very accurately. Unfortunately due to time constraints such tests were not done in the here and they are left for future work.

In the case of the second group of samples, in every case if the packing fraction of a powder mixture of a particular size ratio is higher than the packing fraction of a different mixture, then its UTS will also be higher and visa versa. However, the magnitude of the changes are not seen to be the same. Indeed in one case (the sample with a size ratio of 1.086) a small increase in packing fraction from the previous sample corresponds with a much larger increase in UTS. This may be down to the problems experienced with manufacturing the material discussed below. However, these results do indicate a relationship between packing fraction and tensile strength and that both are altered in the same direction by changing size ratio.

In an attempt to show some of the microstructures of the materials micrographs are presented in chapter 5. The samples which were available to take micrographs were the samples which had been used for the tensile tests. Thus they had been deformed previously and so were not entirely suitable for this purpose, however it is felt that they can still give an indication of the true structure of the material post sintering.

Examining the photographs of the microstructure presented in chapter 5 above we can see the differing ways that the materials tend to sinter as the relative sizes of the particles is varied. In Fig 5.2.5 we see the structure of a material made from 10μm Al with 10% by volume 23μm SiC_p. The size ratio is quite low at 0.43 and the material seems to have been reasonably well sintered. However some porosity can be seen and the shape of the metal particles can still be partly seen, showing that incomplete sintering has occurred. It is known that the SiC_p plays an important in the sintering of Al SiC_p MMCs as upon compaction it tends to puncture through the oxide layer of the aluminium powder and thus allow better sintering to occur [1, 2, 69]. The relatively low volume fraction of the SiC_p in this instance may have played a role in the incomplete sintering seen here.

Fig 5.2.6 shows material made of the same two constituents but with 20% by volume SiC_p. The levels of porosity do appear to be lower here by a certain amount. This figure also has large areas which correspond to where SiC_p particles were torn out during the polishing which the sample underwent to prepare it for the microscope.

Fig 5.2.7 shows a material made of 18μm Al with 20% by volume SiC_p and fig 5.2.8 shows material of the same proportions of 25μm Al and 23μm SiC_p. The size ratios in both cases are close to one at 0.78 and 1.086 respectively and an increase in the porosity throughout the material compared to that shown in fig 5.2.6 can be seen. This would appear to support the idea that when the powder sizes are close together the porosity between them is greater before compaction and that this greater level of porosity is not reduced during subsequent compaction or sintering.

Fig 5.2.9 is a micro-graph of a material made of 38μm Al with 20% by volume SiC_p. Here the size ratio is quite large at 1.65. The edges of the original Al particles are visible in some areas of the graph. This points to incomplete sintering of the material.

No samples which could be said to have sintered properly were produced during this work. The poor strengths of the material are probably due to some problem with the sintering rig used to manufacture them. It seems most likely that the atmosphere in the furnace was not inert and that as such the powders oxidised rather than sintered. Due to the poor strengths of the material produced during this work, and the somewhat inconclusive nature of the microstructural examination above, the decision was taken to continue with discussion of the comparison between the change in packing fraction of poured powders and changes in mechanical strength of material using previously published data.

By far the lowest UTSs are obtained for the samples shown in fig 5.2.9. It has been noted previously by O'Donnell [1] and German [2] that in Al-SiC_p MMCs manufactured by this method, the strength of materials manufactured using larger Al powders tends to be smaller, regardless of the size ratio between the powders. This can be attributed to the larger voids between the particles pre-sintering, which is a feature of the use of larger powder sizes. While the powder of the smaller size could fill these pores were it present in sufficient quantity, in this case the smaller SiCp powder is only 20% by volume and so will only partially fill these large voids. Furthermore the silicone carbide takes no active part in the sintering process. Contrast with the situation where 10μm aluminium and 23μm SiC_p were used. Here the large pores are between the larger SiC_p particles. However the smaller aluminium powder is

still 80% by volume and so can easily fill the large voids in the mixture, pre-compaction. The aluminium powder will also actively sinter to further fill these voids.

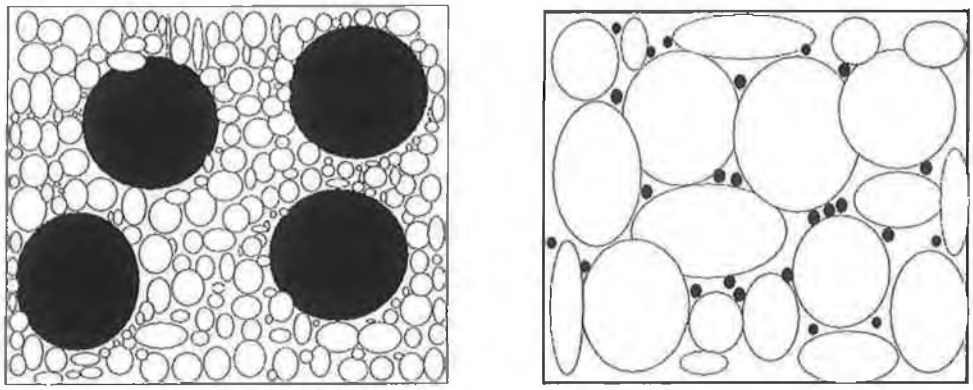

(a) (b)

Fig 6.2.1: (a) A powder mixture where a large amount of the smaller constituent powder is present (b) a powder mixture where a small amount of the smaller constituent powder is present.

In figure 6.2.1 above two powder mixtures are illustrated. One has a large amount of the smaller constituent powder present. The other has a small amount of the smaller constituent powder present in the mixture. Let us take it that the dark particles are SiC_p and that the white particles are Al. When the (dark) SiC_p is large and the (white) Al small there is sufficient Al to fill the voids between the SiC_p and thus the sintered product has higher density. When the Al is larger there is little SiC_p to fill the voids so the large voids remain and large pores may remain after sintering.

Fig 5.2.9 seems to show that as a result of the extra porosity in the powder mixture in mixtures of this type, incomplete sintering has occurred. This can explain the seemingly inherent weakness of materials made in this manner where large Al powders are used. So it seems that the decrease in strength of such materials seen in this work and previously [1,2] can, at least in part, be attributed to this mechanism. So we see that it is important for a good mixture and thus a good mechanical strength to be achieved that sufficient amount of both powders be present in the mixture.

It should also be considered that it was seen in the measurement of packing fraction that the powders containing the large Al powders and no lubrication flowed less smoothly and as a result of this tended to trap air and have lower packing fractions. It is probable that this same effect will be seen when such mixtures flow into the die pre compaction and that this decrease in packing fraction may have a detrimental effect on the mechanical properties of the material, even post sintering.

In figs 5.2.10 and 5.2.11 we see materials which are of the same composition as those shown in figs 5.2.8 and 5.2.9 respectively. However these materials were sintered at a higher temperature and for a longer time than the earlier mixtures. The reduction in porosity can clearly be seen which should naturally lead to a stronger material. German [2] notes that as sintering times and temperatures are increased so the size ratio effect is decreased. This is put down to the increased time and energy of sintering being able to overcome the effects of increased porosity due to the differences in size ratios between the constituent powders. However in this case the overall strength of the materials produced at the higher temperature and longer sintering time was not seen to change discernibly from the strengths of the materials as seen in figure 5.2.3 and the material strengths are seen to vary with size ratio still. Thus the effect of the large Al particles on the strength of the materials does not appear to have dissipated. This seems to contradict German [2]. It is possible that some other fault with the manufacturing process used to produce these samples meant that even though porosity was seen to decrease the strength did not increase. Also, higher temperature and longer time could also give more opportunity for problems such as oxidation or large grain growth, either of which can inhibit strength. Further work needs to be carried out in order to gain an understanding of this problem.

It must also be noted that although we are looking at how the relative sizes of the powders effect the strength of the material, post sintering additional processes have been carried out on the material in the data shown above i.e. they have been precipitation heat treated and age hardened. Naturally, these processes will affect the granular structures of the materials, causing a different grain structure in the material than the one that exists post sintering.

It might be considered that such an action may mask or distort any relationship between the size ratios of the powders and the material strengths of the finished materials that might exist. However the processes used here are exactly those of O'Donnell [1] and in that case the relationship was clearly seen as it was in the work of German [2]. It is this relationship that was investigated in this work and so the manufacturing process was kept exactly the same. It should be noted that in this case we are looking at the relationship between the powder particle size and the mechanical strength rather than between grain size and material strength. The particle sizes are chosen before any processing takes place at all. During the sintering process the particles ought to grow into each other and the voids between them close to a certain degree. Thus the porosity of the material as determine by the size ratio of the powders is determined and set once the sintering process is finished. If is thought that the subsequent processing of the material is at a temperature which is too low to significantly effect this process further and so, though the structure and size of the grains of the material may be altered, the effect of the relative sizes of the particles of the metal and silicon carbide powders should not be greatly altered. However when considering the results presented above the effect of the subsequent processing should be borne in mind and it would be worthwhile in any future work looking at the effect that such post-processing has on any size ratio effect.

The absolute values for UTS obtained in the tests presented above are very low, well below that which might be expected for such a material. This in spite of the fact that the sintering regime used here is exactly that used by O'Donnell [1], which obtained UTSs in the range of 100-200 MPa. The only real change is the introduction of a new kiln into the furnace. In the work done by O'Donnell the kiln used was basically a square metal box that filled the inside of the furnace. This has been replaced by a new kiln with four separate chambers to enable experiments on different sintering times and interrupted sintering to take place in different chambers simultaneously without disrupting processing in another chamber.

The problem with the kiln set-up used in the above tests appears to be in its inability to maintain the correct processing atmosphere, which is so vital for the processing of the material. Unlike in the kiln set-up as used by O'Donnell [1] the lids of the chambers are not clamped down, making it extremely likely that oxygen could defuse

into the chambers. Also there is nothing to prevent the lids of the chambers from "barrelling" slightly when at high temperatures creating an even bigger gap for oxygen to get into the processing chamber. Secondly, the use of fire-block in the lids of the chambers, which contains an oxide material, provides a further source of oxygen contamination in the processing chamber. This leads to a possible oxidation of the material during either, or both, the annealing and the sintering operations.

Tests where the fire-block was removed and weights placed on top of the lids of the processing chamber in order to prevent barrelling have provided powders which, when sintered, have produced samples with UTSs of over 63 MPa. This seemed to suggest that the kiln set-up used to produce these parts was not suitable for the sintering of this material and so the decision was made to return to the box kiln as used by O'Donnell [1]. However on refitting the box kiln no real improvement in the strength of the material manufactured was seen. The strengths increased to the order of 40-50 MPa on average, still well short of the levels reported by O'Donnell although the equipment and methods used were the same. Because no significant improvement was achieved, results from the experiments carried out with the box kiln are not presented here.

6.3 Comparison of packing fraction results with published Tensile Results

In chapter 5 a comparison between packing fraction as calculated using the Yu and Standish [3] model and UTS as measured by O'Donnell [1] for samples of Al SiC_p material made using PM methods can be made from the data shown in figures 5.3.1, 5.3.2, 5.3.3 and 5.3.4. These results show that there is a link between the packing fraction of the powder before compaction and the mechanical strength of the material after processing.

The data for the powder containing 20% by volume SiC_p certainly indicates some relationship between packing fraction and tensile strength. In this case it is clear that as fig 5.3.4 (which shows how packing fraction for the powder mixture as calculated by the Yu and Standish model varies as the size ratio of the mixture is changed) decreases, so fig 5.3.3, (which shows how the UTS of the material varies as packing

fraction is changed) also decreases. Similarly as the packing fraction of the powder starts to increase again as size ratio gets greater than one (i.e. as the powder sizes get further apart again) so strength also increases. So a decrease or increase in packing fraction seems to be matched by a decrease in UTS although the magnitude of the decrease is not the same.

However the tensile strength of the samples made containing 10% by volume SiC_p, figs 5.3.1, did not vary with packing fraction, instead staying reasonably constant throughout a large section of the range of size ratios tried. Furthermore, samples in this group never showed an increase in strength as packing fraction increases at large size ratios. This shows that while packing fraction is a contributing factor to the tensile strength of the material, it is not the only factor which needs to be considered. So why does UTS change with packing fraction for a material containing 20% by vol. SiC_p and not for one containing 10%? One possible answer lies in the fact that the effect of size ratio on packing fraction is dependent on the interaction between particles of two different sizes. Therefore, if there are not enough particles of either size present in the mixture then this interaction will have less of an effect. Below is a graph illustrating the changes in packing fraction with size ratio for a number of mixtures of the same two powders, each one containing different amounts of each powder as calculated from the model of Yu and Standish [3]:

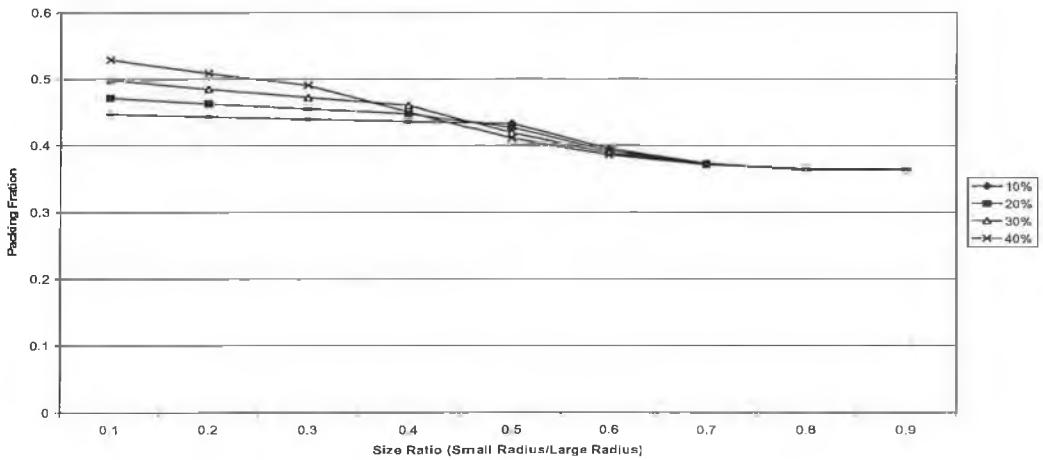

Fig 6.3.1: Variation in packing fraction as with size ratio for a number of mixtures of the same two powders where the % by volume of one of the powders is varied in each mixture

It is clear from fig 6.3.1 that in order to get a significant change in packing fraction as size ratio is changed, there must be a sufficient quantity of both constituent powders present. The closer the mixture is to a 50/50 mix of both powders (by volume) the larger the variation in packing fraction with size ratio will be.

It should also be noted that in fig 6.3.1 there is an area for the powder containing 10% by volume SiC_p where there is very little change in packing fraction with change in size ratio. The region where it remains constant is a size ratio between 0.1 and 0.5. Each of the subsequent mixtures also has a reasonably constant area of packing fraction but for a smaller range of size ratios. In effect this means that there is a reasonable wide range of size ratios for powder mixtures containing small quantities of one powder where no large change in packing fraction will be seen. Thus no change in mechanical properties as a result of changing packing fraction can be expected. However when both powders are present in sufficient quantity (i.e. nearer to a 50/50 mixture) this flat region disappears. Thus, according to the model of Yu and Standish which has been seen to predict packing fractions accurately over a wide range of size ratios and powder sizes, for these powders any change in size ratio will give a change in packing fraction and so any change in size ratio will lead to a change in UTS. The decrease in strength seen in the material which contained 10% by volume SiC_p as size ratio increased can be explained by the effect of the large aluminium powders which were used in their manufacture. It has already been noted here and in [1] and that matrix material made from large powders tends to have a detrimental effect on UTS.

Thus figures 5.3.3 and 5.3.4 show that there is a relationship between packing fraction of the powders and the tensile strengths of the material made from them. As changing size ratio leads to a lower packing fraction, the tensile strengths of the material made from those same powders when compacted and sintered, tends to decrease. However, a sufficient amount of both powders must be present for this effect to become important. Thus size ratio and its effect on packing fraction does have an important role to play in determining mechanical properties and can directly affect them. However, other factors such as the size of each constituent powder and the material chosen as the larger powder also have a role to play in the mechanical properties of the finished material. It has also been shown in figs 5.2.9 and 5.2.12 that if both

powders are not present in the mixture in sufficient quantities that this will lead to a high level of porosity in the mixture as poured that will not necessarily be overcome during the sintering process.

However fig 5.2.7 and fig 5.2.8 certainly show that under the correct conditions packing fraction and tensile strength do change in a similar way as size ratio is changed. This may explain the dependence of the mechanical properties of materials of this type manufactured using these methods on size ratio as noted by O'Donnell [1] and German [2].

6.4 Discussion of Hardness Results

Material samples were manufactured and the hardnesses of them measured as described in chapter 5. How the hardnesses obtained changes with the changing size ratio of the powder mixture was plotted in fig 5.4.2. How packing fraction (as calculated by the Yu and Standish model) changed for the same changes in size ratio was also plotted in fig 5.1.8. Comparing fig. 5.4.2 and fig. 5.1.8 above, a similarity can be observed between the shapes of the plots. For three of the powder mixtures the change in direction (i.e. a positive or negative change) of the curve plotting the hardnesses of the samples is matched by a corresponding change in direction of the curve for the packing fraction e.g. the hardness of the sample manufactured using a powder mixture with a size ratio (Al/SiC_p) of 0.43 is lower than that of a sample manufactured using a powder with a size ratio (Al/SiC_p) of 0.98 and the packing fraction of the mixture with a size ratio of 0.43 is also lower than that of the mixture with the size ratio of 0.98.

However the powder mixture with the size ratio of 1.65 does not behave in this way. For this powder the predicted packing fraction is higher than that for a powder mixture with a packing fraction of 1.43. However the hardness measured for a sample sintered using a powder mixture with a 1.65 size ratio is lower than the hardness of a sample manufactured from a powder mixture with a size ratio of 1.43. The explanation for this is that the Al powder used in the mixture with size ratio of 1.65 was a 38μm Al powder, the largest Al powder used in these tests. As with the tensile response of the material discussed in section 6.2, the hardness of the material appears to be adversely

effected by the use of the large Al powder due to the increased porosity around such powders pre-compaction and the inability of the sintering process to fill these large voids at the times and temperatures used in these tests.

It is seen that as the size ratio of the powder mixtures changes the packing fraction the mechanical properties of the finished material are affected. However, as with the tensile strength of the material, other factors, such as the actual size of the powders, will also influence these properties.

Chapter 7: Conclusions and Future Work

7.1 Conclusions

The aim of this project was to explore the relationship between the mechanical properties of Al SiC_p metal matrix composites manufactured using powder metallurgical methods, and the size ratios of the powder mixtures used to manufacture them. Having looked at the options, it was decided that a possible cause of this relationship, which had been noted elsewhere, was to be found in the changing packing fraction of the powder before compaction which results with the change in size ratio. The model of Yu and Standish [3] was chosen to try to effectively predict the packing fraction of the material due to its simplicity and its use of the size ratio of the powder being used as prescribed information, therefore guaranteeing that the effect of the size ratio on packing fraction could clearly be seen and tested.

The testing carried out on the model has shown that it is useful for predicting the packing fraction of such metal/silicon carbide powder mixtures. The materials used here are of irregular shape. Also the work above assumes all particles are of a uniform size when, in fact, their sizes are distributed around a mean. In spite of this packing fractions as predicted by the model are within a maximum difference of 10% generally well within the 8% difference level reported by the authors when compared with measurements obtained in the laboratory. Thus the model of Yu and Standish [3] can be used to predict the packing fraction of these and other metal powder mixtures with some degree of accuracy. Its simplicity and ease of calculation also recommend it. It is also extremely useful in any circumstance where, as in the above work, size ratio needs to be explicitly taken into account. However if a higher degree of accuracy is required then another model, possibly one of the other models discussed in Chapter 2 may be needed.

Having proven the accuracy of the model for predicting packing fractions for these materials, the proposed correlation between changes in packing fraction and changes in mechanical properties of finished material was investigated. It did not prove possible to manufacture material of a sufficiently high quality to rigorously test the

theory, even though the same methods and equipment as used by O'Donnell [1] were used in this work. The tests on the material produced do give an indication that a relationship does exist between packing fraction and strength and that both changed in the same manner as size ratio was changes. However, using the data that O'Donnell produced it was possible to test for any relation between packing fraction and strength. It was found that a correlation between packing fraction and mechanical properties does exist in the correct circumstances. An increase in the packing fraction of the powder mixture before compaction and sintering was seen to lead to an increase in the mechanical strength of the final material. However the magnitude of the increase in strength or hardness was not the same as the increase on packing fraction caused by the size ratio effect partly because the size ratio effect is dependent on the percentage volume of both powders present.

It is possible to conclude that in cases where there is a sufficient amount of both materials present to create a significant change in packing fraction as size ratio is varied, the change in packing fraction will be mirrored in changes in mechanical strength. The compaction and sintering regimes investigated by O'Donnell can therefore be said to have been insufficient to overcome the increased porosity of the powder mixture as the sizes of the constituent powders get close to each other. However this is not to say that other compaction and sintering regimes may not cancel out this effect by closing up this extra porosity.

The model of Yu and Standish shows in fig 6.3.1 that in order for the size ratio effect to have a large impact on packing fraction, sufficient volumes of both powders (in the case of a binary mixture) must be present in the mixture. If both powders are not present in sufficient quantities there will be much less of a reduction in packing fraction as the sizes of the powders get close together. This would also appear to have an effect on mechanical properties with mechanical properties of materials containing small amounts of one constituent part showing less of a correlation to packing fraction changes.

This work shows that it is to be possible to pick powder sizes and quantities which will create mixtures with inherently high packing fractions. These materials will have lower porosities pre-compaction. They should therefore be easier to compact to high

density and thus should sinter better at lower temperatures and shorter times, leading to a saving in expenditure.

In summary then, it has been shown in this work that the effect of size ratio on mechanical properties as noted by O'Donnell [1] and German [2] may be attributed to the change in size ratio dependent packing fraction. However it has been shown that other factors such as the size of the matrix powder, time and temperature of sintering can also modulate the material's mechanical strength and may even, in some cases, be used to overcome the size ratio effect.

7.2 Future Work

The aim of this project is to investigate the relationship between the mechanical strength of Al SiC_P MMCs manufactured using PM methods and the size ratios of the powders used to manufacture them. Much work remains to be done to understand the true nature of this relationship. There is little doubt that the inherently better packing provided by powders with a large difference in their sizes improves the sintering process. However the amount of both powders present in the mixture is also of critical importance. The interaction between the amount of each powder present in the mixture and how size ratio affects the mechanical properties of the material remain to be investigated.

It has been shown in section 5.3 that as mixtures containing powders with different size ratios, and thus having different packing fractions, are used to manufacture material, the changing packing fractions do have an effect on the mechanical strength of materials. Certainly in the case of materials sintered using relatively low temperatures and short times changes in packing fraction caused by changes in size ratio between the powders do seem to relate to changes in mechanical properties i.e. better packing fractions give materials with better strength. However, there is a suggestion [2] that if times of sintering or temperatures are increased then the effect may be to be negated. It is assumed that this is because the material has more time and/or energy to fill the larger pores due to the decrease in packing fraction caused by changes in size ratio.

A detailed examination of samples where size ratio, r, is close to one (i.e. the constituent powder sizes are close together), some of which have had shorter times and lower temperatures and some of which have had longer times and/or temperatures, under a Scanning Electron Microscope (SEM) ought to give an insight into what is happening when sintering times or temperatures are increased. Density measurements of samples should also be carried out as this could easily and accurately determine whether increased times and temperatures lead to decreased porosity. It should also be possible to discover the best and most efficient method of sintering in order to overcome the effect altogether if this is possible. The transition point between a mode where the size ratio effect is in play and where it times and temperatures are

sufficient to overcome it may also tell us a lot about the best way to sinter such materials. If it is possible to pick materials which have inherently high packing fractions then the need for using high temperature and long times may be negated, thus saving on processing costs. The full potential for this type os saving needs to be investigated.

The samples prepared to give the data provided in this work have all proved to be significantly less strong than might be expected. This is in spite of the fact that times, temperatures and gas flows laid out by O'Donnell [1] have been followed and he reported UTSs, which are comparable to standard strengths for such materials. Indeed even the same equipment that O'Donnell used is still in use. Work needs to be done to discover why there is a discrepancy between the samples prepared in this work and in that of O'Donnell [1].

All samples of material tested in this work have been processed post-sintering. It is possible that this post-processing has altered the structure of the material in such a way as to change the effect of the size ratio of the powders on the mechanical properties. Any future work on this subject ought to examine what this effect is and quantify it if it exists.

The fact that the powder sizes are distributed needs to be taken into account. All calculations above use an average value for the sizes of the powders. However it is known that this is not the true size of the powders. It is possible for the distribution of the powder size to be taken into account in the Yu and Standish [3] model. The distributions of the powders can be measured using laser measurement techniques on the powders. Such results can be seen in Appendices B-E. However a problem still remains in taking the distribution into account in the measurement of the packing fraction of the powders on their own which is a prescribed piece of information for the model. This problem must be resolved in order to see if it is entirely reasonable to measure packing fraction as was done in this work or if a more detailed method is necessary.

References

[1] Gareth O'Donnell, Process Optimisation and Numerical Modelling of Powder Metallurgical Aluminium Matrix Composites, Thesis for PhD, Dublin City University, 1999

[2] R.M. German. Sintering theory and practice. John Wiley and Sons. 1996. IBSN: 0 471-05786-X

[3] A.B. Yu and N. Standish, Powder Technol, 52 (1987) 233.

[4] N. Standish and A.B. Yu, Powder Technol., 49 (1987) 249.

[5] H. Scheffe, J. Roy. Stat. Soc., B25 (1963) 235.

[6] M. Leitzelment, Cho Seng Lo and J.A. Dodds, Powder technol., 41 (1985) 159.

[7] N. Ouichiyama and T. Tanaka, I&EC Fundam., 23 (1984) 490.

[8] P.Z. Cai, G.L. Messing, D.L. Green, J Am. Ceram. Soc. 80 (2) (1977) 445-452. [9] N. Standish and A.B. Yu, Powder Technol., 53 (1987) 69.

[10] N.R. Draper and R. St. John, Tehnometrics, 19 (1977) 177.

[11] R.K. McGeary, J.Am. Ceram Soc., 44 (1961) 513

[12] C.D. Scott, Nature, 188 (1962) 908

[13] R. Rutgers, Nature, 193 (1962) 465

[14] M. Cross, W.H. Douglas and R.P. Fields, Powder Technol., 43 (1985) 27.

[15] S.M.K. Rassouly, Powder Technol., 103 (1999) 145.

[16]W.O. Smith, P.D. Foote, P.F. Busang, Phys. Rev. 34 (1929) 1271.

[17] K. Ridgeway, K.J. Tarbuck, Br Chem. Eng. 12 (1967) 384.

[18] S.M.K. Rassouly, PhD Thesis, University of London, King's Collage, 1982.

[19] A.E.R. Westman, J.Am.Ceram. Soc., 19 (1936) 127.

[20] M.Song, K.T.Chuang and K.Nandakumar, Ind. Eng. Chem. Res.,37(1998) 3490.

[21] T. Stovall, F, De Larrard and M. Buil, Powder Technol., 48 (1986) 1.

[22] A. Marmur, Powder Technol., 44 (1985) 249.

[23] W.A. Gray, The packing of Solid Particles, Chapman and Hall Ltd, 1968. IBSN B6812808

[24] Druckler D.C., Prager W, Quarterly Appl Math 10 (1952) 157

[25] Alan C.F. Cocks, Constitutive modelling of powder compaction and sintering, Progress in Materials Science, 46 (2001) 201-299.

[26] Schofeild A, Wroth GA. Critical state soil mechanics. London: McGraw-Hill, 1968.

[27] Hédi Chtourou, Michel Guillot and Augustin Gakwaya International Journal of Solids and Structures, Volume 39 (2002) 1059-1075.

[28] Hédi Chtourou, Augustin Gakway, Michel Guillot, International Journal of Solids and Structures 39 (2002) 1077-1096.

[29] R.J. Henderson, H.W. Chandler, A.R. Akisanya, C.M. Chandler, S.A. Nixon, , Journal of the Mechanics and physics of solids, 49 (2001) 739-759.

[30] Paul, B, Prediction of elastic constants of multiphase materials. Trans. ASME 218, 36-41.

[31] Chang, C.S., Liao, C.L.. Appl Mech Rev., 47, (1994) 197,

[32] Pia Rednaz, , Int. J. Sci. 40 (1998) 11, 1175-1189,

[33] Gurson, A.L., ANME 99 (1977) 2-15

[34] Fleck, N.A., Kuhn, L.T. and McMeeking, 40 (1992) 5, 1139-1162.

[35] R.S. Ransing, D.T. Gethlin, A.R. Khoei, P. Mosbah, R.W. Lewis, 21 (2000) 263 269.

[36] R.M. German, Met. Trans. 23A (1992) 1455-1465

[37] K. Shinagawa, Computational Material Science, 13(1999) 276-285.

[38] A. Jogta, P.R. Dawson, Acta Metall. 36 (1988)2551.

[39] J. Svoboda, H. Riedel, H. Zipse, Acta Metall. Mater. 42 (1994) 435.

[40] Michael Gasik, Baosheng Zhang; 18 (2000) 93-101

[41] A. Kazaryan, Y. Wang and Bruce R. Patton; Scripta Materialia, 41 (1999).5, 487 492.

[42] G. Tomandl, P. Varkoly; Materials Chemistry and Physics, 67 (2001) 12-16.

[43] Eugene Olevsky, Alain Molinari, International Journal of Plasticity, 16 (2000) 1 37.

[44] Olevsky, E, Skorohod, V., Technological and Design Plasticity of Porous Materials, IPMS NAS Ukraine, (1988) 97

[45] Scherer, G.W., J Non- Cryst. Solids 34 (1979) 239.

[46] Helle, A.S., Easterling, K.E., Ashby, M.F., Acta Meatll. 12 (1985) 2163-2174

[47] Eugene A. Olevsky, Material Science and Engineering, R23 (1998) 41-100.

[48] R.L. Coble, J Appl. Phys. 32 (1961)

[49] R.A. Gregg, F.N. Rhines, Metall. Trans. 4 (1973) 5 1365-1374.

[50] W Beere, Acta Metall. 23 (1975) 1, 195-203.

[51] A.C.F. Cocks, Overview No 117. Acta Metall. 42 (1994) 7, 2191.

[52] M.F. Ashby, Background reading, HIP 6.0 University of Cambridge, U.K. (1990)

[53]R.M. McMeeking, L.T.Kuhn, Acta Mater. 40 (1992) 5, 961.

[54] A.C.F. Cocks, N.D. Apacicio, Acta Metall. 43 (1995) 2, 731.

[55] V.V. Skorohod, Naukova Dumka, Kiev, (1972).

[56] V.V. Bhanu Prasad, B.V.R Bhat, Y.R. Mahajan, P. Ramakrishnan, , Material Science and Engineering, A 00 (2002) 1-7. Uncorrected Proof.

[57] R.M.Christensen, Mechanics of Composite Materials, Wiley-Interscience,1979.

[58] Z. Xue, Y Huang, M. Li, Acta Materialia, 50 (2002) 149-160.

[59] Yoshihiro Tomita, Yoshikazu Higa, Takehiro Fujimoto, 42 (2000) 249-2260

[60] M.S. Bruzzi, P.E. McHugh, F. O'Rourke, T. Linder, International Journal of Plasticity, 17 (2001) 565-599.

[61] L.H. Dai, G. J. Huang, International Journal of Mechanical Sciences, 43 (2001) 1179-1193.

[62] Dai, LH, Huang, ZP, Wang, R, Polymer Composites 19 (1998) 506-513.

[63] L.H. Dai, Z. Ling, Y.L. Bai, Composites Science and Technology, 61 (2001) 1057-1063.

[64] G.L. Heness, B. Ben-Nissan, L.H. Gan, Y-W. Mai, Computational Material Sciences (1999) 259-269.

[65] J. Boselli, P.D. Pitcher, P.J. Gregson, I. Sinclair, Materials Science and Engineering, A300, (2001) 113-124.

[66] H.Z Ding, O. Hartmann, H. Biermann, H. Mughrabi, Materials Science and Engineering, A2000 (2001), Uncorrected proof.

[67] D. Steglich, T. Siegmund, W. Brocks, Computational Materials Science, 16 (1999) 404-413.

[68] V. Tvergaard, A. Needlemann, Acta Metall, 32 (1984) 1, 157-169.

[69] S.C Baxter, M.I. Hossain, L.L. Graham, International Journal of solids and Structures, 38 (2001) 9209-9220.

[70] Pindera, M.-J., Bednarcyk, B.A., Compos. Part B (Engng.) 30 (1999) 1, 87-105

[71] Baxter, S.C., Graham, L.L., J. Engng. Mech. 126 (2000) 4, 389-404.

[72] T. Wilkins, Y.-L. Shen, Computational Materials Science, 22(2001) 291-299

[73] Metal Powder Industries Federation, Standard Test Methods for Metal Powder Metallurgy Products, 1999, IBSN

[74] G. O'Donnell and L. Looney, Production of Aluminium Matrix Composite Components Using Conventional PM Technology, Materials Science & Engineering, A303, 2001, pp 292-301.

Appendix A

Section A.1: How Far does the top disc sit into the gap created by the two beneath it.

If we consider a triangle between the centres of the discs all sides of the triangle are equal to 2R. Therefore the triangle is equilateral and so all the angles are at 60°. This implies that the section of the disc which is in the triangle has and area equal to 1/6 that of the disc as a whole. Therefore the area of the discs in the triangle $=1/2\pi R^2$. The area of the whole triangle $= 1/24R^2\text{Sin}60=\sqrt{3}/4R^2$. Thus the area of the gap in between the discs can be seen to be

$$=\frac{\sqrt{3}}{4}R^2-\frac{1}{2}\pi R^2$$

$$=0.16R^2$$

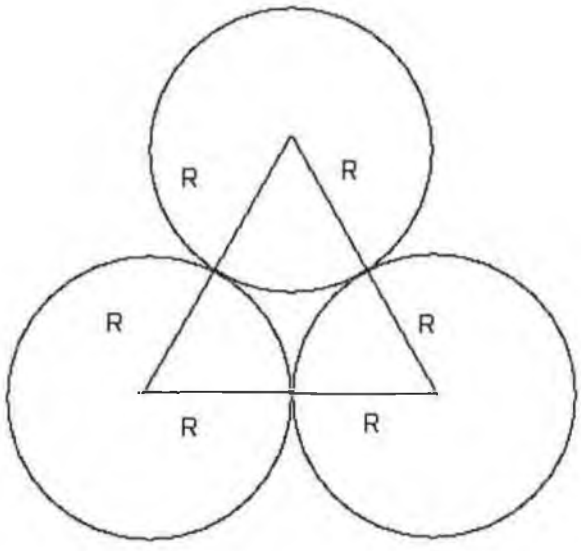

Fig A.1: Triangle Drawn between the centres of the discs.

We now want to find the distance between the bottom of the gap and the bottom of the disc on top. Again, consider a triangle as shown.

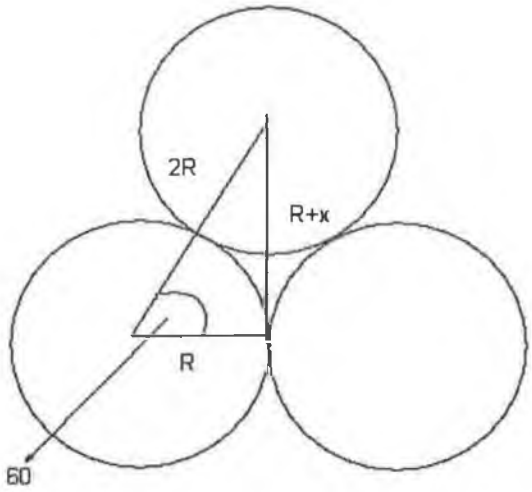

Fig A.2: Triangle to find the size of the gap.

$$\text{Sin}60 = \sqrt{3}/2 = \frac{R+x}{2R}$$

$$2\sqrt{3}R = 2R + 2x$$

$$\Rightarrow x = 0.732R$$

$$\Rightarrow r < 0.366R$$

For the top disc to sit as shown above then we can also say the following.

$$\text{Cos60=R/2R=1/2}$$

$$\therefore Cos60 = \frac{\frac{1}{2}R}{R} = \frac{1}{2}$$

i.e. we can see the following in relation to where the top disc sits.

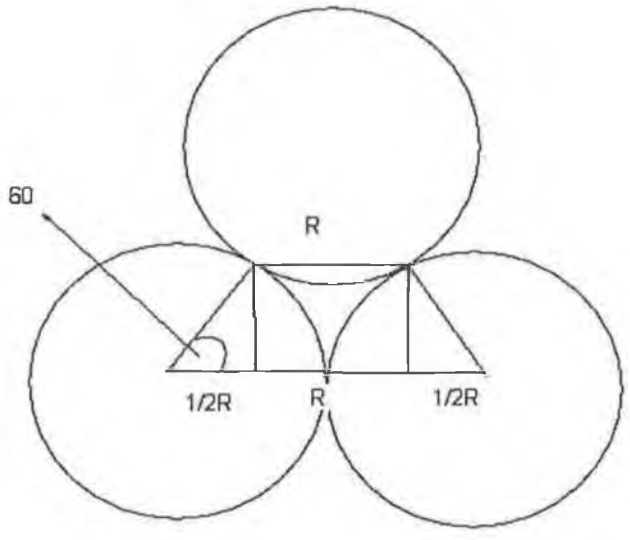

Fig A.3: Consider the following shape in order to calculate the length of the chord where the top disc sits

So the top sphere sits down to a depth where a chord =R. This implies that if we place a disc in this area then we can draw a triangle as shown.

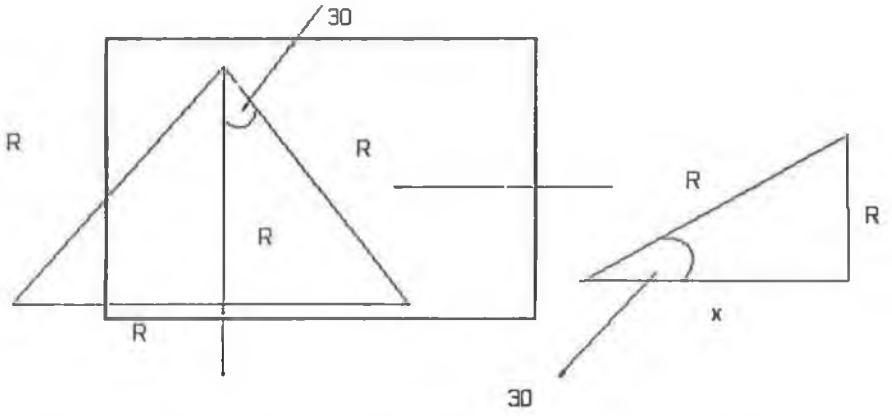

Fig A.4: We draw the following triangle inside the top disc. The length of the whole vertical line is R. However the length of this line inside the triangle is the unknown x. This must be calculated to discover how far into the gap the top disc sits.

$$\text{Cos}30=\sqrt{3}/2=x/R$$

$$\therefore x=\frac{\sqrt{3}}{2}R$$

So we can see that the top disc sits into the gap by a distance of 0.134 of a radius when in this formation. Also each disc added to the mixture adds four additional unit cells. Two will be shared with the discs already present. Therefore we multiply the unit cell area by four times the number of discs present to get the unit cell area for the whole mixture. This assumes that there are a large number of discs present.

Appendix B

MALVERN INSTRUMENTS **MASTERSIZER**

Version 2.16 — **The Aluminium Powder Company** — 15 Jul 2003 12:12PM

6061 +10 -38 :Run Number 60

Source: Analysed

Measured on: 15 Jul 2003 12:11PM

Presentation: 2OHD Very Polydisperse model	Volume Result	Focus = 300 mm.
Residual = 0.371 %	Concentration = 0.048 %	Obscuration = 15.89 %
d (0.1) = 13.38 µm	*d (0 .5) = 24.81 µm*	*d (0.9) = 45.37 µm*
Below 4.50 um = 0.66 %	*Below 6.00 um = 1.07 %*	*Below 10.00 um = 3.87 %*
Below 12.00 um = 7.03 %	*Below 20.00 um = 31.91 %*	D [4, 3] = 28.40 µm
Span = 1.29	*Below 45.00um = 89.71 %*	*Below 75.00um = 98.10 %*
Sauter Mean (D[3,2]) = 20.65 um		Specific Surface Area = 0.2905 sq.m./cc

Size (Lo) µm	Result In %	Size (Hi) µm	Result Below %
0.50	0.10	1.32	0.10
1.32	0.06	1.60	0.16
1.60	0.05	1.95	0.21
1.95	0.07	2.38	0.28
2.38	0.09	2.90	0.37
2.90	0.11	3.53	0.48
3.53	0.14	4.30	0.62
4.30	0.21	5.24	0.84
5.24	0.38	6.39	1.22
6.39	0.71	7.78	1.92
7.78	1.35	9.48	3.28
9.48	2.92	11.55	6.20
11.55	5.61	14.08	11.81
14.08	9.63	17.15	21.44
17.15	13.91	20.90	35.35
20.90	16.93	25.46	52.28

Size (Lo) µm	Result In %	Size (Hi) µm	Result Below %
25.46	16.63	31.01	68.91
31.01	13.21	37.79	82.12
37.79	8.36	46.03	90.48
46.03	4.69	56.09	95.17
56.09	2.30	68.33	97.47
68.33	1.13	83.26	98.60
83.26	0.56	101.44	99.16
101.44	0.34	123.59	99.52
123.59	0.20	150.57	99.72
150.57	0.12	183.44	99.84
183.44	0.07	223.51	99.91
223.51	0.04	272.31	99.96
272.31	0.02	331.77	99.98
331.77	0.01	404.21	99.99
404.21	0.01	492.47	100.00
492.47	0.00	600.00	100.00

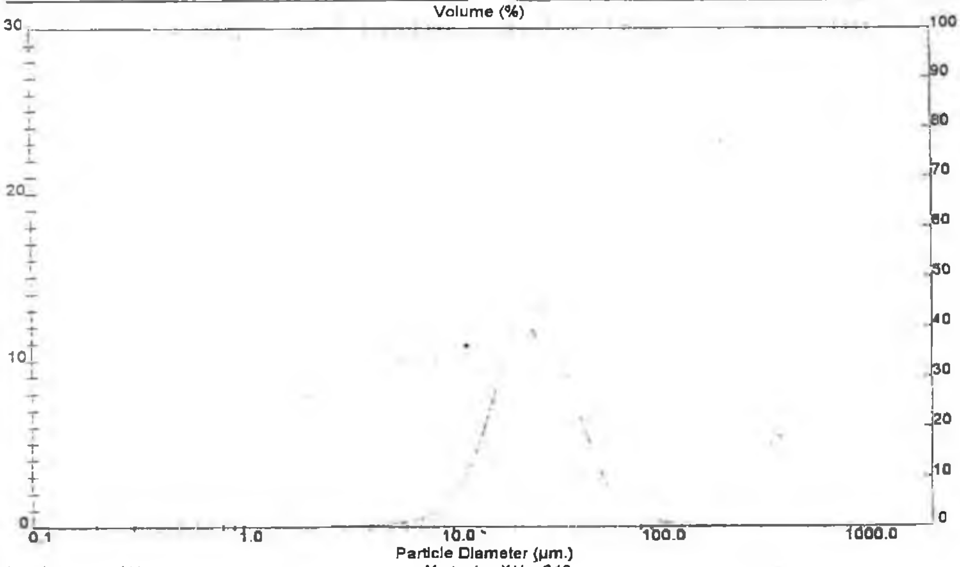

Malvern Instruments Ltd.
Malvern, UK
Tel:=+[44] (0)1684-892456 Fax:+[44] (0)1684-892789

Mastersizer X Ver. 2.18
Serial Number: 6551

p. 6
15 Jul 03 12:1

Appendix C

MALVERN MASTERSIZER

Version 2.18 — The Aluminium Powder Company — 15 Jul 2003 12:32PM

6061 +35 -45 :Run Number 62

Measured on: 15 Jul 2003 12:31PM — Source: Analysed

Presentation: 2OHD
Very Polydisperse model

Volume Result

Focus = 300 mm.

Residual = 0.434 %
d (0.1) = 16.43 µm
Below 4.50 um = 0.59 %
Below 12.00 um = 4.13 %
Span = 1.32
Surface Mean (D[3,2]) = 26.08 um

Concentration = 0.056 %
d (0.5) = 33.26 µm
Below 8.00 um = 0.88 %
Below 20.00 um = 16.69 %
Below 45.00um = 75.08 %

Obscuration = 16.37 %
d (0.9) = 60.38 µm
Below 10.00 um = 2.51 %
D [4, 3] = 38.02 µm
Below 75.00um = 95.09 %
Specific Surface Area = 0.2300 sq.m/cm

Size (Lo) µm	Result In %	Size (Hi) µm	Result Below %
0.00	0.00	1.32	0.00
1.32	0.06	1.60	0.15
1.60	0.05	1.95	0.20
1.95	0.07	2.38	0.27
2.38	0.08	2.90	0.35
2.90	0.09	3.53	0.45
3.53	0.11	4.30	0.56
4.30	0.16	5.24	0.72
5.24	0.28	6.38	0.98
6.38	0.44	7.78	1.42
7.78	0.78	9.48	2.20
9.48	1.52	11.55	3.72
11.55	2.77	14.08	6.48
14.08	4.74	17.15	11.22
17.15	7.39	20.90	18.61
20.90	10.82	25.46	29.43
25.46	14.59	31.01	44.02
31.01	17.16	37.79	61.18
37.79	15.48	46.03	76.66
46.03	10.83	56.09	87.48
56.09	5.92	68.33	93.41
68.33	2.92	83.26	96.33
83.26	1.47	101.44	97.79
101.44	0.84	123.59	98.63
123.59	0.51	150.57	99.13
150.57	0.33	183.44	99.46
183.44	0.21	223.51	99.68
223.51	0.14	272.31	99.82
272.31	0.09	331.77	99.91
331.77	0.05	404.21	99.96
404.21	0.03	492.47	99.99
492.47	0.01	600.00	100.00

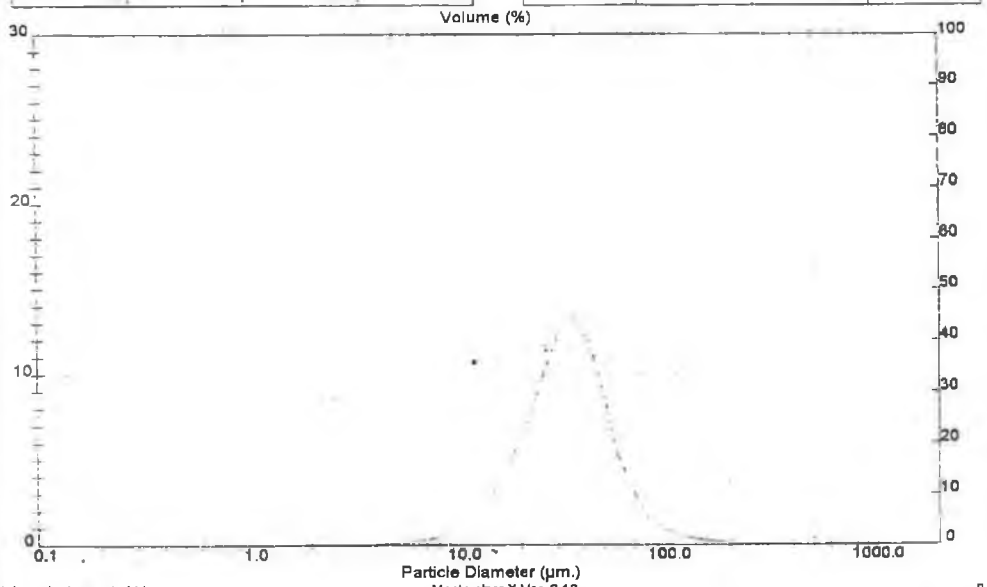

Malvern Instruments Ltd.
Malvern, UK
Tel:=+[44] (0)1684-892456 Fax:+[44] (0)1684-892789

Mastersizer X Ver. 2.18
Serial Number: 8551

p. 6
15 Jul 03 12:3

Appendix D

MASTERSIZER

Version 2.18

The Aluminium Powder Company

15 Jul 2003 12:24PM

6061 +45 -53 :Run Number 61

Source: Analysed

Measured on: 15 Jul 2003 12:24PM

Presentation: 2OHD
Very Polydisperse model

Volume Result

Focus = 300 mm

Residual = 0.446 %
d (0.1) = 20.96 µm
Below 4.50 um = 0.04 %
Below 12.00 um = 2.11 %
Span = 1.09

Concentration = 0.076 %
d (0.5) = 38.94 µm
Below 6.00 um = 0.21 %
Below 20.00 um = 8.78 %
Below 45.00um = 65.35 %

Obscuration = 15.58 %
d (0.9) = 63.58 µm
Below 10.00 um = 1.26 %
D [4, 3] = 42.08 µm
Below 75.00um = 94.48 %

Size (Lo) µm	Result In %	Size (Hi) µm	Result Below %
0.58	0.00	1.32	0.00
1.32	0.00	1.80	0.00
1.80	0.00	1.95	0.00
1.95	0.00	2.38	0.00
2.38	0.00	2.90	0.00
2.90	0.00	3.53	0.00
3.53	0.02	4.30	0.03
4.30	0.08	5.24	0.11
5.24	0.18	6.39	0.27
6.39	0.28	7.78	0.54
7.78	0.53	9.48	1.07
9.48	0.82	11.55	1.89
11.55	1.47	14.06	3.36
14.06	2.45	17.15	5.81
17.15	4.11	20.90	9.92
20.90	6.92	25.46	16.84
25.46	11.68	31.01	28.52
31.01	18.32	37.79	46.83
37.79	20.76	46.03	67.59
46.03	16.07	56.09	83.67
56.09	8.67	68.33	92.33
68.33	4.01	83.26	96.35
83.26	1.84	101.44	98.19
101.44	0.92	123.58	99.11
123.58	0.46	150.57	99.58
150.57	0.24	183.44	99.81
183.44	0.11	223.51	99.92
223.51	0.05	272.31	99.97
272.31	0.02	331.77	99.99
331.77	0.01	404.21	100.00
404.21	0.00	492.47	100.00
492.47	0.00	600.00	100.00

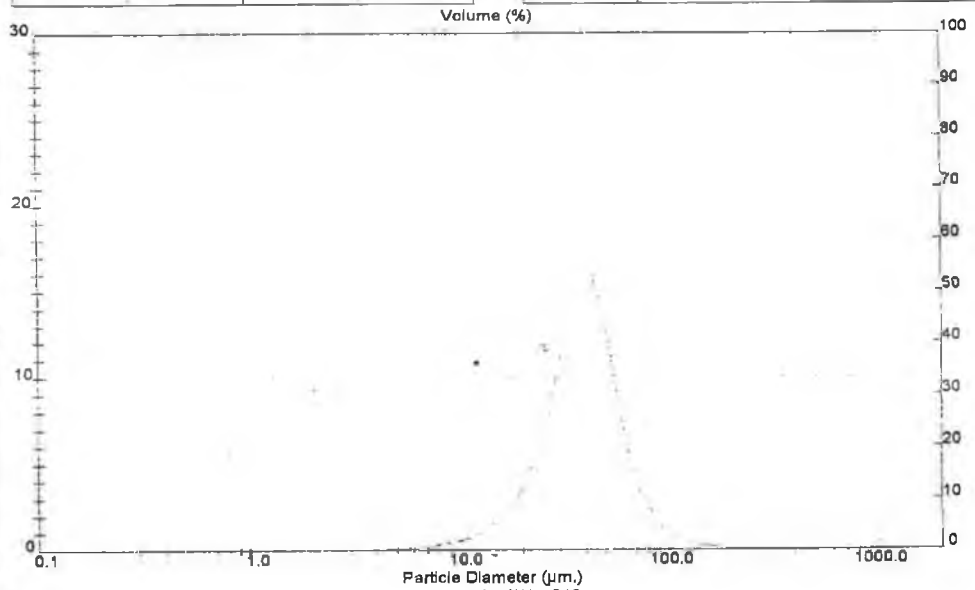

Malvern Instruments Ltd.
Malvern, UK
Tel:=+[44] (0)1684-892456 Fax:+[44] (C)1684-892789

Mastersizer X Ver. 2.18
Serial Number: 6551

p. 8
15 Jul 03 12:2

Appendix E

Tensile Test Sample Dimensions